Does cement mantle thickness really matter?

Jonathan Caruana

Centre for Biomedical Engineering
Institute of Orthopaedics & Musculoskeletal Science
University College London

Supervisors: Prof. Gordon W. Blunn and Dr. Jia Hua

A dissertation submitted in partial fulfilment of the requirements for the degree of Doctor of Philosophy of University College London

January 2008

ProQuest LLC
789 East Eisenhower Parkway
P.O. Box 1346
Ann Arbor, MI 48106-1346

If you believe in God, it should take a great deal to shake your faith.
If you believe in Science, all it takes is one PhD.

Declaration

I, Jonathan Caruana, confirm that the work presented in this thesis is my own. Where information has been derived from other sources, I confirm that this has been indicated in the thesis.

Acknowledgements

Ah, this is just like an award acceptance speech. Where do I start? This is so *unexpected* – I could never imagine that the day would come when I'd be writing a foreword like this, the remainder of the thesis complete. I thought it was going to last forever, and I certainly wasn't alone.

It has been both an honour and a privilege to work in the company of razor-sharp minds that not only probe incisively at the bleeding edge of orthopaedic research but also do a pretty neat job of stitching it up so that it seems almost human.

Gordon Blunn knows a great deal about almost everything from *achnanthes subsessilis* to zirconia. His support, knowledge and vision have empowered me, and his endless faith in me has provided a constant and much-needed boost to my morale, if somewhat baffling.

Jia Hua offers the insight only possible from a clinician who defected to academia; always good at keeping things in perspective, usually a light-hearted one, and always full of obfuscatory wit and wisdom.

I am indebted to Anish Sanghrajka, Paul Whittingham-Jones and Debbie Higgs, without whose diligence in the collection, measurement and cataloguing of medical records and radiographs the surgical approach study would not have been possible; also to Claudia Hon for her assistance in preparing and analysing samples following fatigue testing.

Everyone at the Centre for Biomedical Engineering who makes it such a warm and friendly environment: thank you for your kindness, support and endless cups of coffee. Particularly those friends who offered a ray of sunshine to distract me, intentionally or otherwise, from my thesis writing.

Meanwhile, tucked away behind the Department, a dark workshop beckons. Behind the roaring and clanking machinery, amidst the piles of bones and old surgical equipment and the stench of bovine serum and mineral oil, a team of superheroes is at work. Keith Rayner, Bob Skinner and Mark Harrison achieve the impossible, on a daily basis. Thank you for your help.

In Nijmegen, Nico Verdonschot kindly provided me with Jan Stolk's subroutines and Dennis Janssen was immensely helpful and patient in teaching me how to use them.

This project was supported by the Scales Trust and by Biomet Europe, who kindly supplied implants, surgical tooling and bone cement, as well as providing surface treatment to the conical taper implants.

Whilst writing this thesis felt at times like it was slowly draining my lifeblood, Michiko has always been there, providing life support, supplying food and fluids and the intensive care required to keep the creative juices flowing in my veins.

And lastly, to my parents: I've finished! (You can talk to me again now...)

Abstract

The thickness of the cement mantle around the femoral component of total hip replacements is a contributing factor to aseptic loosening and revision. Nevertheless, various designs of stems and surgical tooling lead to cement mantles of differing thicknesses. This thesis is concerned with variability in cement thickness around the Stanmore Hip, due to surgical approach, broach size and stem orientation, and its effects on stress and cracking in the cement.

The extent to which cement mantle thickness varies in clinical practice as a result of surgical approach was investigated, through retrospective radiographic analysis. The posterior approach was associated with a thicker and more uniform cement mantle.

Stress distributions in the cement mantle around Stanmore hips and surrounding cortical bone were investigated using finite element analysis, under a simulated gait load. Thicker cement was found to produce lower maximum principal stress in the cement and to reduce the likelihood of bone resorption due to stress shielding. Bone density was found to strongly affect stress levels in the bone and cement, but not to alter this result.

Stanmore Hips were implanted into synthetic femurs with different cement thicknesses and stem alignments. Crack measurement and analysis was conducted, following fatigue testing under a simulated stair-climbing load. Crack length was found to be independent of overall cement mantle thickness, suggesting that thinner mantles would fail sooner. However, crack length was highly sensitive to local cement thickness, with regions of 1 mm or less containing longer and more concentrated cracks. Stem alignment and cement mantle uniformity are thus more critical to cement damage than broach size.

Finite element simulations incorporating creep and nonlinear damage accumulation were performed to investigate cracking in the cement mantles around Stanmore Hips with varied cement thickness, interfacial bonding and collar design. Simulations represented the simple stair-climbing joint contact load used in fatigue tests and a more realistic stair-climbing load incorporating muscle forces and physiological bone properties. In all cases, damage levels were much higher when the stem-cement interface was bonded. Cement mantle thickness was of limited importance to cement damage in debonded cases, in agreement with fatigue test results, but was critical in bonded and collarless cases. Damage around a smooth, debonded stem with a collar is thus much less sensitive to cement thickness than around rough/bonded or collarless stems.

Table of contents

List of figures

List of tables

Chapter 1

Introduction

1.1 Total hip replacement

1.1.1 What is total hip replacement?

Total hip replacement is one of the most commonly performed orthopaedic procedures, with an estimated one million operations per year worldwide. Its primary purpose is to restore function to diseased hip joints, where the joint bearing surfaces have degenerated, usually as a result of osteoarthritis. It is a highly successful procedure for improving patient quality of life (Charnley 1972), with implant failure within five years postoperatively now occurring in as few as 2.3 percent of cases overall (Herberts *et al.* 2005). Nevertheless, the high cost per primary operation (estimated to be around $24,000) and much higher cost ($31,000) and complication risk of revision operations (Bozic *et al.* 2005) – coupled with the sheer numbers of procedures performed – mean that any improvements to implant survival duration, however slight, may be highly significant from both clinical and economic perspectives.

Total hip replacement (THR) involves the removal of the diseased femoral head and acetabular bearing surface, and their replacement with an artificial joint comprising of a femoral and an acetabular component, as shown in **Figure 1.1**. The acetabular component is a cup made of metal, plastic or both and fixed into the reamed acetabulum. The femoral component is a metal shaft (or 'stem') fixed into the medullary canal of the femur and supporting a spherical metal or ceramic head which articulates with the acetabular component. The fixation of either component to the surrounding bone may be

achieved either by the use of polymethylmethacrylate (PMMA) bone cement, or by means of bony ingrowth to porous or osseoconductive implant coatings.

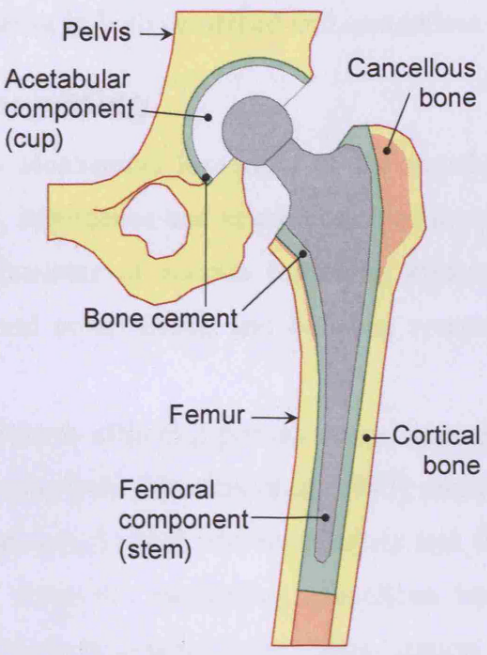

Figure 1.1. Schematic of a cemented total hip arthroplasty.

1.1.2 Why do hip replacements fail?

The most common reasons for revision are aseptic loosening, dislocation, and deep infection. Aseptic loosening alone accounts for more than 75 percent of all revisions, whilst deep infection and dislocation each lead to around seven percent of revisions (Herberts *et al.* 2005). The issue of deep infection has been addressed by the use of surgical protocols which minimise bacterial exposure, the postoperative delivery of antibiotics, and the use of antibiotic-laden bone-cements. Dislocation arises as a result of the altered joint morphology and the loss of support from muscle which has been damaged during surgery; surgical technique and postoperative care are major contributors to this problem.

By contrast, aseptic loosening has been observed to be affected not only by surgical technique but by a host of other design-related factors, including the wear-resistance, stiffness, shape and surface morphology of the implants

used. As the most common cause for revision and the one over which we appear to have the most control through the design of implants, materials and surgical procedures, it is scarcely surprising that aseptic loosening has attracted so much research interest in both cemented and cementless cases.

1.1.3 Aseptic loosening

Aseptic loosening is mechanical loosening of the prosthesis from the bone, leading to local pain, subsidence and micromotion of the prosthesis relative to the bone. The mechanisms of aseptic loosening appear to differ between acetabular and femoral components, and between cemented and cementless implant types.

The main problems afflicting porous coated cementless implants seem to be periprosthetic osteolysis (Havelin *et al.* 1995) and poor, inconsistent or incomplete bony ingrowth, in both the acetabulum and femur, or fracture of this bony ingrowth from the supporting cancellous bone. In the case of hydroxyapatite-coated cementless implants, disintegration or resorption of this coating appears to be a major problem (Hirakawa *et al.* 2004). According to the Swedish Hip Arthroplasty Registry, revision within thirteen years of primary THR is three times more likely with a cementless implant than a cemented one, and twice as likely with a hybrid implant (Herberts *et al.* 2005). It is therefore likely that hip surgeons will continue to choose cemented implants for patients over the age of sixty for the foreseeable future. Only in younger and more active patients are cementless femoral implants widely accepted, due to their preservation of bone, which facilitates revision.

In the case of the cemented acetabular component, a layer of granulomatous tissue, containing wear particles, has been observed to invade the cement-bone interface from the periphery (Charnley 1979; Fornasier *et al.* 1991; Schmalzried *et al.* 1992b). This suggests a predominantly biologic aetiology for osteolysis and aseptic loosening where particulate wear debris plays the key role in implant failure (Hirakawa *et al.* 2004). Multivariate survival analysis indicated that aseptic loosening of the acetabular component

was associated only with rapid wear of the polyethylene (Kobayashi *et al.* 1997). Although many other factors have also been thought to influence survival of the acetabular component, such as the cup design and patient age or activity level, many of these factors are also contributors to wear. Thus efforts to save the cemented acetabular component may be focused on improvement of the wear properties of articular bearing surfaces.

However, studies of the cemented femoral component have not yielded such clear-cut results. Many aspects of bone geometry, prosthetic design and selection, and surgical technique have been associated with increased risk of aseptic loosening. These include the following, from large-cohort survival analysis studies:

- Design of femoral component;
- Brand of bone cement;
- Surgical approach used;
- Cement not mixed under vacuum;
- No pulsatile lavage;
- No proximal femoral seal;
- No distal femoral plug;
- No retrograde fill;

(Malchau *et al.* 2000)

- Brand of bone cement;
- Low viscosity bone cement;
- Cement without gentamicin;

(Espehaug *et al.* 2002)

- A thin (less than 1 mm) cement mantle;
- Defects in the cement mantle;

(Mulroy *et al.* 1995)

- Canal filling by the stem of less than 75 percent;
- Less than 1 cm of cement distal to the stem tip;
- Varus alignment of the stem;

- Calcar resorption and atrophy of the femoral cortex;

(Kobayashi and Terayama 1992)

- 'Stovepipe' medullary canal geometry.

(Kobayashi *et al.* 2000)

Clearly, there are many design parameters and surgical factors implicated in the process of aseptic loosening of the cemented femoral component. Broadly, the design parameters relate to the implant itself and the surgical factors to the preparation of the cement mantle. These are examined in later sections.

1.1.4 Mechanism of aseptic loosening

To improve fixation of the cemented femoral component, it is necessary to understand the underlying processes by which failure occurs. The earliest hip replacements often fractured as a result of metal fatigue of the femoral component (Galante 1980), but improved material selection and processing have almost entirely eradicated this problem. This leaves the femoral bone, the cement mantle, and the interfaces between implant, cement and bone as potential sites for failure – the 'weak-link zones' (Lewis 1997). The current understanding of the failure mechanism for cemented femoral components is that all of these sites are involved sequentially in the process of implant loosening.

Until the 1990s, opinion on the causes of aseptic loosening of the femoral component was divided between two camps.

On the one hand were those who believed this to be primarily a mechanical phenomenon, resulting from the breakdown of the bone cement or its interfaces with metal and bone. Thus implant survival was thought to depend mostly on strength and fatigue resistance at these locations, and on the stresses to which they are subjected. Much research focused on measuring, predicting, or controlling these unknowns (Crowninshield *et al.* 1980; Rohlmann *et al.* 1983; Lewis *et al.* 1984; Miles and Dall 1985).

Others believed that aseptic loosening was principally a biological response to implanted foreign materials. Goldring *et al.* (1986) observed a synovial-like membrane at the bone-cement interface of loose femoral components, capable of synthesizing prostaglandin E2 and collagenase which cause bone resorption. This membrane was found to contain particulate PMMA and polyethylene particles. The presence of cement fragments, and the growth of this membrane around the cement mantle, led to the belief that this was an immune response to cement, and to the nicknaming of periprosthetic bone loss as 'bone cement disease' for many years.

However, later evidence suggested that this kind of periprosthetic bone loss was a response to polyethylene wear debris, rather than cement. Anthony *et al.* (1990) noticed that focal osteolytic lesions around well-fixed stems were only located adjacent to defects in the cement mantle. Schmalzried *et al.* (1992a) noted linear (diffuse) and lytic (localised) areas of periprosthetic bone loss around loose and well-fixed femoral components, remote from the articular surfaces, and characterised by macrophages containing intracellular submicron particles of polyethylene. They found that the number of macrophages in a microscopic field was directly related to the concentration of particulate polyethylene debris, and that the number of macrophages present had a direct relationship to the degree of bone resorption that was seen. This indicates that joint fluid containing wear debris penetrates along the interface between the prosthesis and bone and into the periprosthetic tissues – more extensively than previously thought. They suggested the concept of the 'effective joint space' to include all periprosthetic regions accessible to joint fluid and thus to particulate debris.

Jasty *et al.* (1990) observed debonding at the stem-cement interface and cracking of the cement mantle in well-fixed femoral components, indicating that debonding and cement damage precede periprosthetic bone loss and loosening. They also noted that the extent of cement damage was consistent with length of time *in vivo*.

From this evidence, it appears that aseptic loosening of the femoral component is a sequential process, the phases of which may overlap. "The mechanism of initiation of loosening of cemented femoral components is now known. It is debonding at the cement-metal interface." (Harris 1992) Initially, debonding of the stem-cement interface allows the stem to subside, altering the stresses present in the cement mantle, as well as extending the effective joint space to include the stem-cement interface. Stresses in the cement mantle lead to cracks forming and propagating in the cement mantle over time. Ultimately, through-thickness cracks and defects in the cement mantle then serve to extend the effective joint space as far as the periprosthetic bone, as indicated in **Figure 1.2**. This serves as a direct path for particulate wear debris in the pressurised joint fluid (Robertsson *et al.* 1997) to reach bone, where the biological process of lytic bone resorption and loosening begins.

A body of fractographic evidence from Topoleski *et al.* (1990; 1993; 1995) indicts fatigue failure and fatigue crack propagation as the primary cement failure mechanisms that contribute to aseptic loosening of the prosthesis. Weakening of the cement mantle by cracking may even enable subsidence and mechanical loosening which is independent of wear particle ingress (Noble *et al.* 2005). The accumulation of damage in the cement mantle may therefore be considered an enabler of aseptic loosening and a useful indicator for predicting likely rates of aseptic loosening in mechanical testing and simulation where the accompanying biological processes are absent (Stolk *et al.* 2003a)

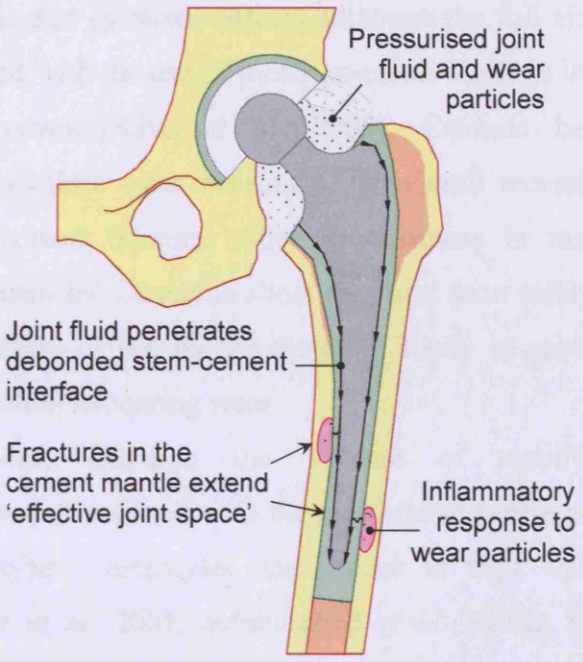

Figure 1.2. The effective joint space, showing the wear-debonding-damage pathway.

1.2 Implant design

1.2.1 Articular bearing surfaces

In theory, it should be possible to eliminate aseptic loosening altogether by improving the wear resistance of articular bearing surfaces. Charnley's highly successful Low Friction Arthroplasty originally consisted of a stainless steel prosthesis articulating against a PTFE cup, later replaced by a polyethylene cup due to poor wear resistance and adverse tissue reactions to PTFE. While metal implants and polyethylene cups are still the most popular combination today, others have been tested, principally to reduce wear debris and tissue reactions. Metal-on-metal and ceramic-on-ceramic bearings have been developed which produce less wear debris.

However, these solutions are not without their own problems. Whilst polyethylene wear debris is relatively inert, remaining within the effective joint space until absorbed into periprosthetic tissues, metal wear debris releases metal ions which enter the serum and blood stream. These are known to have

both carcinogenic and cytotoxic effects, although the full extent of these, and the risk associated with the use of metal-on-metal bearings in hip replacement, are not yet known (Silva *et al.* 2005). Ceramic bearings, although demonstrating excellent wear resistance, have until recently been prone to occasional component fracture, although advances in manufacturing may reduce these incidences. Concerns about the short term safety of ceramics and the long term safety of metals are therefore likely to prevent or delay any widespread reduction in bearing wear.

Furthermore, although the volume of reactive periprosthetic inflammatory tissue associated with metal-on-metal bearings is less than with metal-on-polyethylene, osteolysis does occur in hips with metal-on-metal bearings (Beaule *et al.* 2001; Schmalzried *et al.* 1996a; Schmalzried *et al.* 1996b). Aspenberg (1998) observed an osteolytic response to pressurised synovial fluid, even where no wear particles were present. So the problem of aseptic loosening may be reduced by the avoidance of polyethylene, but not entirely eradicated.

If osteolytic response to wear particles cannot be avoided, and debonding cannot be prevented, then it falls to the cement mantle to act as a barrier between the effective joint space and the surrounding bone. It is thus clear that the cement mantle and its interfaces with bone and implant have a crucial role to play in delaying or preventing aseptic loosening.

1.2.2 Stem material

The materials commonly used in cemented femoral stems are cobalt-chromium, stainless steel, and titanium. Titanium was once favoured due to its lower elastic modulus, giving titanium implants a bending stiffness closer to that of the femur so that bone stresses would be preserved. However, this increased flexibility is believed to lead to higher proximal cement stresses and more rapid debonding (Verdonschot 2005), which is thought to account for the relatively high failure rates observed clinically (Bowditch and Villar 2001; Ebramzadeh *et al.* 2003; Jergesen and Karlen 2002; Lichtinger *et al.* 2000).

Titanium is also prone to crevice corrosion (Hallam *et al.* 2004; Thomas *et al.* 2004; Willert *et al.* 1996). Most femoral components are now made of forged cobalt-chromium or stainless steel.

1.2.3 Surface finish

Many attempts have been made to enhance fixation of the stem-cement interface by roughening the surface of the femoral stem with grit-blasting or bead-blasting, and in some cases pre-coating it with a layer of cement. Implants had previously been given a polished or matte finish. Roughening and pre-coating were intended to prevent debonding from occurring, which was thought to reduce cement damage. However, clinical follow-up revealed that rough stems often performed worse that their smooth-finished precursors (Collis and Mohler 1998; Dowd *et al.* 1998; Cannestra *et al.* 2000; Sylvain *et al.* 2001; Collis and Mohler 2002; Ong *et al.* 2002; Della Valle *et al.* 2005). Although debonding may have been delayed by the improved interfacial shear strength, it was not prevented altogether. In fact, surface roughness does not seem to improve the interfacial fatigue debond response (Damron *et al.* 2006). Furthermore, once debonding occurs, the rough stem begins to wear abrasively against the cement mantle. This may allow more rapid subsidence or rotation than would normally be expected (Mohler *et al.* 1995), increasing cement stresses, generating PMMA wear particles, and opening up the wear particle pathway, thus accelerating the loosening process. Stems with rough surfaces have recently declined in use.

1.2.4 Implant shape

The shapes of commercially available stems are typically complex and incorporate many design parameters. Hence, it is difficult to establish the precise effects of any of these parameters in isolation. Broadly speaking, the axial cross-section contributes chiefly to the torsional stiffness and stability of the implant, and the mediolateral thickness contributes towards the principal bending stiffness and stability under physiological loads.

Torsional stiffness is proportional to the polar moment of area, which depends equally on anteroposterior and mediolateral thickness; thus, a thicker implant is stiffer. Torsional stability depends on how well stress is imparted to the cement mantle, and is increased by both thickness and cross-sectional complexity; thus, a thicker implant is more stable, whilst an implant with a circular cross section is less stable than one with an angular cross-section. Since sharp corners impart large stresses to the cement mantle, they are best avoided, so most implants have cross-sections which are either roughly elliptical or rectangular with fillet radii of at least 2 mm.

Implants generally transfer stresses to the bone mostly at the proximal and distal ends. Increased bending stiffness generally focuses the stresses more around the distal tip. Accordingly, stems are generally thinner distally, so that stresses are not too concentrated around the distal tip.

Design features such as double and triple tapers have been introduced with aims such as sustaining hoop stress in the femoral cortex as the implant subsides, although this may in turn be more damaging to the cement mantle. Since many of these design features are conceived as solutions to idealised, two-dimensional or axisymmetric models, it is often unknown whether they are truly beneficial to implant fixation. Furthermore, since available implants each incorporate a mix of design features, clinical evaluation of individual features is nearly impossible.

1.2.5 Design philosophy

Verdonschot (2005) asserts that a design philosophy should be chosen and design features be selected to fit that philosophy. Two such philosophies are the 'force-closed' and 'shape-closed' paradigms (Huiskes *et al.* 1998). A force-closed design (generally tapered) is stabilised by hoop stresses and frictional forces as it subsides, whilst a shape-closed design (generally collared) is supported in place by the bone and cement mantle such that major axial subsidence is prevented. Features such as implant shape and surface finish should be chosen to support the design philosophy.

Two clinically successful femoral components which demonstrate each philosophy are the Exeter Hip and the Lubinus SPII, shown in **Figure 1.3**. The Exeter Hip has a highly polished finish and no collar, to allow subsidence, a double-taper to generate cortical hoop stress, and a rectangular cross section for torsional stability. It embodies the force-closed paradigm, and results in large but stable, continuous axial migration (Huiskes *et al.* 1998) and steadily increasing cement damage (Stolk *et al.* 2003a). The Lubinus SPII, a shape-closed design, features a collar and a more anatomical shape, with a near-elliptical cross-section. It does not subside much axially, but does experience torsional rotation. The rates of both migration and cement damage are thought to decrease over time, so that very little further rotation or damage is seen after a few hundred thousand loading cycles (Stolk *et al.* 2003a).

Failure to adhere to such a philosophy leads to arbitrary mixing of features, which is unlikely to result in well-designed, stable implants. For example, the Scientific Hip Prosthesis was designed with an optimised shape to minimise cement stress. It was described as a 'shape-closed' design (Huiskes *et al.* 1998), and the shape optimization was based on the assumption that no debonding would occur (Huiskes and Boeklagen 1989). However, it later became apparent than there was significant debonding and migration (Nivbrant *et al.* 1999), and hence more cement damage than expected, leading to early loosening. Had this implant been given a collar to prevent migration, like other shape-closed designs, it may have been more successful. The flanged Capital Hip, essentially a copy of a successful (shape-closed) Charnley design, was made available in Titanium with a rough finish. Its flexibility, incompatible with a shape-closed philosophy, promoted debonding and its roughness had an abrasive effect, leading to extensive cement damage and wear (Janssen *et al.* 2005a).

Figure 1.3. Three femoral components demonstrating different design philosophies. Left to right: polished Exeter stem (force-closed), Stanmore Hip, and Lubinus SPII (shape-closed) showing projections of its anatomically-curved profile. Images courtesy of Stryker Corp., Biomet, Inc., and Waldemar Link GmbH, respectively.

1.2.6 The Stanmore hip

The Stanmore Hip is the only design to have remained on the market for over four decades without any substantial design changes to the femoral component (except for modularity) since its introduction. It was designed by Professor John Scales in Stanmore during the early sixties, and does not adhere strictly to the 'design philosophies' later advocated by Verdonschot, having both a smooth, straight, double-taper design similar to that of the Exeter stem, but with a collar to minimise migration.

Nevertheless, excellent survival rates are reported in the Swedish Hip Registry between 1994 and 2005 (Kärrholm *et al.* 2006): 98.6 percent survival at five years for all diagnoses and revisions (n=610), and 100 percent survival for osteoarthritis and aseptic loosening only (n=293). Survival rates of 91 percent at 22 years are reported elsewhere (Gerritsma-Bleeker *et al.* 2000). These results are similar to those of other widely used prostheses such as the Exeter and Lubinus SP-II (Kärrholm *et al.* 2006).

1.3 The cement mantle

1.3.1 Early use of bone cements

The very first hip replacement is thought to have been performed by Gluck (1890) in Germany, consisting of a carved ivory ball and socket fixed in place with a novel bone cement composed of pine resin, pumice powder, and plaster of Paris. Prior to this, the only intervention possible in diseased hip joints had been femoral head resection, leading to pseudarthrosis or fusion, or the interposition of various tissues and man-made materials. Wiles (1958) implanted stainless steel femoral and acetabular components, both held in place by screws which subsequently loosened and failed. Haboush (1953) first used a two-part self-polymerising polymethylmethacrylate (PMMA) bone cement, already popular in dental applications, to fix in place a vitallium resurfacing prosthesis consisting of concentric femoral and acetabular cups. However, it was not until Charnley introduced his low friction arthroplasty in 1962, consisting of a stainless steel femoral stem and a high density polyethylene cup, both cemented into place with acrylic bone cement, that long term results improved dramatically.

1.3.2 Evolution of cementing techniques

Acrylic bone cement was such a successful improvement on Gluck's interesting concoction that its formulation has not substantially changed since it was first introduced. It remains the only material used for anchoring cemented arthroplasties to the contiguous bones (Lewis 1997). However, when mixed and cured *in situ*, its mechanical properties are dramatically inferior to those of PMMA produced industrially under controlled conditions, leaving considerable scope for improvement. Attempts both to improve the quality and to reduce the variability of its material properties and of its fixation to bone have led to progressive improvements in cementing technique.

First generation

Initially, bone cement was mixed in a bowl. This introduced micro-porosity as air between the powder granules became trapped during mixing. Surgical staff would also have been exposed to noxious fumes released by the monomer fluid. The cement would then have been manually finger-packed into a reamed and irrigated bony cavity. This would trap pockets of air (macro-pores) between layers of packed cement, and would not force the cement to displace blood and fat in order to interlock tightly with cancellous bone. Blood and marrow could also intrude into the cement, leading to more large inclusions. The prosthesis would then be inserted and held in place until the cement had cured.

Second generation

Many early failures of fixation of the femoral component were observed to result in a 'pistoning' motion (Gruen *et al.* 1979) of the cement mantle within the medullary cavity, as a result of the low interfacial strength of the cement-bone interface. As a filler or grout, rather than an adhesive, bone cement does not form any bond with bone, so fixation relies instead on the cement forming a macro-interlock with the surrounding cancellous bone. The so-called 'second generation' cementing technique consisted of a number of new steps, proposed primarily as a way to improve this bony interlock. Preparation of the medullary canal was seen to take on new importance, with high pressure pulsatile lavage now used to clear blood and fat away more aggressively. The medullary canal was then swabbed with haemostatic agent in order to absorb water and minimise bleeding. High-viscosity bone cement was injected in a retrograde fashion using a pressurising gun to create a steady influx of cement with no layers trapping air. Pressurisation was further enhanced by the use of a distal plug or cement restrictor. The pressurised, high-viscosity cement would then transmit pressure more effectively to the cement-bone interface during insertion of the implant, enhancing interdigitation and the displacement of blood and fat.

Third generation

The adoption of second generation cementing techniques provided improved fixation at the cement bone interface, leading to a reduction in revisions due to aseptic loosening of the femoral component (Estok and Harris 1994; Mulroy *et al.* 1995). However, this exposed the cement mantle itself and the stem-cement interface to greater scrutiny as surgeons now sought to eliminate failure associated with debonding and cracking of the cement mantle. 'Third generation' techniques were introduced with the intention of preventing these failures by improving the strength and fatigue resistance of the cement and stem-cement interfaces. Firstly, cement was either centrifuged or mixed under vacuum at pressures of between –30 and –80 kPa, in order to reduce micro-porosity. Vacuum mixing also dramatically reduced the exposure of theatre staff to methacrylate fumes. Secondly, cement ingredients were pre-chilled so that working time was increased and cement remained more fluid during mixing, facilitating the release of trapped air under vacuum or centrifugation. Thirdly, to improve the integrity of the stem-cement interface, femoral components with matt and rough surface finishes were introduced, sometimes pre-coated with a layer of PMMA produced under controlled manufacturing conditions. To further enhance pressurisation of the cement during filling of the medullary canal, a proximal femoral seal was introduced. To address the issue of cement failure around poorly-aligned prostheses, thought to arise due to high cement stresses and cracking around thin mantle regions, centralisation devices were added to the distal tip of many femoral components.

Inconsistencies

The individual steps within each subsequent 'generation' were advocated throughout the 1980s and 1990s by a number of researchers and have been gradually adopted in a piecemeal manner by surgeons. It is therefore difficult to categorise technical advances as being 'second' or 'third' generation, with precise definitions of what constitutes a second or third generation technique varying from author to author. For example, optional centrifugation and

vacuum mixing at pressures of around –30 to –40 kPa are sometimes cited as part of the second generation technique (Dunne and Orr 2001). The above descriptions are therefore necessarily generalisations for the sake of clarity.

It is also difficult to ascertain how mainstream surgical techniques evolved over time, as new techniques have typically taken decades to become widespread. For example, it was reported a decade ago that 'modern' cementing techniques had been fully adopted by only 25 percent of surgeons in the UK, accounting for only 26 percent of hips implanted in this country (Hashemi-Nejad *et al.* 1994). In contrast, surgeons in Sweden and Norway, whose National Hip Arthroplasty Registers have allowed large scale statistical analysis of the effects of new techniques on implant survival, have been quick to adopt successful methods and to reject those with less success (Herberts and Malchau 1998).

1.3.3 Composition of bone cement

The chief utilities of PMMA bone cement are (*a*) that it can be mixed to form a fluid consistency which cures *in situ* within minutes and at temperatures which generally pose no significant threat of thermal necrosis to surrounding tissues, and (*b*) that, once cured, it forms a relatively strong, biocompatible solid; few other materials, if any, could be used in this way. The main constituents of bone cement are methylmethacrylate (MMA) monomer liquid and PMMA polymer powder, along with extremely small amounts of chemical catalysts which initiate, accelerate and stabilise the polymerisation process. In addition to these, small quantities of antibiotics, such as gentamicin, and radiopacifiers, such as barium sulphate or zirconium dioxide, are often added to reduce the risk of deep infection and enhance radiographic appearance, respectively. The relative proportions of all these ingredients vary between brands, and affect both the fluid viscosity of the cement and its mechanical properties once cured.

1.3.4 Physical properties of bone cement

During mixing and curing

Mixing of bone cement begins with bringing together the monomer fluid and polymer powder constituents. Polymerisation gradually increases molecular weight, so the mixture's viscosity increases over time (Dunne and Orr 1998). Since this reaction is highly temperature dependent, the initial temperature of the cement components and the ambient temperature have a strong effect on curing time, such that temperatures only a few degrees higher can dramatically reduce working time (Baleani *et al.* 2001; Hansen and Jensen 1990; Lewis 1999). The exothermic reaction causes the cement to reach high temperatures after around 10–20 minutes, as the cement reaches a solid state – typically around 67–124 °C (Wang *et al.* 1995) at the core of the thickest regions.

Molecular weight

Different brands of bone cement have different molecular weights and powder-to-liquid ratios. These influence the viscosity of curing cement as well as its mechanical properties once cured. Those cements with the highest molecular weights, such as Simplex and Palacos, have the highest viscosities before curing and also the highest stiffness, tensile strength, fracture and fatigue resistance after curing (Graham *et al.* 2000; Harper and Bonfield 2000). Sterilisation by beta or gamma irradiation has been shown to reduce molecular weight, leading to reduced tensile strength, modulus, strain to failure, fracture resistance and fatigue life (Harper *et al.* 1997; Lewis and Mladsi 1998); sterilisation with ethylene oxide gas does not influence fracture or fatigue properties, and is therefore preferable (Graham *et al.* 2000).

Additives

Antibiotics and radiopacifiers are routinely added in small quantities to most brands of bone cement, usually by the manufacturer. Whilst radiopacifiers have been observed to stiffen the cement (Holm 1977), both antibiotics and radiopacifiers have been shown to reduce its ultimate and fatigue strengths

(Armstrong *et al.* 2002; Baleani *et al.* 2003; Lee *et al.* 1977; Vallo 2002). However, this material weakness is offset by clinical benefits, namely the prevention of deep infection and the improvement of diagnostic clarity through enhanced radiographic appearance. Conversely, optimal dosing of radiopacifier particles has been used (Freitag and Cannon 1977) as a means of improving fatigue resistance, and the addition of other reinforcing additives, such as polybutylmethacrylate particles, silanated hydroxyapatite particles, and fibres of titanium, PMMA, carbon, or polyethylene terephthalate, have been shown to increase fatigue life or strength by 55 to 88 percent (Lewis 2003). Colourants, such as chlorophyll, are used in much smaller quantities to improve cement visibility, primarily for the benefit of the revision surgeon, and have been shown to have no significant effect on fatigue life (Davies and Harris 1992).

Time dependent properties

Like many other polymers, bone cement exhibits time-dependant mechanical properties. Ultimate tensile strength is known to be strain-rate dependent (Lee *et al.* 1977). Viscoelastic properties are affected by brand of bone cement, time since mixing, and temperature history, as well as the presence of water, blood and/or lipids (Holm 1980; Lee *et al.* 2002). Viscoelasticity is usually referred to in terms of two phenomena: creep, which is the gradual strain increase arising under sustained stress; and stress-relaxation, which is the gradual reduction of stress arising under sustained strain. Viscoelastic properties of different brands of bone cement, and with a range of ageing and test environments, have been characterised through tests involving stress relaxation (Holm 1980; Yetkinler and Litsky 1998), creep under static load (Arnold and Venditti 2001; Chwirut 1984) and under dynamic tensile (Jeffers *et al.* 2005b; Verdonschot and Huiskes 1994) and compressive (Verdonschot and Huiskes 1995) loads. Whilst Holm (1980) and Norman *et al.* (1995) found that Palacos-R cement creeps more than other brands, Lee *et al.* (2002) concluded that environmental and ageing factors can be more influential than brand formulation on the viscoelastic behaviour of bone cements.

Environment, ageing and residuai stress

The environments in which test samples are stored and tested have been shown to affect their mechanical properties. Although the peak curing temperature, occurring just after cement solidifies, is usually seen by surgeons as the endpoint in the curing process, polymerisation is not complete: stiffness continues to increase gradually over time for many days afterwards, and increased temperature accelerates this process (Baleani *et al.* 2001). The ductility of bone cement is also affected by ageing environment: samples stored in water, Ringer's solution or lipid demonstrate higher ductility than dry samples, which has been attributed to the plasticising effect of fluid ingress (Hailey *et al.* 1994; Watson *et al.* 1990), whilst samples stored at body temperature are more brittle than those stored at room temperature. Thermal contraction, during and after curing, leads to irregularly distributed residual stresses throughout the cement; these stresses can be large enough to initiate cracking (Lennon and Prendergast 2002; Orr *et al.* 2003). The strong effect of curing times and temperatures on fracture resistance (Watson *et al.* 1990) may be attributed to a combination of these factors. Mechanical properties such as strength are known to deteriorate over longer periods of time in samples *in vivo* (Kon 1981), which is thought to be caused by molecular weight reduction resulting from prolonged exposure to an oxidative environment (Hughes *et al.* 2003).

Porosity and mixing technique

Porosity arises from five sources (Lewis 1997): air initially surrounding the liquid monomer or powder constituents, entrapment of air during wetting of the powder by the liquid monomer, entrapment of air during mixing of the constituents, the evaporation of the volatile liquid monomer during the curing stage, and the entrapment of air during the transfer of the dough to the syringe or gun. The presence of porosity has a detrimental effect on the mechanical properties of bone cement. Greater pore size and pore density have marked effects on crack initiation and growth, dramatically reducing fatigue life

(Ishihara *et al.* 2000). Murphy and Prendergast (1999; 2002) describe the relationship between stress, porosity and non-linear damage accumulation, noting that cracks generally appear to originate at pores, and that different porosity levels account for the variability in damage accumulation between specimens. Although Topoleski *et al.* (1993) speculated that pores may play a role in blunting crack growth, a wealth of evidence to the contrary has led to the general consensus that porosity should be minimised (Lewis 1997). A number of studies have investigated the effect of different mixing systems on porosity and mechanical properties. General observations include superior results from vacuum mixing and centrifugation in terms of reduced porosity as well as increased stiffness, strength, fatigue strength and fracture resistance, when compared to hand-mixing (Dunne and Orr 2001; Dunne *et al.* 2003; Graham *et al.* 2000; Wilkinson *et al.* 2000). More specifically, the best results are obtained with the use of a syringe-type, or 'sealed, combined mixing, collection and delivery system', such as the Optivac, at pressures of around –80 kPa (Dunne and Orr 2001; Mau *et al.* 2004; Wilkinson *et al.* 2000). Pressurisation during or after mixing has also been observed to increase strength (Guidoni and Vallo 2002) and fatigue resistance (Dunne *et al.* 2003; Freitag and Cannon 1977).

Porosity distribution

Whilst the gross level of micro-porosity is dependent principally on the amount of trapped air, its distribution is affected by thermodynamic factors. Polymerisation occurs most rapidly where the temperature is highest. As the heat generated by the exothermic reaction is dissipated by the implant, bone and body fluids, the cores of the thickest regions of cement generally polymerise first, driving dissolved impurities and gases towards the last regions to polymerise and increasing thermal shrinkage in these regions. Since the metal implant is cooler and more thermally conductive than bone, the implant-cement interface is generally the last to polymerise, and most of the porosity is therefore concentrated at this interface. Preheating the stem has been shown to

accelerate polymerisation (Dall *et al.* 1986) and to reduce the porosity at the stem-cement interface (Bishop *et al.* 1996), thus increasing interfacial shear strength (Iesaka *et al.* 2003) without affecting bulk cement material properties like elastic modulus, fracture toughness or fatigue strength (Parks *et al.* 1998).

1.3.5 Cement mantle thickness and continuity

Strain, damage, osteolysis and loosening

Cement mantle thickness has been frequently indicted as a critical factor affecting the outcome of femoral component fixation. Thin cement (usually defined as less than 1 or 2 mm thick), or defects (flaws or windows) in the cement mantle, lead to an increased incidence of loosening (Massoud *et al.* 1997; Mulroy *et al.* 1995), particularly in the proximal medial (Ebramzadeh *et al.* 1994; Malik *et al.* 2005) and distal medial regions (Ritter *et al.* 1999; Star *et al.* 1994). Osteolysis is seen most commonly around cement mantle defects and thin mantle regions (Joshi *et al.* 1998; Kawate *et al.* 1999; Maloney *et al.* 1990).

This is unsurprising, given that cracks are found mostly in thin mantle regions (Kawate *et al.* 1998), and appear to originate preferentially in thin or defective mantle regions (Jasty *et al.* 1991; Jasty *et al.* 1992; Koster *et al.* 1999). *In vitro* studies indicate that through-thickness cracks in the cement mantle are more likely to form in thin regions, under torsional (Hertzler *et al.* 2002) and stair-climbing loads (Mann *et al.* 2004). It is thought that this damage occurs in thin regions as a result of the critical influence of cement thickness on cement strains, especially near the tip: peak strains are minimised both through reducing the stem thickness and by ensuring neutral alignment of the stem (Estok *et al.* 1997; Fisher *et al.* 1997; Lee *et al.* 1993; Lee *et al.* 1994; Schmolz *et al.* 2000).

Cement mantle thickness is sometimes expressed in terms of the proportion of the medullary canal which is filled by the stem (usually calculated as the ratio of their diameters at a specified distance along the

implant). A canal-filling ratio of less than 50–60 percent is associated with osteolysis and failure (Ebramzadeh *et al.* 1994; Joshi *et al.* 1998).

Definition and measurement of cement mantle thickness

Although these findings appear to agree on thick cement as optimal, the way in which cement mantle thickness is measured or defined can be confusing. Experimental and finite element studies tend to use an idealised, uniform cement mantle and vary its thickness; clinical studies measure thickness locally on radiographs or sections. Thus, recommendation of 'thick' cement can sometimes be taken to mean 'without thin regions'.

To add to this confusion, the thickness of cement measured from radiographs generally includes the interdigitated regions of cancellous bone, whose properties are inferior to those of pure cement (Jofe *et al.* 1991) and which offers lower resistance to fatigue crack growth (Race *et al.* 2003) and wear particle ingress. Moreover, routine anteroposterior and lateral radiographs tend to underestimate the prevalence of both thin cement mantles and defects (Kawate *et al.* 1998; Valdivia *et al.* 2001), as further voids and thin or defective regions become apparent on additional radiographs taken at different angles (Kawate *et al.* 2003; Smith *et al.* 1998).

Optimal cement mantle thickness

There is a general consensus that the cement mantle should preferably be 2–5 mm thick, so as to minimise the risks of both thermal necrosis and mechanical loosening. Removal of cancellous bone specifically in the region of the calcar femoris, ensuring a thick mantle in this area, also leads to lower peak cement strains (Ayers and Mann 2003) and a reduced risk of loosening (Massoud *et al.* 1997; Ebramzadeh *et al.* 1994). Breusch and Malchau (2005) recommend a composite thickness of 5 mm at the calcar and 2–3 mm distally.

Femoral components from most manufacturers are generally provided to the surgeon with a set of rasps, each specially designed for an implant size and shape, to over-ream the medullary canal by a uniform amount, thus (in theory) creating a uniform cement mantle thickness around the implant.

Despite the body of research concerning cement mantle thickness, the thickness of this mantle varies from implant to implant (Langlais *et al.* 2003; Mellor *et al.* 2004).

Skinner *et al.* (2003) assert that a very thin, discontinuous mantle may be at least as good as a thick, continuous one. Their finding is based on the method favoured in francophone countries of cementing a canal-filling, press-fit (line-to-line reamed) prosthesis; their excellent results call into question the received wisdom surrounding prostheses with thick mantles. Langlais *et al.* (2003) suggest that this so-called 'French paradox' arises as a result of the entirely different mechanisms of load transfer and failure for the two different philosophies: direct cortical contact may enhance load transmission to the femur, keeping strains low in the cement, while very thin films of cement might be strengthened and toughened through an extrusion process as the prosthesis is inserted.

Distal centralisers

The use of a distal centraliser is known to improve alignment and reduce the incidence of thin or deficient distal regions (Berger *et al.* 1997; Breusch *et al.* 2001; Goldberg *et al.* 1998; Hanson and Walker 1995; Scheerlinck *et al.* 2006). However, some designs of centraliser may trap air as they are pushed through the cement, introducing voids (Noble *et al.* 1998). Not all centralisers are effective (Kawate *et al.* 2001).

1.4 Finite element modelling

1.4.1 What is finite element analysis?

It is often useful to understand the distribution of stress in a structure, in order to investigate if, and how, it would fail. Mathematics can be used to solve differential equations relating force, displacement, stress, and strain analytically in simple shapes. However, the complex anatomical shapes and materials commonly encountered in orthopaedics are not suited to this method.

The finite element method solves this problem by breaking down a structure into a smaller mesh of simple geometric 'elements', within each of which these differential equations can be easily solved. Elements are typically rods, plates or blocks connected together at shared 'nodes', each element having its own constitutive properties. Calculations for each element are solved iteratively until agreement is reached between adjacent elements, and until forces and displacements are globally compatible with stresses and strains. Thus, as mesh density increases, the solution approaches a true analytical solution. The accuracy of finite element analyses is often checked by increasing mesh refinement until there is no significant change in numerical results, known as convergence testing. Although the finite element method is most widely used for finding stress and strain, it is used for solving thermal, electrical, fluid mechanics, and other problems involving vector and tensor fields.

The finite element method has been used since the early 70s in orthopaedics, initially for predicting stress fields in bone, and later for investigating implant, cement and bone stresses. Initially, only coarse, one- and two-dimensional and axisymmetric models were used, with linear-elastic material properties, due to computer processing limitations. As processing power has increased, models have increased in complexity, with refined three-dimensional models, anisotropy, frictional contact, and non-linear constitutive relationships now commonplace. During the last decade, adaptive models have also been developed which incorporate growth and remodelling, tissue differentiation, and damage propagation.

A major limitation of the finite element method is the problem of validity: numerical empiricism in the selection of material properties, geometric simplification, or boundary assumptions, reduce the validity of results, limiting the relevance of many publications. For this reason, it is often considered necessary to validate a finite element model by checking all or part of the numerical results against the observed response of a physical model.

However, it is often difficult to achieve this in practice, as biological tissues are difficult to instrument and results highly variable.

The finite element method has been applied in virtually every conceivable area of orthopaedics, as well as other areas of medicine, especially where mechanical devices are implanted into human tissues.

1.4.2 Finite element modelling of hip replacement

Within orthopaedics, the hip poses a difficult biomechanical challenge: loads of several times body weight must be sustained over many years. The very earliest mathematical models in orthopaedics investigated functional loading of the femur, and modelling of the femoral construct in total hip arthroplasty in particular has sustained enormous interest over the years.

Femoral component design

Numerous and varied investigations of stem design have been conducted using finite element analysis, a few of which are outlined here. Implants with reduced bending stiffness due to material or geometry have been observed to generate more physiological stresses in the proximal medial bone, but also increased proximal cement and interfacial stresses (Yettram and Wright 1979; Crowninshield *et al.* 1980; Lewis *et al.* 1984; Fagan and Lee 1986b; Rohlmann *et al.* 1987; Prendergast *et al.* 1989; Huiskes *et al.* 1992; Cheal *et al.* 1992; Janssen *et al.* 2005a). A collar which contacts the medial calcar has been shown to both increase bone stress and reduce cement stress proximally (Crowninshield *et al.* 1980; Lewis *et al.* 1984; Fagan and Lee 1986a; Prendergast and Taylor 1990; O'Connor *et al.* 1996). Attempts have been made to mathematically optimise implant shape so as to mimimise cement or interfacial stresses (Huiskes and Boeklagen 1989; Yoon *et al.* 1989; Hedia *et al.* 1996; Katoozian and Davy 2000). Optimal distal centraliser design has also been sought, with distal truncation of the stem to accommodate a centraliser observed to adversely affect cement stress (Estok *et al.* 1997; Estok and Harris 2000; Schmolz *et al.* 2000).

Damage accumulation

Stresses in the cement mantle and at its interfaces are generally used in these studies as criteria for optimising or distinguishing between designs. Verdonschot (1995) simulated the processes of creep and damage accumulation in bone cement using continuum damage mechanics in a three-dimensional finite element model, in order to better simulate the comparative lifetimes of prostheses. Further development of this model (Stolk *et al.* 2004) has enabled the accurate prediction of crack locations and orientations around prostheses, sufficient for pre-clinical testing. Crack growth rates are generally not well predicted and are dependent on mesh density, but the use of a stress-averaging algorithm can counter these problems, allowing adjustment of crack growth rates to fit experimental data, remaining independent of mesh refinement (Stolk *et al.* 2003b).

The effect of porosity on damage accumulation has been simulated, demonstrating a less favourable and much more variable fatigue response. The accuracy of such damage simulations is improved by the inclusion of porosity (Jeffers *et al.* 2005a). However, while uniaxial tensile fatigue tests are highly sensitive to porosity, torsional implant loading is much less so, explaining the limited effect of third-generation cementing techniques on clinical outcome (Janssen *et al.* 2005c). Micro-scale finite element simulations have demonstrated that pores can slow down or speed up cracking, depending on the pore location relative to local stress intensities (Janssen *et al.* 2005b).

Debonding

The process of debonding has been modelled using both fracture mechanics approach and interfacial shear stress failure criteria, and has been observed to initiate at the proximal medial and distal regions and to progress stably along the stem until fully debonded (Verdonschot and Huiskes 1997a; Damron *et al.* 2006).

The effect of debonding on implant fixation is a contentious issue. Some authors report a significant increase in peak cement stress levels as a

result of debonding (Harrigan and Harris 1991; Verdonschot and Huiskes 1997a; Chang *et al.* 1998). In constrast, others have observed reduced tensile and shear stresses in the cement due to debonding (Wheeler *et al.* 1997; Massin *et al.* 2003), as well as more favourable stresses in the bone and at the cement-bone interface (Verdonschot and Huiskes 1996a; Massin *et al.* 2003).

A microscale finite element model of surface asperities predicts an intermediate level of surface roughness ($R_a \sim 10–20$ μm) to be the most damaging; a polished surface allows slip and minimises local cement stress, whilst a sufficiently rough surface may maintain stability, also limiting cement stress. Thus, it appears that implants should either be given a polished microstructure, minimising the transmission of shear stress, or be macroscopically profiled so as to prevent migration (Verdonschot *et al.* 1998).

Residual stress

Coupled thermal and stress analyses have demonstrated that polymerisation initiates at bone-cement interface and moves towards the prosthesis, generating residual stresses which are highly dependent on curing history. Pre-chilling the stem or cement has been shown to reduce the temperature at the cement-bone interface, but in doing so slows down polymerisation which may weaken the cement. Pre-heating the prosthesis reverses the polymerisation direction, reducing residual stress at stem-cement interface, and does not significantly raise the temperature at the cement-bone interface (Li *et al.* 2003; Li *et al.* 2004).

Finite element simulations have demonstrated the sensitivity of damage accumulation to residual stresses due to curing: these can be large enough to initiate pre-load cracking, which further accelerates fatigue damage under loading (McCormack and Prendergast 1999; Lennon and Prendergast 2002; Nuno and Avanzolini 2002).

Cement mantle thickness

Finite element stress analyses have generally shown a thicker cement mantle to be preferable, reducing stresses in the bulk cement and around voids, especially

around the prosthesis tip – whether by removing more cancellous bone or by reducing the prosthesis diameter (Lee *et al.* 1994; Estok *et al.* 1997; Powers *et al.* 1998; Schmolz *et al.* 2000; Ayers and Mann 2003).

Cyclic torsional loading of cornered implants demonstrated crack growth rates to be independent of cement thickness, thinner mantles failing first as cracks had to propagate less far. Finite element damage simulations of these tests revealed that stress intensity decreased with increasing crack length, explaining the stable crack growth rates (Hertzler *et al.* 2002).

Thermal modelling of the polymerisation process revealed that even thick mantles of up to 10 mm would not lead to thermal osteonecrosis of the femoral bone (Swenson *et al.* 1981).

Loading

Finite element simulations have shown stair climbing to be more damaging than walking, leading to greater and more widely distributed cement stress and damage (Harrigan and Harris 1991; Stolk *et al.* 2002; Kleemann *et al.* 2003). Shear stress at the cement-bone interface has been shown to depend strongly on patient activity levels (Chang *et al.* 1998).

1.5 Aims and objectives

This project is primarily concerned with causes and effects of varying cement mantle thickness around the femoral components of total hip replacements. Variation in cement mantle thickness is approached both in terms of the local thickness, determined by the position of the femoral component, and global or average thickness, determined by the relative femoral stem and broach sizes.

The effect of surgical approach to the hip on cement mantle geometry is investigated, as well as the effect of cement mantle geometry on the level of stress and damage accumulation in cement mantle and on stress shielding of the calcar femoris. Other factors, including cancellous bone density and various prosthesis design parameters are also investigated to establish how these factors influence the effects of cement thickness on cement stress and damage.

Chapter 2

Surgical approach

2.1 Introduction

2.1.1 Surgical approaches to the hip

A surgical approach to the hip was first described by Von Langenbeck in 1874, and later refined by Kocher in 1907, that exposed the joint from the posterior aspect (Gibson 1950). Watson-Jones (1936) described an anterolateral approach, Smith-Petersen (1949) an anterior approach, and McFarland and Osborne (1954) a posterolateral approach. The transtrochanteric approach (Jergensen and Abbott 1955) was advocated by Charnley (1961) for his Low Friction Arthroplasty. Lateral approaches include those proposed by Harris (1967; 1975), Bauer (1979), and Hardinge (1982). There have been many subsequent suggested modifications to all of these types of approach (Lindgren and Svenson 1988; Light and Keggi 1980; Keggi *et al.* 1993; Frndak *et al.* 1993; Pai 2002; Gammer 1985; Soni 1997; Lombardi *et al.* 2000; Hedley *et al.* 1990; Johnsson *et al.* 1981; Shaw 1991; Pellicci *et al.* 1998).

These many approaches involve different techniques and soft tissue dissections, but can broadly be divided into three categories, according to the direction from which the femoral neck is approached: the transtrochanteric approach involves removal of the greater trochanter and its musculature to enable a clear lateral view of the femoral neck, while all other approaches must bypass the gluteus medius to provide either an anterolateral or posterolateral exposure. Due to the complications associated with reattachment of bone, the transtrochanteric approach is generally used only in problematic cases such as

revisions, where unimpeded access to the proximal femur is of prime importance. The approaches most commonly used today are variations on the transgluteal (anterolateral) and posterior approaches.

Figure 2.1. Transverse section of the hip indicating the soft tissue dissection paths of common anterior (A), anterolateral/transgluteal (B), and posterolateral (C) approaches to the hip. The iliopsoas (1), sartorius (2), rectus femoris (3), tensor fasciae latae (4), gluteus medius (5), gluteus maximus (6), pelvitrochanteric muscles (7) are shown. Adapted from Nazarian *et al.* (1987).

2.1.2 Factors influencing choice of approach to the hip

The relative merits of these different approaches are a matter of some contention. Many studies have compared approaches with respect to a number of intra- and post-operative variables.

Dislocation

The posterior approach has long been associated with an increased risk of postoperative dislocation, with dislocation rates of 2–9% reported (Berry *et al.* 2005; Grossmann *et al.* 1994; Hedlundh *et al.* 1995; Kwon *et al.* 2006; Masonis and Bourne 2002; Pascarel *et al.* 1989; Ritter *et al.* 2001; Vicar and Coleman 1984; Zimmerma *et al.* 2002); this is the most frequently cited reason for avoidance of the posterior approach. However, enhanced soft tissue repair

to stabilise the joint redresses this balance, reducing dislocation rates to around 1% or less (Dixon *et al.* 2004; Kwon *et al.* 2006; Pellicci *et al.* 1998; Suh *et al.* 2004; van Stralen *et al.* 2003; Weeden *et al.* 2003); this is comparable with other approaches. The posterior approach may increase the sensitivity of dislocation risk to surgical experience (Hedlundh *et al.* 1995), although this finding is contested (van Stralen *et al.* 2003).

Nerve damage

Damage to the superior gluteal nerve is a particular cause of concern with the lateral and anterolateral approaches (Bos *et al.* 1994; Picado *et al.* 2006; van der Linde and Tonino 1997), where the risk is greater than with the posterior approach (Jolles and Bogoch 2004).

Heterotrophic bone

There is no consensus on effect of surgical approach on heterotrophic bone formation; results are conflicting and studies have small numbers of patients (Barber *et al.* 1996; Bischoff *et al.* 1994; Vicar and Coleman 1984).

Gait and function

Some authors report no difference between approaches in terms of limp, abductor strength, trendelenburg test, range of motion, or Harris Hip Score (Barber *et al.* 1996; Downing *et al.* 2001; Jolles and Bogoch 2004), whilst others report more normal gait, improved function and abductor strength, less pain, and faster return to function with the posterior approach (Gore *et al.* 1982; Roberts *et al.* 1984; Pascarel *et al.* 1989; Masonis and Bourne 2002; Zimmerma *et al.* 2002; Madsen *et al.* 2004).

Intra-operative factors

Compared to other approaches, the posterior approach takes half the operative time and reduces blood loss (Hovelius *et al.* 1977; Patiala *et al.* 1984; Roberts *et al.* 1984).

Alignment, subsidence and the cement mantle

Very few studies have looked at positioning of the stem within the cement mantle or subsidence. No difference has been observed in initial stem position or subsidence, although greater internal rotation of the stem may occur with posterior approach (Glyn-Jones *et al.* 2006; Jolles and Bogoch 2004). Conversely, the posterior approach has been associated with better anatomical positioning of the implant (Gore *et al.* 1982). No difference has been observed between approaches in terms of the acetabular or medial calcar cement mantle thicknesses; other regions of the femoral cement mantle were not investigated (Vicar and Coleman 1984).

2.1.3 Aseptic loosening and the femoral cement mantle

Aseptic loosening is the most frequent long-term complication of total hip arthroplasty, accounting for over 75% of all revision operations (Herberts *et al.* 2005). The cement mantle is widely regarded as the 'weak link' in the femoral prosthesis-bone construct, requiring careful quality control by the surgeon. A number of studies have demonstrated the importance of cement mantle thickness and continuity in preventing mechanical loosening (Bragdon *et al.* 1995; Kawate *et al.* 1998; Star *et al.* 1994).

The Swedish Hip Arthroplasty Register is to our knowledge the only study to have investigated the effect of surgical approach on risk of revision:

"The analysis shows a significantly lower risk for revision for the posterior incision (lateral position) and the lateral incision with trochanteric osteotomy than the transgluteal (lateral or supine position). The reason for this finding is not associated to certain implants, and in the analysis only includes cemented implants. We have no explanation for this observation." (Malchau and Herberts 1998)

A link between surgical approach and the quality of the cement mantle would offer an explanation for this finding.

2.1.4 Objective

The purpose of this study was to determine whether the surgical approach used to perform total hip arthroplasty affects the quality of the femoral cement mantle, in terms of thickness and continuity, around Stanmore Hip replacements.

2.2 Materials and methods

2.2.1 Patient selection

Over 400 cases of primary Stanmore total hip arthroplasty performed over a fifteen-year period at the Royal National Orthopaedic Hospital, Stanmore, were identified using administrative and theatre records. Cases were selected for this study if they met all of the following inclusion criteria:

1. Primary total hip arthroplasty, using the Stanmore femoral implant;
2. High quality postoperative anteroposterior and lateral radiographs;
3. Documentation of the operative procedure and surgical approach used.

During this period, only 90 operations had been performed using the posterior approach, reflecting surgical preferences. Fifty cases met the inclusion criteria. These cases were under the care of eight surgical teams. Anterolateral cases were selected from the same eight teams to minimise inter-surgeon variability between the two groups. As the transgluteal approach has been modified over time, the most recent 50 cases that met the inclusion criteria were used.

2.2.2 Measurement and analysis

The notes were analysed to record the date of surgery, the principal diagnosis, the side, the components used and the grade of operating surgeon. One orthopaedic surgeon analysed all radiographs, as poor inter-observer agreement during radiographic assessment of a cement mantle has been demonstrated (McCaskie *et al.* 1996). In order to eliminate bias, the radiographs of all 100

cases from both groups were pooled randomly, blinding the investigator to the surgical approach used.

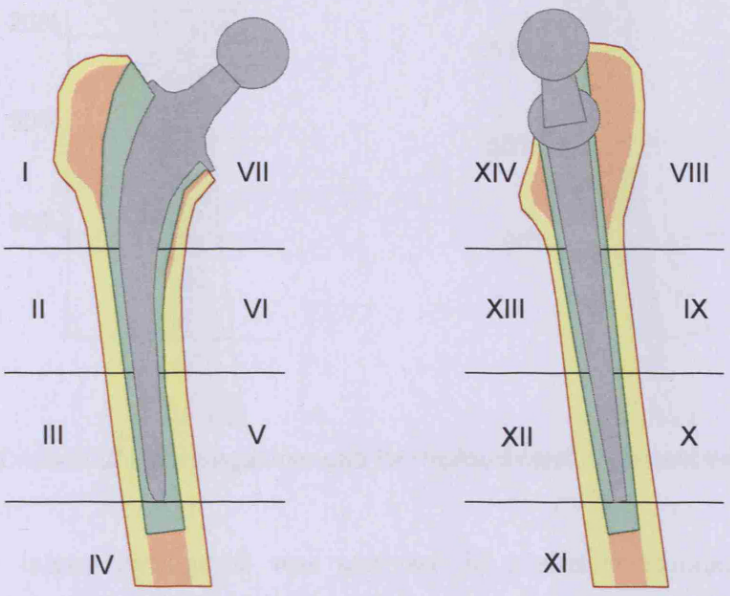

Figure 2.2. Zones defined for radiographic analysis by Gruen (left) and Johnston (right).

The cement mantle around the femoral stem was analysed on the anteroposterior radiograph using the seven radiographic zones described by Gruen (1979), as shown in **Figure 2.2**. The number of defects in each zone was recorded. Defects were defined as regions which appeared to have no cement mantle on the radiograph, either because the stem appeared to be in direct contact with bone or because the cement appeared discontinuous. The stem length was measured from the lateral stem-collar junction to the stem tip on the AP film and measurement lines plotted perpendicular to the axis at 25%, 50%, and 80% of the stem length, as shown in **Figure 2.3**. Cement mantle thickness could thus be measured at reproducible points within each Gruen zone. Due to the difficulties in separating cement from cortical bone and in establishing precise boundaries around cement mantles with rough or blurry edges, measurements were taken to the nearest millimetre.

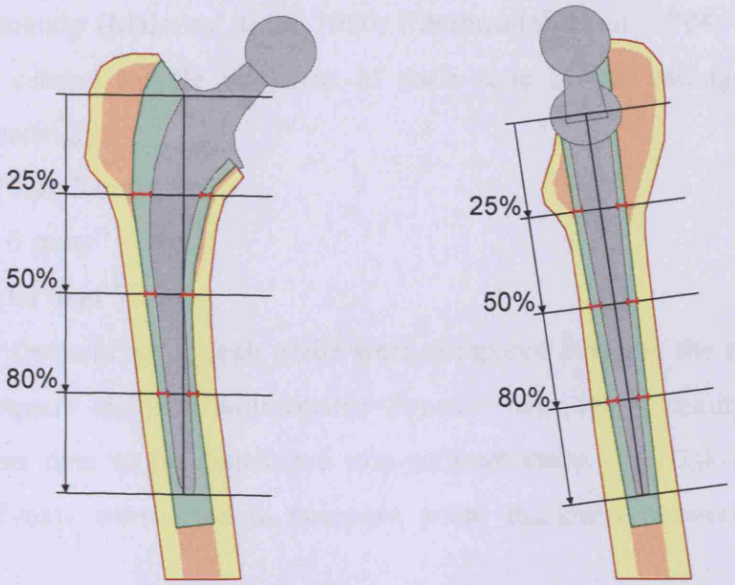

Figure 2.3. Division of stem length into grid for measurement of cement thickness.

The lateral radiograph was analysed in a similar manner, with the cement mantle delineated into the additional seven zones (VIII–XIV) originally described by Johnston (1990); see **Figure 2.2**. The approximate centre of the collar and the distal tip were used as the reference points for the fixed line on these views.

Zones IV and XI, which represent the cement mantle beneath the tip of the stem, were excluded from the study, as the standard use of cement restrictors has ensured that there is always a substantial thickness of cement in this area. It was apparent from an early stage in the study that incorporating these zones would confound the results, and that they would have to be excluded from analysis.

The frequency of cement mantle defects between the two groups was compared using the Chi-square test. Chi-square tests were also used to determine whether the primary diagnosis, grade of surgeon, or side of operation affected the incidence of defects, both within each group and collectively.

Several previous studies have suggested that a femoral cement mantle thickness of 2–5 mm has a better outcome than stems implanted with a thicker

or thinner mantle (Maloney *et al.* 1990; Ebramzadeh *et al.* 1994; Star *et al.* 1994); the cement mantle thickness of each zone on the radiographs was graded accordingly:

(*a*) less than 2 mm;

(*b*) 2 to 5 mm;

(*c*) greater than 5 mm.

The frequencies of each grade were compared between the two groups using Chi-square analysis. Kolmogorov-Smirnov tests for normality revealed the thickness data to be distributed non-parametrically ($p < 0.001$). Mann-Whitney U-tests were used to compare zonal thickness between the two groups.

2.3 Results

2.3.1 Demographics

The anterior group comprised 50 arthroplasties performed between 1995 and 2003, in 44 patients. Nineteen patients were male and 25 female, with an age range of 44 to 88 years. The principal diagnoses were osteoarthritis in 40 cases, avascular necrosis in six cases, and one case each of pathological fracture, rheumatoid arthritis, chondrolysis, and osteomalacia.

The posterior group comprised 50 arthroplasties performed between 1990 and 2003, in 46 patients. Fifteen patients were male and 31 female, with an age range of 37 to 91 years. The principal diagnoses were osteoarthritis in 47 cases, and one case each of central dislocation, epiphyseal displasia, and rheumatoid arthritis.

Table 2.1 shows the distribution of side, grade of operating surgeon and defective cement mantles observed in each group.

Table 2.1. Distribution of defects by grade of operating surgeon, side and approach.

Surgical approach	Grade of surgeon			Defective mantle		Total
				Complete	Defective	
Anterior	SpR	Side	Left	11	3	14
			Right	8	3	11
		Total		19	6	25
	Consultant	Side	Left	11	2	13
			Right	6	6	12
		Total		17	8	25
Posterior	SpR	Side	Left	13		13
			Right	6	1	7
		Total		19	1	20
	Consultant	Side	Left	12	2	14
			Right	15	1	16
		Total		27	3	30

2.3.2 Cement mantle defects

Fourteen cases (28%) had defects in the anterior group, while 4 cases (8%) had defects in the posterior group ($p < 0.01$). Twenty-eight radiographic zones (4.7%) had defects in the anterior group, while 6 zones (1.0%) had defects in the posterior group ($p < 0.001$), as shown in **Figure 2.4**. Four zones accounted for 82% of all defects in the anterolateral group (see **Figure 2.5**). Defects in zones I and VIII were exclusively associated with defects in zone V and XII respectively. Although 54% of stems in the anterolateral group were implanted on the left side, they accounted for only 25% of the defects, suggesting that a disproportionately high number of defects occurred on the right side. A chi-square test indicated that this was significant ($p < 0.005$). There was no significant effect of primary diagnosis or grade of operating surgeon either within groups or in general, and no significant effect of operated side in the posterior group.

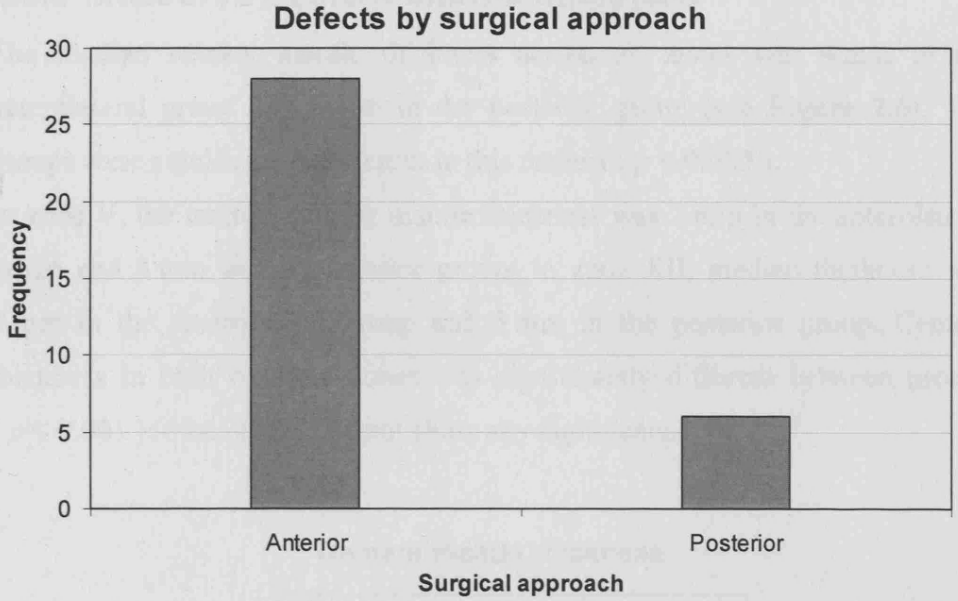

Figure 2.4. Total number of defective zones observed within each group. The posterior approach is associated with significantly fewer defects ($p < 0.001$).

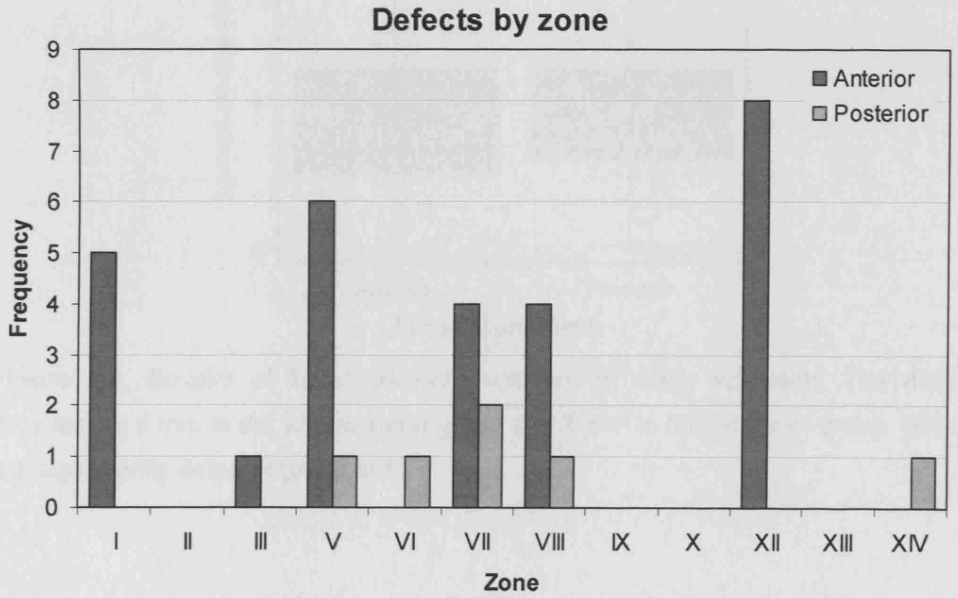

Figure 2.5. Graph showing the frequency of defects in each radiographic zone. Defects in the anterolateral group are primarily found in zones I, V, VIII and XII.

2.3.3 Measured cement mantle thickness

The median cement mantle thickness across all zones was 4 mm in the anterolateral group and 5 mm in the posterior group (see **Figure 2.6**). The groups were significantly different in this respect ($p < 0.005$).

In zone V, the median cement mantle thickness was 2 mm in the anterolateral group and 3 mm in the posterior group; in zone XII, median thickness was 3 mm in the anterolateral group and 5 mm in the posterior group. Cement thickness in each of these zones was significantly different between groups ($p < 0.001$); other zones did not show any significance.

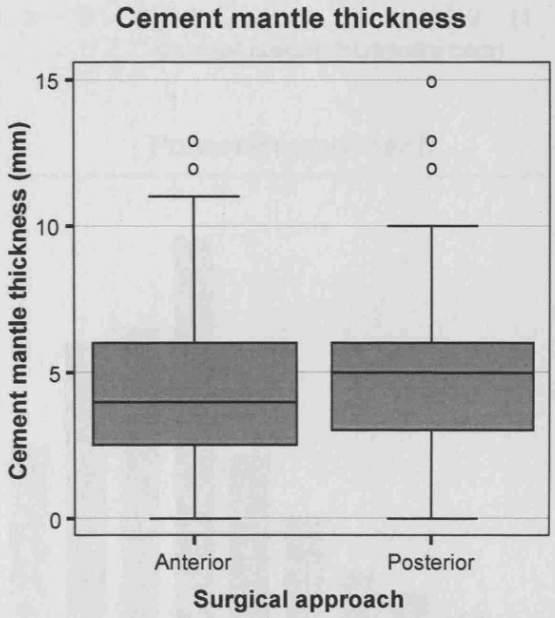

Figure 2.6. Boxplot of zonal cement thickness for each approach. The median thickness is 4 mm in the anterolateral group and 5 mm in the posterior group. Groups are significantly different ($p < 0.005$).

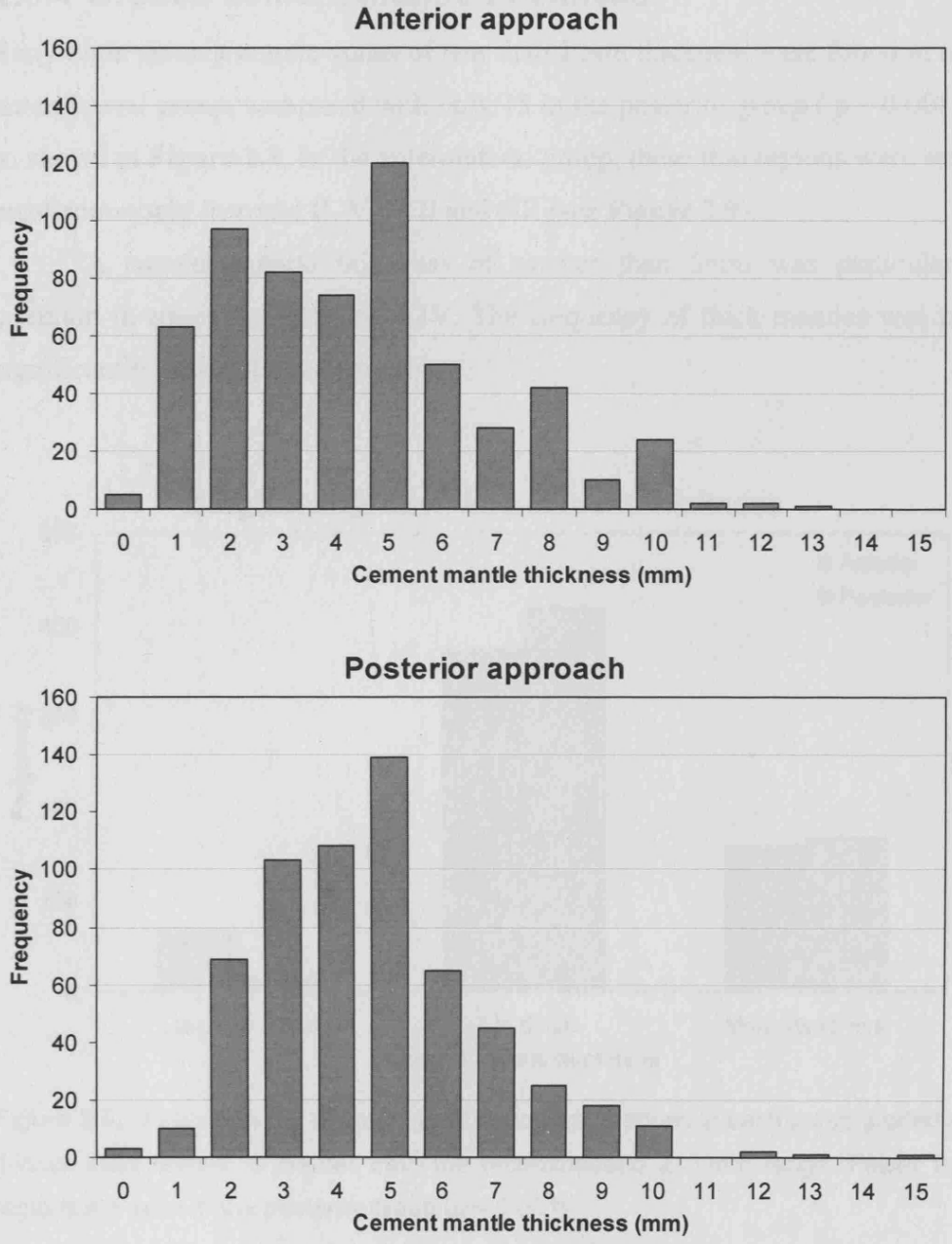

Figure 2.7. Zonal cement mantle thickness frequency distributions for each approach.

2.3.4 Graded cement mantle thickness

Sixty-eight cement mantle zones of less than 2 mm thickness were found in the anterolateral group, compared with only 15 in the posterior group ($p < 0.001$), as shown in **Figure 2.8**. In the anterolateral group, these thin regions were seen most commonly in zones II, V, VIII and XII (see **Figure 2.9**).

A cement mantle thickness of greater than 5mm was particularly common in zones X, XIII, and XIV. The frequency of thick mantles was not significantly different between groups.

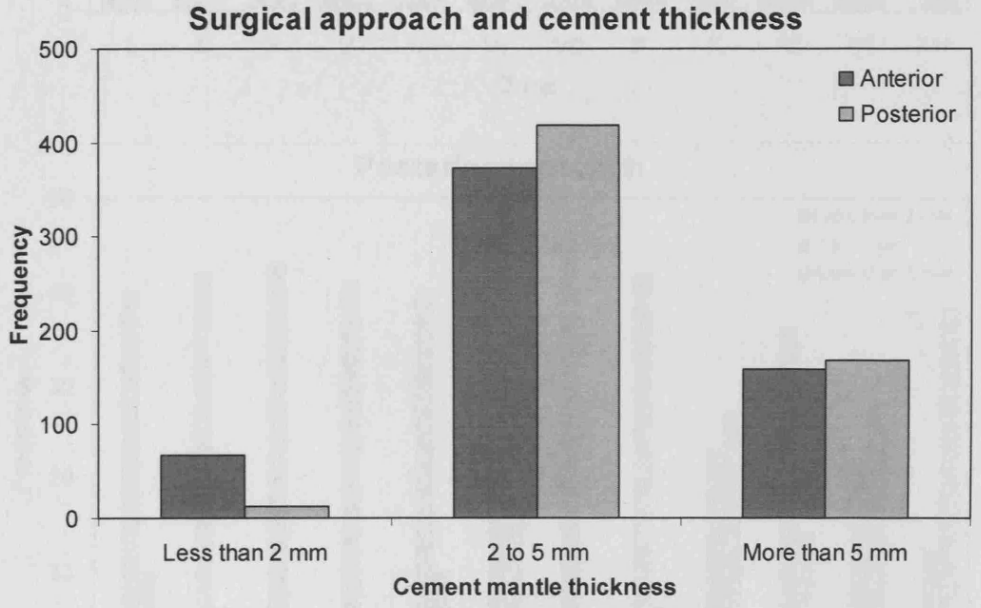

Figure 2.8. Graph showing the number of radiographic zones in each group graded as thinner than, within, or thicker than the recommended 2–5 mm range. Fewer thin regions are seen in the posterior group ($p < 0.001$).

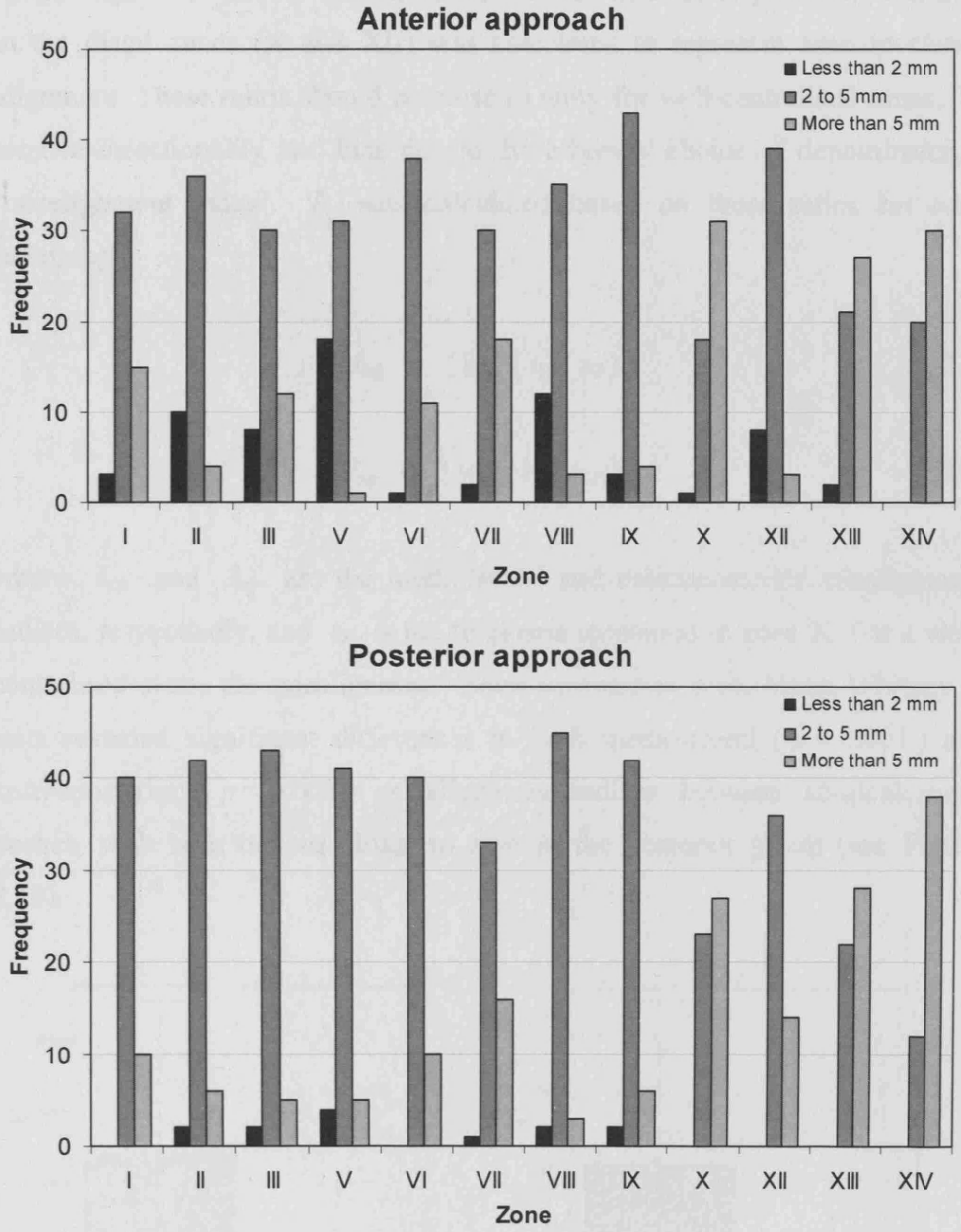

Figure 2.9. Graphs showing cement mantle thickness graded by zone as thinner than, within, or thicker than the recommended 2–5 mm range.

2.3.5 Centralisation

The ratio of lateral to medial thickness measured in the distal zones (III and V) was calculated for each cement mantle, as a measure of the degree of

varus/valgus orientation. Similarly, the ratio of anterior to posterior thickness in the distal zones (X and XII) was calculated to represent anteroposterior alignment. These ratios should be close to unity for well-centralised stems. To remove directionality and bias due to the arbitrary choice of denominator, a 'misalignment index' I was calculated based on these ratios for each radiograph:

$$I_{ml} = |\log(t_{III}/t_V)| \quad (2.1)$$

$$I_{ap} = |\log(t_X/t_{XII})| \quad (2.2)$$

where I_{ml} and I_{ap} are the mediolateral and anteroposterior misalignment indices, respectively, and t_X is the thickness measured in zone X. For a well-centralised stem, the misalignment index approaches zero. Mann-Whitney U tests revealed significant differences in both mediolateral ($p < 0.001$) and anteroposterior ($p < 0.001$) misalignment indices between surgical appr-oaches, with both indices closer to zero in the posterior group (see **Figure 2.10**).

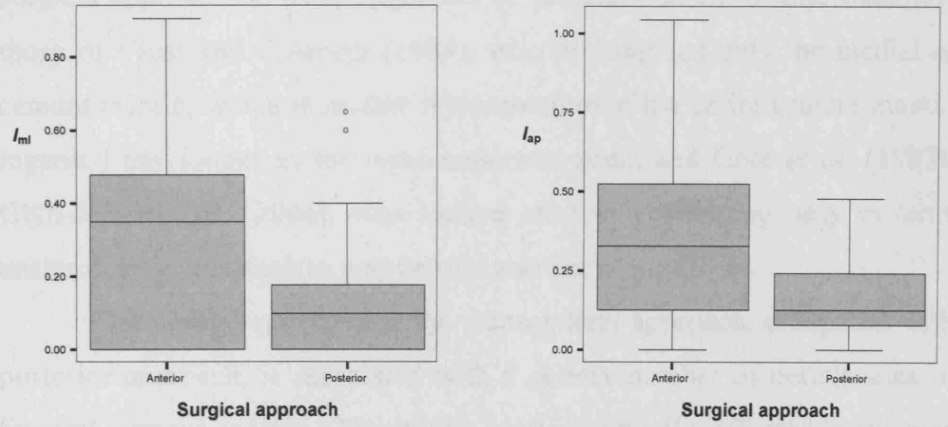

Figure 2.10. Box plots of mediolateral (left) and anteroposterior (right) misalignment indices, as explained in equations (2.1) and (2.2). In both cases, the posterior group has a median value closer to zero ($p < 0.001$), indicating better centralisation.

2.4 Discussion

It is widely accepted that both the anterolateral and posterior approaches provide good exposure of the acetabulum and proximal femur. Much work has been performed on the merits and shortcomings of the various surgical approaches to the hip. As explained earlier, there is an increased risk of dislocation with the posterior approach, which can be avoided through enhanced soft tissue repair; there are increased risks of nerve damage, inferior gait and abductor strength, and less anatomic implant positioning associated with anterolateral approaches. Importantly, the risk of revision due to aseptic loosening is lower with the posterior approach.

The importance of the cement mantle in the initiation of aseptic loosening is well documented, and several studies, cadaveric and clinical, have shown that poor cementation is a significant predictor of aseptic loosening (Star *et al.* 1994; Bragdon *et al.* 1995; Kawate *et al.* 1998). Cement mantle fractures are believed to cause osteolysis and the formation of granulomas, with passage of wear particles from the metal-cement interface to the bone-cement interface (Jasty *et al.* 1991).

To our knowledge, the only studies to have investigated the effect of surgical approach on stem alignment or femoral cement mantle thickness are those of Vicar and Coleman (1984), who investigated only the medial calcar cement mantle, which is neither representative of the entire cement mantle nor regarded any longer as the most important zone; and Gore *et al.* (1982) and Glyn-Jones *et al.* (2006), who looked at stem positioning only in terms of anatomical factors such as anteversion and neck length.

Our study suggests that the anterolateral approach, compared with the posterior approach, is associated with a greater number of deficiencies in the femoral cement mantle. The zones most commonly affected were zone V (often in association with zone I), and zone XII (often associated with zone VIII); the pattern of these deficiencies suggests that the anterolateral approach

results in an increased prevalence of valgus and posterior tilted (i.e. 'front-to-back') stem positioning within the reamed canal, as shown in **Figure 2.11**.

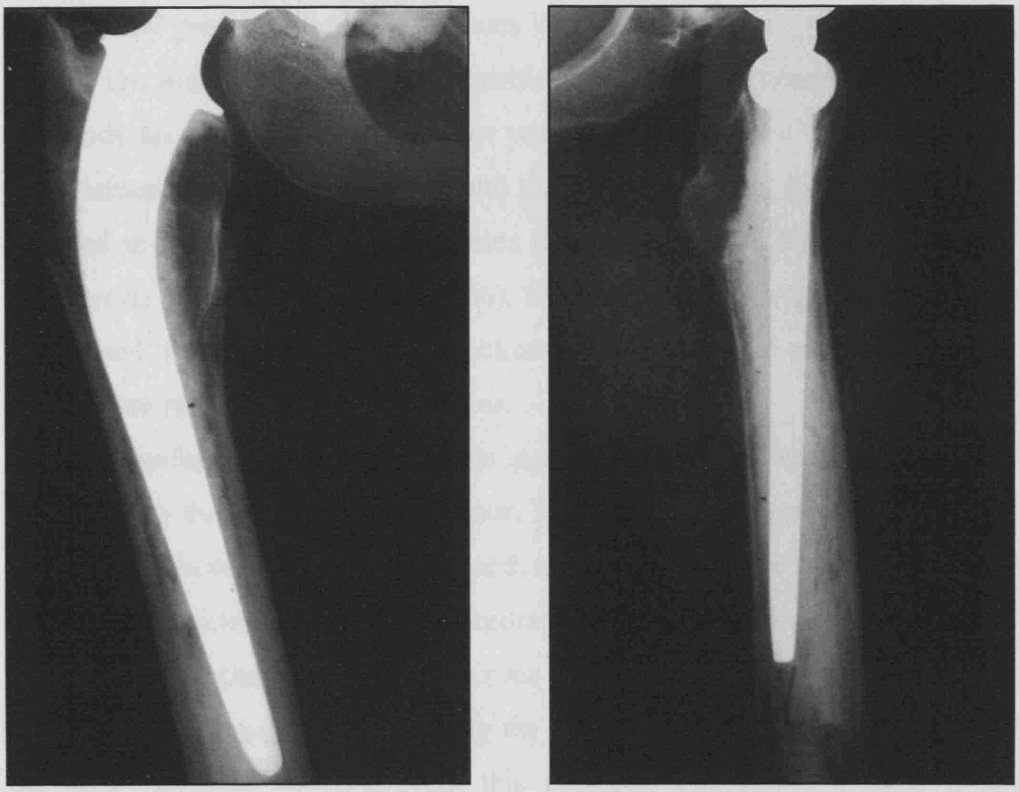

Figure 2.11. Anteroposterior (left) and lateral (right) radiographs showing valgus and posterior tilted stem positioning.

There is an increasing trend to perform only an AP radiograph post surgery; over 50% of patients had to be excluded from the study as a lateral radiograph had never been performed. Forty percent of the defects in this study were found in the lateral radiographs, emphasising the need for good quality postoperative lateral radiographs.

The five stems which had defects in both zone I and V were all inserted on the right side, and stems inserted on the right side had significantly more defects. A possible explanation for this finding is that the natural arc of movement of the surgeon's arm as they broach and rasp the femoral canal, and then insert the prosthesis, may lead to valgus positioning of the stem.

The posterior surgical approach allows a more uniform cement mantle to be produced around the femoral stem. The frequency of 'thin' areas within the cement mantle (less than 2 mm thick) was significantly greater in the anterolateral group, particularly in zones V and XII.

The high frequency of thin mantles and defects in zones V and XII in this study are of particular importance with respect to aseptic loosening. It has been demonstrated, both clinically and experimentally, that loosening may be initiated in these highly-stressed zones (Star *et al.* 1994; Ritter *et al.* 1999; Kwak *et al.* 1979; Caruana *et al.* 2006). Estok *et al.* (1997) suggest that a well-centralised stem with a mantle thickness of at least 2.5 mm near the tip experiences much lower cement strains.

Crawford *et al.* (1999) have ascribed problems with neutral stem placement to the anatomy of the femur. The true medullary axes of the femur and of the femoral neck are not aligned, as shown in **Figure 2.12**. This means that a stem inserted central to the femoral neck will tend to come into contact proximally with the anterior cortex (zone VIII), due to its natural concavity in this region. They suggest that placing the stem more posteriorly at the level of the neck resection would prevent this problem. The abductor mass in an anterolateral approach is difficult to retract away, making access to this site difficult. Furthermore, Gore *et al.* (1982) report that the anteversion necessary for anatomical stem positioning is best achieved via a posterior approach; insufficient anteversion associated with an anterolateral approach would compound this problem, as indicated in **Figure 2.12**.

The results from our study support Crawford's theory, as defects in zones VIII and XII were significantly more frequent in the anterolateral group. If an anterolateral approach is used, the attachment of the gluteus medius to the proximal femur would also interfere with broaching the femoral canal laterally and rasping against the lateral wall. This would account for the increased prevalence of valgus tilting of the femoral stems seen in our study.

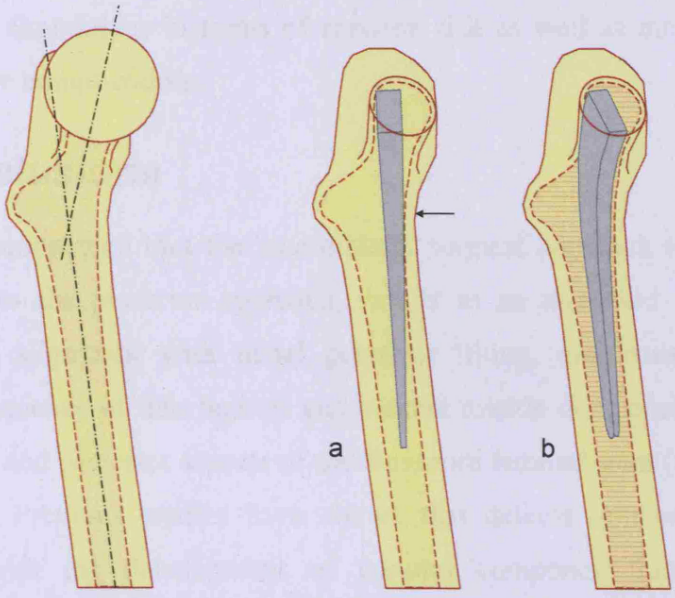

Figure 2.12. Schematic of the medial aspect of the proximal femur, showing the internal surfaces of the cortex in the neck and shaft (left). The axes of the neck and medullary canal are angled. This means that the stem is likely to contact the cortex antero-proximally (a), unless sufficient anteversion is achieved (b).

Improved centralisation of the distal femoral stem can optimise the distal cement mantle thickness, potentially reducing the risk of mechanical loosening (Egund *et al.* 1990; Berger *et al.* 1997). Our results show better distal centralisation in stems inserted using a posterior approach. We advise that effective centralising devices be used with all femoral components inserted via an anterolateral surgical approach, to overcome the tendency for stem misalignment and cement mantle deficiencies.

It would not be appropriate to advise all surgeons to immediately adopt the posterior surgical approach; there is a learning curve associated with any newly-adopted technique, and there is strong evidence to suggest that, in general, surgical experience critically affects the clinical outcome of hip arthroplasty (Katz *et al.* 2001; Fender *et al.* 2003). However, if the higher dislocation risk associated with the posterior approach is addressed by the use of enhanced soft tissue closure techniques, this approach appears preferable to

anterolateral alternatives in terms of revision risk as well as most intra- and post-operative complications.

2.5 Conclusions

We have demonstrated that the anterolateral surgical approach to the hip, in comparison to the posterior approach, results in an increased incidence of valgus stem alignment with distal posterior tilting, and consequently an increased frequency of thin regions and cement mantle deficiencies along the distal medial and posterior aspects of the Stanmore femoral stem (Gruen Zones V and XII). Previous studies have shown that defects in these zones are associated with the development of femoral component loosening. The posterior approach is thus preferable, providing a greater likelihood of achieving a thick, continuous cement mantle and hence a reduced risk of revision.

Surgeons should be aware of this potential hazard of the anterolateral approach, so that active effort can be made to avoid suboptimal positioning of the femoral component and a defective cement mantle. The gluteus medius needs to be adequately released and retracted, to allow adequate lateral broaching and posterior placement of the stem at the level of the neck cut. An effective distal centraliser may also help avoid these problems, thereby reducing the potential for mechanical loosening and subsequent failure.

Given that the anterolateral approach is widely used, it is apparent that thin cement mantles and defects may occur frequently. The remainder of this thesis will investigate the effects of cement mantle thickness around the Stanmore Hip.

Chapter 3

Stress analysis

3.1 Introduction

3.1.1 Cement mantle thickness

The thickness of the femoral cement mantle is widely considered to be a critical factor in determining the outcome of total hip arthroplasty. Thin cement regions have been frequently observed to increase the incidence of osteolytic bone loss (Joshi *et al.* 1998; Kawate *et al.* 1999; Maloney *et al.* 1990) and aseptic loosening (Massoud *et al.* 1997; Mulroy *et al.* 1995; Ebramzadeh *et al.* 1994; Malik *et al.* 2005; Ritter *et al.* 1999; Star *et al.* 1994).

It is also well known that cement mantle thickness affects the level of stress or strain in the cement, a thicker mantle providing a reduction in peak stress (Estok *et al.* 1997; Fisher *et al.* 1997; Kwak *et al.* 1979; Lee *et al.* 1993; Lee *et al.* 1994; Schmolz *et al.* 2000). Crack growth rates in the cement are highly stress-dependent.

Using a centraliser can improve the uniformity of the cement mantle thickness. However, the overall thickness of the cement mantle must be controlled through choice of either broach size or stem size. The broaches provided for use with each stem design are generally intended to provide a constant thickness of cement around a given size of stem. This thickness varies substantially between different stem designs (Mellor *et al.* 2004), and according to the preferences of surgeons in different countries (Langlais *et al.* 2003). This phenomenon is exemplified by the Stanmore Hip, which is provided with two different-sized sets of rasps (a UK-designed set in Europe

and a US-designed set in the Americas), to suit the different preferences of surgeons on either side of the Atlantic. For a given size of femoral stem, the US rasp is broader by around 3 mm, so as to create a thicker cement mantle.

Previous clinical studies have generally focused on outcome in relation to locally-measured cement thickness from radiographs or sectioned retrievals, while experimental studies have sought to vary the gross cement mantle thickness by changing the stem size. To the author's knowledge, no investigation of the effect of broach size on cement mantle geometry and cement stress has been made. This is likely to differ substantially from the effect of stem size, since variation of rasp size would leave the bending stiffness of the stem unchanged, and the shape of the cement mantle would be partially dependent on the anatomic geometry of the medullary canal, regardless of selected rasp size.

3.1.2 Bone density

Finite element analysis in orthopaedics is often conducted using a standardised or 'average' patient data set. For example, the hip is frequently modelled using a standardised geometry and material properties, consistent with synthetic bone analogues used in biomechanical testing. This setup should eliminate the experimental variability associated with the different geometry and density of bone between patients and over time, and should allow comparison both with experimental results and between FE studies (Viceconti *et al.* 1996; Huiskes and Vroemen 1986).

However, these idealised models are representative of only a small subset of patients with 'average' bone geometry and properties. It is rare for researchers to assess the validity of their conclusions for a wider range of patients. Several studies have reported significant changes in the levels of micromotion and stresses or strains in the bone, prosthesis, cement, and at the cement-bone interface, when the elastic modulus of cancellous bone is varied around both cemented and cementless femoral components (Wong *et al.* 2005; Brown *et al.* 1988; Taylor *et al.* 1995).

3.1.3 Objectives

The aims of the study reported in this chapter were to investigate:

(1) the effect of rasp size on cement geometry around a cemented femoral component;

(2) the effects of a clinically realistic variation in cement mantle thickness, due to the use of two different broach sizes, on stresses in the cement mantle and cortical bone;

(3) the extent to which these effects are influenced by patient bone density;

(4) whether a more sophisticated model than linear-elastic stress analysis is needed to facilitate choice between rasp sizes.

3.1.4 Hypotheses

(1) The US and European femoral rasps provided for use with the Stanmore Hip produce different cement mantle geometries, with the larger US rasp allowing a thicker mantle.

(2) The larger US rasp leads to a cement mantle with reduced levels of cement stress, indicating lower rates of cement damage.

(3) The larger US rasp generates a cement mantle which imparts higher stress levels to the femoral cortex, indicating lower rates of bone resorption due to stress shielding.

(4) Variation of cancellous bone density will affect stress levels in the cement and cortical bone, but will not change which rasp size performs better in terms of cement and bone stress.

(5) A linear-elastic analysis of cement and bone stress allows adequate comparison of rasp sizes.

3.2 Materials and methods

3.2.1 Preparation of femurs

A pair of fresh-frozen adult femurs from the same donor was stripped of soft tissue and preserved in formal saline. The femurs were radiographed

anteroposteriorly and the required implant sizes chosen using the Stanmore Hip surgical templates. Size-3 standard-shaped implants were selected. Both femurs were prepared using the standard surgical procedure for the Stanmore Hip system, using surgical rasps in ascending order of size, with the shape of the medullary cavity controlled by the choice of final rasp size. For one femur, the UK-designed rasp set was used, and for the other, the larger, US-designed rasp set, in both cases finishing with the size-3 rasp from each set (**Figure 3.1**).

3.2.2 Insertion of femoral components

To enable CT scanning of the implanted femurs without radiographic artefacts, replica Stanmore Hip femoral components were used. The implants were fabricated from polyurethane resin (Easyflo 60, Polytek Development Corp., Easton, Philadelphia) poured into a silicone rubber casting of a standard size-3 Stanmore Hip femoral component (see **Figure 3.2**).

Both femurs were cleaned using pulsatile lavage and dried with surgical swabs. Vacuum-mixed Palacos-R bone cement was injected under pressure into the medullary canal of each femur using an Optivac cement mixing gun (Biomet, Inc., Warsaw, Indiana) in a retrograde fashion. The plastic replica femoral components were then inserted with distal centralisers and held in place until curing was complete. Both preparation of the femurs and stem insertion were performed by an experienced trainee orthopaedic surgeon.

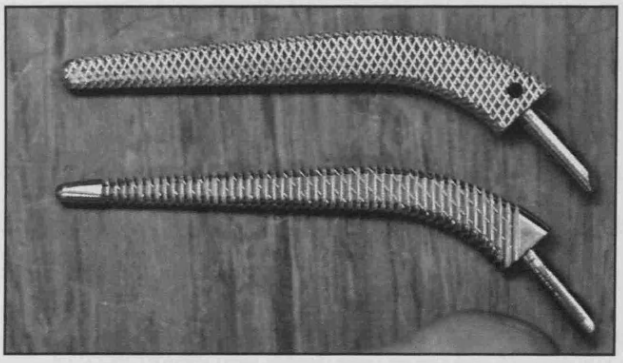

Figure 3.1. Thick/US (top) and thin/UK Stanmore Hip rasps for use with standard size-3 stem.

Figure 3.2. Replica Stanmore Hip stems cast in polyurethane resin.

Anterior-posterior and lateral radiographs were then taken to ensure that the cement mantles were complete and that they resembled those commonly observed in postoperative clinical radiographs.

3.2.3 Scanning and geometric modelling

Axial serial CT scans were taken of both femurs with slices 1 mm apart and a resolution of 0.3 mm. These were imported into Mimics (Materialise, Leuven, Belgium) software for conversion into surface data using a thresholding method. Regions of cortical and cancellous bone, prosthesis and bone cement were isolated and exported as stereolithography (.stl) curve files. These were imported into the MSC.Mentat finite element pre-processing environment.

On the CT scans, it was difficult to distinguish cortical bone from cement and pure cement from regions where the cement was interdigitated with cancellous bone, causing concern over the accuracy of the thresholded geometric models. For this reason, the femurs were then sectioned at 5 mm intervals using a water-cooled, diamond-coated saw (Exakt Vertriebs GmbH, Norderstedt, Germany) and surface images and contact radiographs taken. These images and radiographs were analysed using KS300 image analysis

software (Carl Zeiss AG, Oberkochen, Germany), and the coordinates of cement surfaces and interdigitation measured and recorded for alternate sections at eight 45-degree intervals about the centre of the prosthesis, as shown in **Figure 3.3**.

These coordinates were input into the MSC.Mentat environment, forming a three-dimensional data set. This consisted of three coplanar rings of eight points representing the outer limits of the stem, cement and interdigitation, occurring at 10 mm intervals in the axial direction. Points from the radiographs were assumed to be mid-section measurements and were therefore axially offset by 2.5 mm relative to the points from surface images.

The radiographic and surface image data showed good registration. Aligning these with the CT scan curves also revealed good agreement for all interfaces except for that separating pure cement from interdigitated regions. It was decided that the higher resolution CT scan curves be used to guide all finite element mesh construction except for the cement-bone interfaces, which were fitted to the surface image and contact radiograph points.

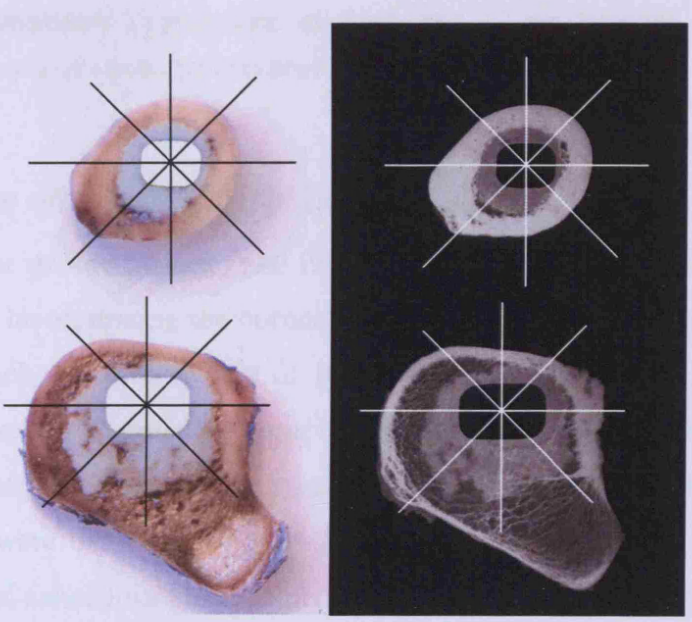

Figure 3.3. Images and contact radiographs of two sections from the thick/US cement mantle, showing the radial lines along which measurements were made.

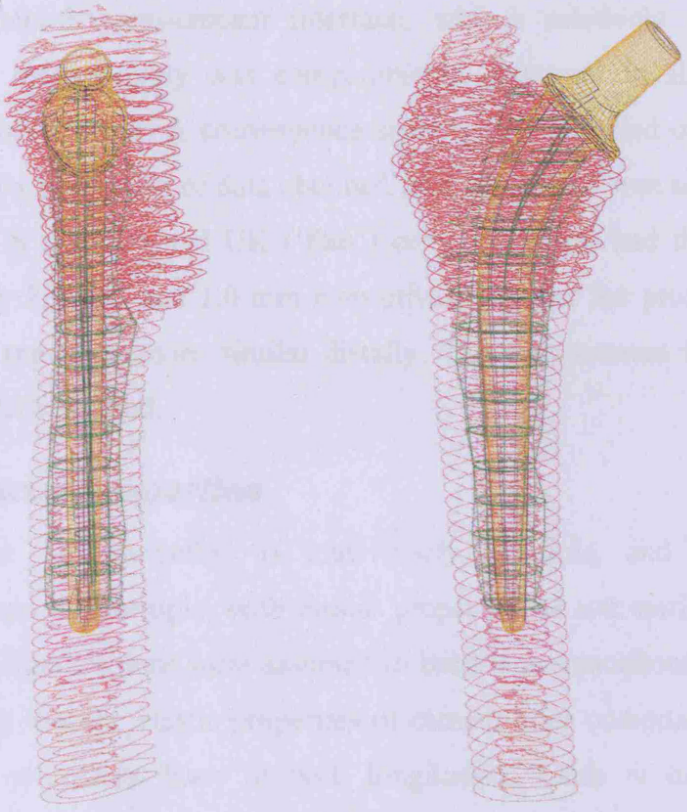

Figure 3.4. Plots of interface coordinates for the thin/UK mantle, showing CT scan (pink) and radiographic (green) data at 3 mm and 10 mm intervals, respectively. Stanmore Hip surface model (yellow) provided by Biomet.

3.2.4 Finite element model construction

Based on these geometric data, two finite element meshes were constructed in MSC.Mentat, incorporating the cortical and cancellous bone, bone cement and prosthesis. Each model consisted of 10,300 eight-noded brick elements, with elements in the femur radiating from the central prosthesis to provide a mesh that was finest at the stem-cement interface. Element edge length ranges for both models were 0.4–16.6 mm, 0.7–29.0 mm, 0.2–10.4 mm and 0.1–5.9 mm for cortical and cancellous bone, cement and prosthesis, respectively.

Choice of mesh density is always a compromise between computational expense and numerical accuracy. Element sizes were chosen to give a

reasonably smooth stem-cement interface, with a relatively coarse outer surface. The mesh density was comparable to that used in similar, recent studies by other authors. A convergence study was not carried out due to the limitation of the resolution of data obtained from alternate 5 mm sections.

The US ('thick') and UK ('thin') cement mantles had thicknesses of approximately 2.5 mm and 1.0 mm respectively, around the proximal half of the implant, and were more similar distally. The stem-cement interface was modelled as fully bonded.

3.2.5 Material properties

Cortical bone was modelled as transversely isotropic, and cortical and cancellous bone as isotropic, with elastic properties as summarised in **Table 3.1**. Interdigitated regions were assumed to behave as cancellous bone, based on the finding that the elastic properties of cement-bone composites are close to those of cancellous bone in both longitudinal (Jofe *et al.* 1991) and transverse (Williams and Johnson 1989) directions.

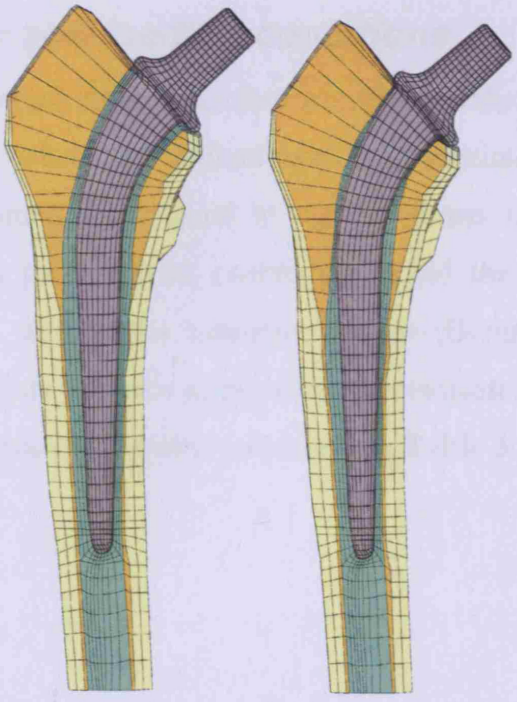

Figure 3.5. The two meshes created, with thick/US (left) and thin/UK mantles.

Table 3.1. Elastic properties assigned to materials in the finite element models

Material	Elastic modulus (GPa)	Poisson's ratio
CoCr stem	$E = 220$	$v = 0.3$
Palacos-R cement	$E = 2.7$	$v = 0.3$
Cancellous bone	$E = 0.04–4.0$	$v = 0.3$
Cortical bone*	$E_1 = E_2 = 11.5$	$v_{12} = v_{21} = 0.58$
*Transversely-isotropic properties from Reilly and Burstein (1975). Third axis is longitudinal direction.	$E_3 = 17.0$ $G_{12} = 3.6$	$v_{13} = v_{23} = 0.31$
	$G_{13} = G_{23} = 3.28$	$v_{31} = v_{32} = 0.46$

In order to assess the impact of variability in patient bone density on choice of cement mantle, analysis was repeated with the isotropic elastic modulus of cancellous bone assigned to five different values ranging from 40 to 4000 MPa, based on the range of anisotropic cancellous bone moduli observed in the proximal ($E_{\text{longitudinal}} = 200–4500$ MPa) and distal femur ($E_{\text{longitudinal}} = 200–4000$ MPa , $E_{\text{transverse}} = 40–1880$ MPa) (Morgan *et al.* 2003; Kaneko *et al.* 2004; Ashman and Rho 1988).

3.2.6 Boundary and loading conditions

Analysis was performed using boundary conditions selected to represent the stance phase of gait where the implant loading is maximal. The nodes of the femur were constrained 5 cm distal to the prosthesis tip, and forces were applied representing the hip joint contact force and the resultants of glutei, tensor fasciae latae, and vastus lateralis muscles (Bergmann *et al.* 2001b). Locations of the points of force application are indicated in **Figure 3.6** and magnitudes of the force components are shown in **Table 3.2**.

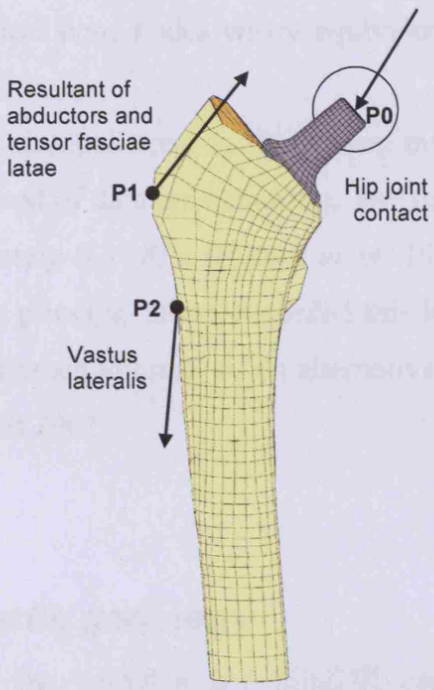

Figure 3.6. Schematic of gait load applied, indicating points of application of joint and muscle forces. The distal end of the model is fixed in all degrees of freedom.

Table 3.2. Force components applied to represent the stance phase of gait for a body weight of 750 N. Based on data from HIP98 (Bergmann *et al.* 2001b).

Description of force	Force magnitudes (N)			Point of application*
	X (medial)	Y (posterior)	Z (proximal)	
Hip joint contact	-405.0	246.0	-1719.0	P0
Abductors and tensor fascae latae	485.3	-114.0	605.3	P1
Vastus lateralis	-6.8	-138.8	-696.8	P2

*see **Figure 3.6** for points of application.

3.2.7 Outcome measures

The equivalent stress in the femoral cortex and specifically the medial calcar region was investigated as an indicator of the likelihood of loss of bone stock due to stress shielding. Bone atrophy is thought to occur below a threshold strain of approximately 200 με (Prendergast 2002), which in a state of uniaxial stress would equate to an equivalent stress of around 3.4 MPa in cortical bone.

The proportion of cortical bone nodes where equivalent stress fell below this level was also assessed.

The maximum principal stress in the cement mantle was analysed as a predictor of the likelihood of damage occurring. The fatigue limit for Palacos-R cement is approximately 8.3 MPa (Fritsch *et al.* 1996). The proportion of nodes where maximum principal stress exceeded this level was also obtained, based on the idea of 'stressed volume' as an alternative measure to peak stress (Lennon and Prendergast 2001).

3.3 Results

3.3.1 Cement mantle geometry

Visual comparison of the thick/US and thin/UK cement mantles revealed geometry which was quite similar in the distal half, but differed more in thickness in the proximal half. The extents of the proximal interdigitated regions were very similar. The stems were poorly centralised in the medullary canal despite the use of distal ring centralisers in both cases, requiring some adjustment to the FE mesh to ensure good alignment and centralisation.

3.3.2 Stress in the cement mantle

The distribution of stress in each cement mantle was broadly similar. In all cases, a focal peak maximum principal stress occurred posteromedially to the prosthesis tip (corresponding to radiographic zones V and XII). The lateral side of the cement mantle experienced generally higher maximum principal stress than the medial side, as would be expected given that the femur-implant construct is loaded primarily in bending. See **Figure 3.9**, **Figure 3.7** and **Figure 3.8**.

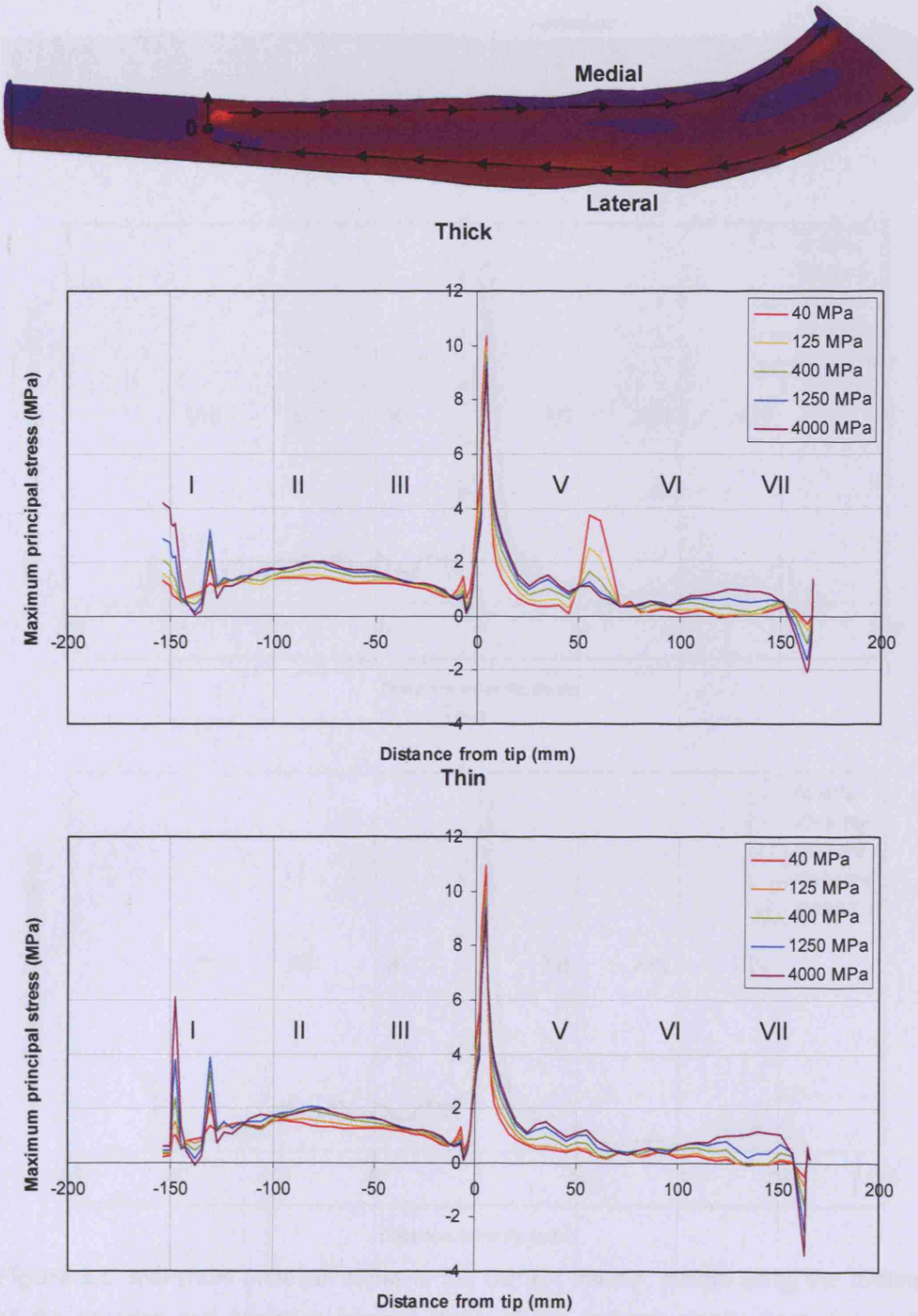

Figure 3.7. Maximum principal stress in the cement mantle, plotted along the midline of the medial and lateral internal faces of the cement mantle from zone I (proximal medial) to VII (proximal lateral). Coloured lines represent different cancellous bone moduli. Peak stress occurs in zone V.

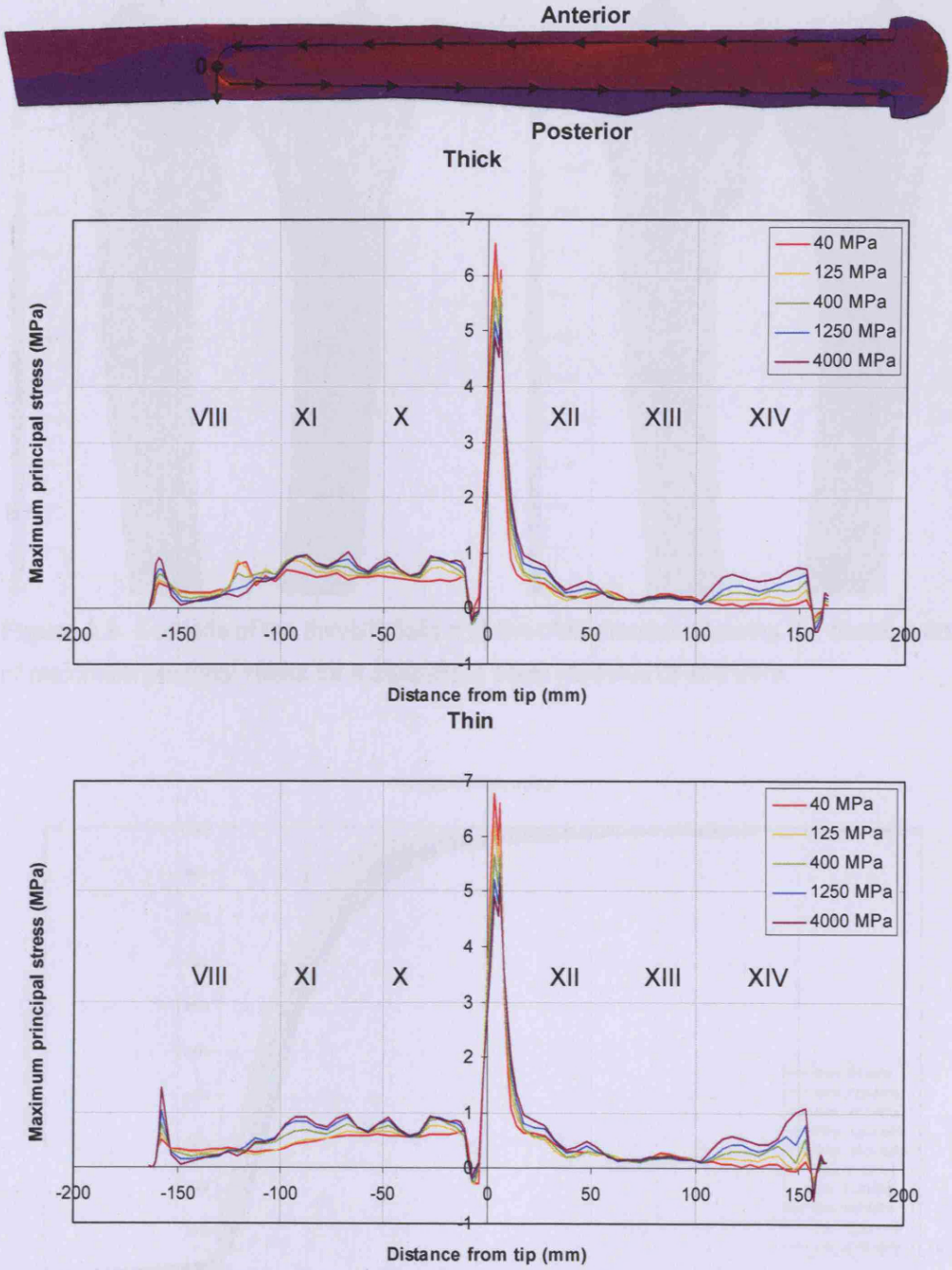

Figure 3.8. Maximum principal stress in the cement mantle, plotted along the midline of the anterior and posterior internal faces of the cement mantle from zone VIII (proximal anterior) to XIV (proximal posterior). Coloured lines represent different cancellous bone moduli. Peak stress occurs in zone XII.

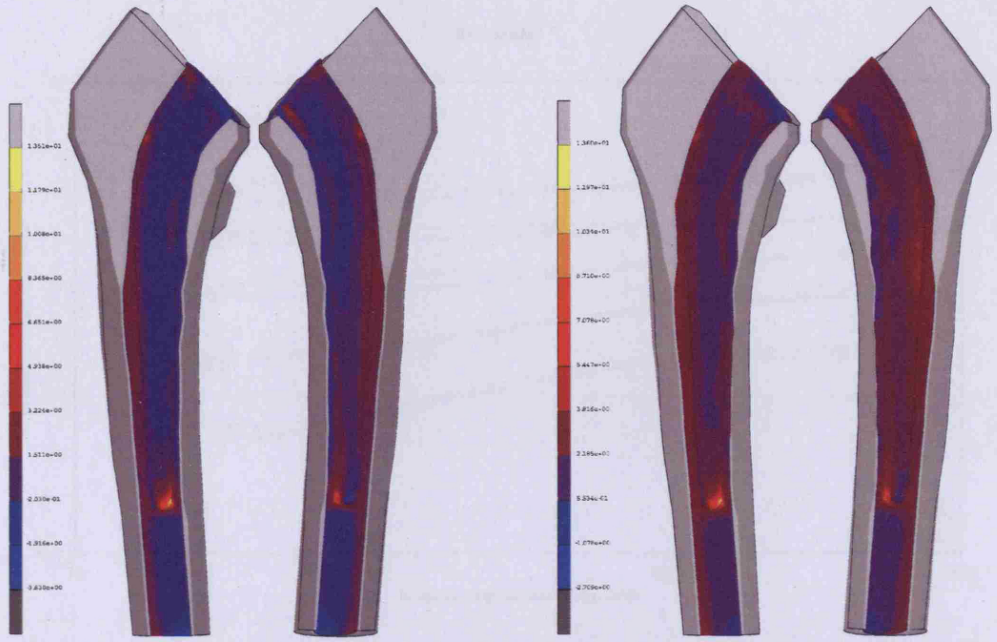

Figure 3.9. Sections of the thin/UK (left) and thick/US mantles showing the distribution of maximum principal stress for a cancellous bone modulus of 400 MPa.

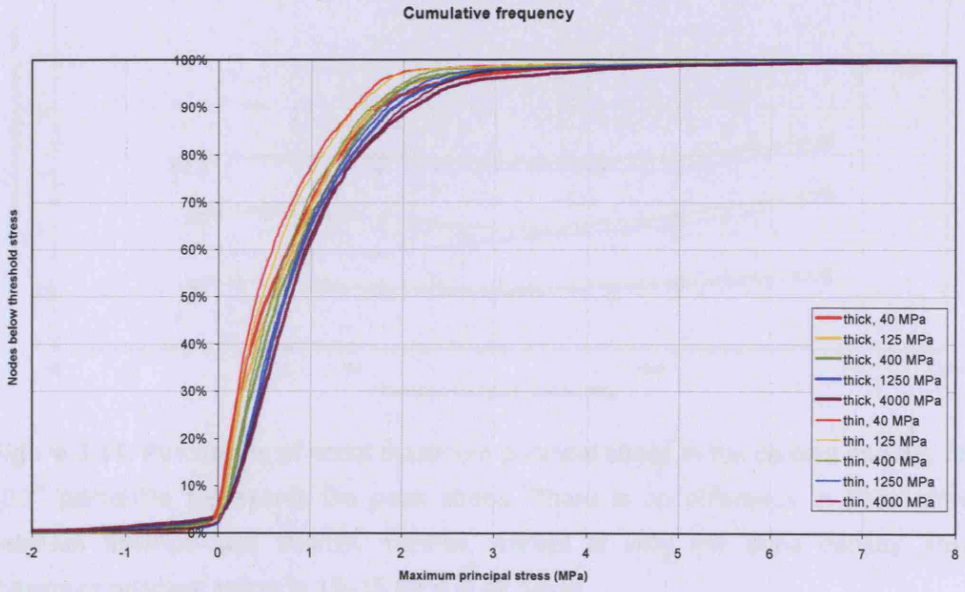

Figure 3.10. Cumulative frequency graph of nodal maximum principal stress in the cement mantle. Coloured lines represent the use of different cancellous bone moduli; thick and thin lines represent thick/US and thin/UK cement mantles, respectively.

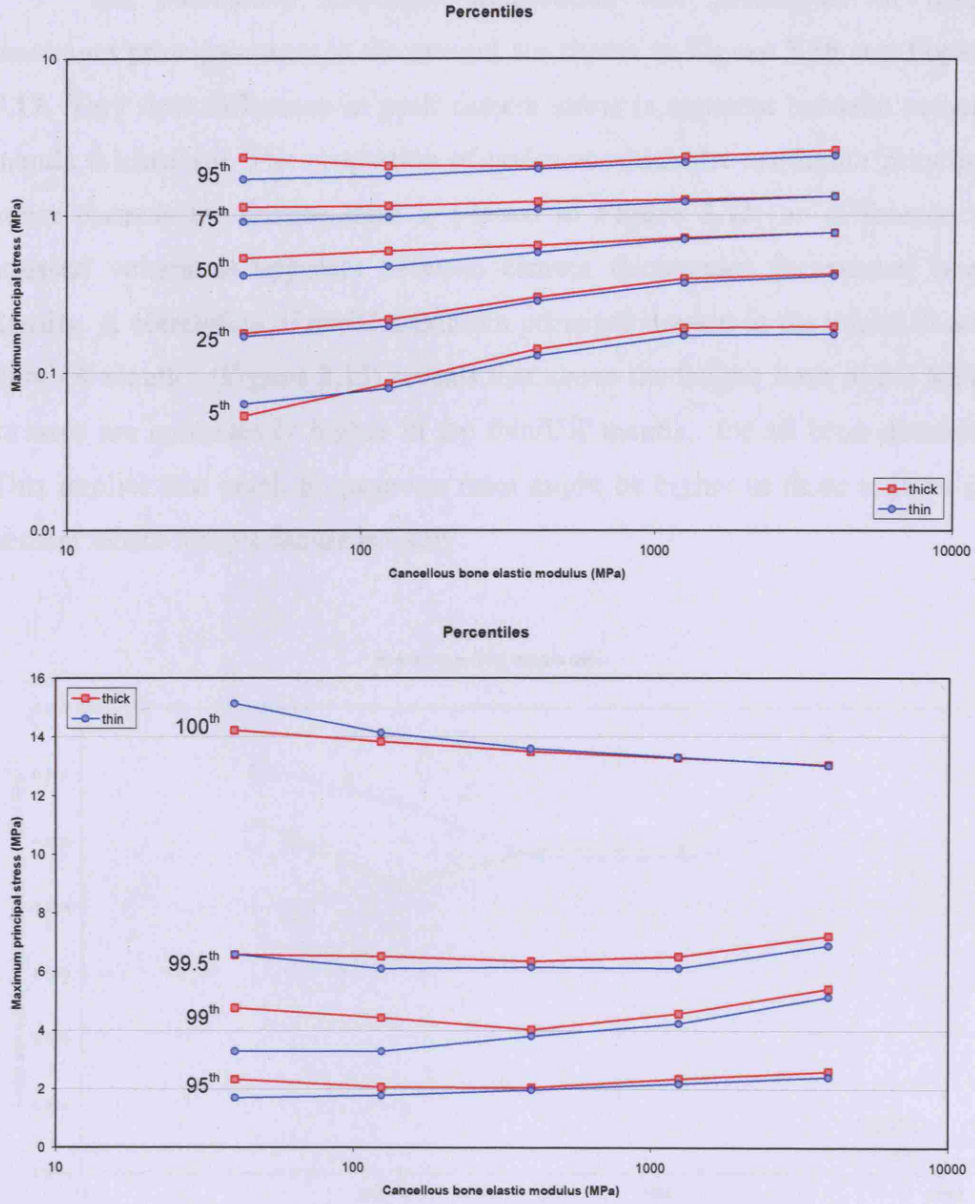

Figure 3.11. Percentiles of nodal maximum principal stress in the cement mantle. The 100th percentile represents the peak stress. There is no difference in peak stress between thick/US and thin/UK mantles, except at very low bone density. Peak maximum principal stress is 13–15 MPa in all cases.

The cumulative frequency distribution and percentiles of nodal maximum principal stress in the cement are shown in **Figure 3.10** and **Figure 3.11**. Very little difference in peak cement stress is apparent between cement mantle thicknesses. The proportion of nodes at which the maximum principal stress exceeds the fatigue limit is plotted in **Figure 3.12**; no difference in stressed volume is apparent between cement thicknesses for normal bone density. A correlation of nodal maximum principal stresses in the thick/US and thin/UK mantles (**Figure 3.13**) reveals that above the fatigue limit of 8.3 MPa, stresses are consistently higher in the thin/UK mantle., for all bone densities This implies that crack propagation rates might be higher in those regions of cement where fatigue failure is likely.

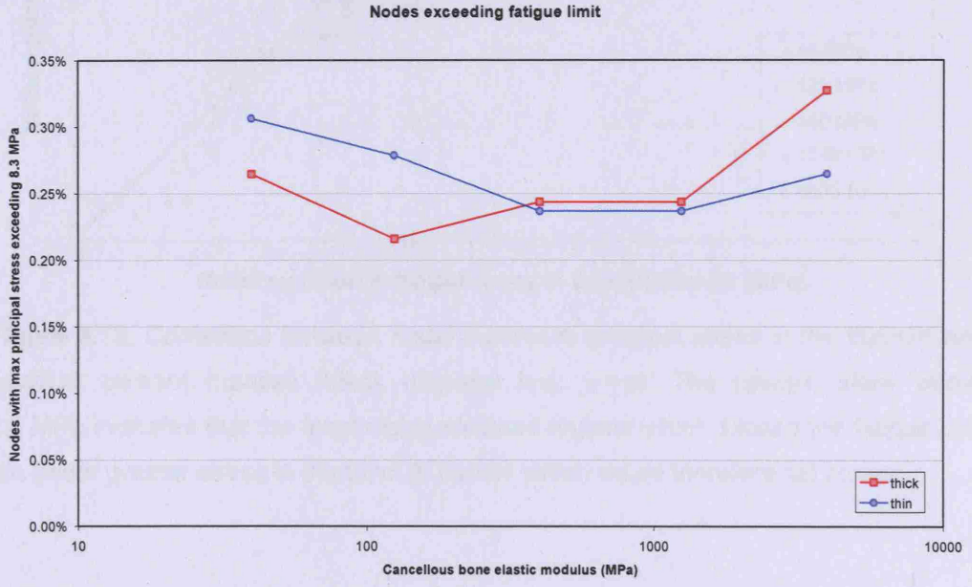

Figure 3.12. Nodes in the cement mantle exceeding the fatigue limit of 8.3 MPa (Fritsch *et al.* 1996). There is little difference between the thick/US and thin/UK mantles over a normal/healthy range of cancellous bone density. For very dense cancellous bone, the thick/US mantle has more nodes exceeding the fatigue limit, while for low bone densities it has fewer.

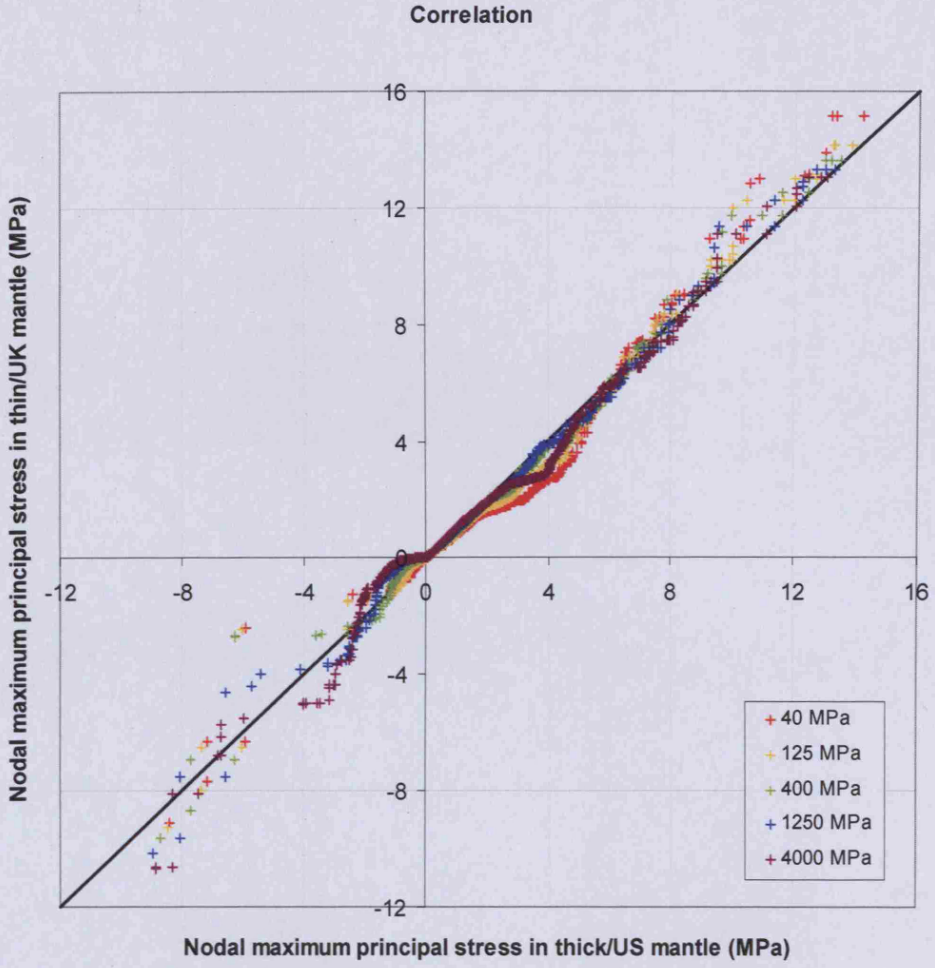

Figure 3.13. Correlation between nodal maximum principal stress in the thin/UK and thick/US cement mantles (black diagonal line: $y = x$). The upward skew above 8.3 MPa indicates that the most highly-stressed regions which exceed the fatigue limit are under greater stress in the thin/UK mantle which would therefore fail sooner.

3.3.3 Stress in the cortical bone

Plots of equivalent stress along the midlines of the anterior, posterior, lateral and medial aspects of the external surface of the femur are shown in **Figure 3.14** and **Figure 3.15**. Anterior, posterior and lateral stresses are strongly affected by bone density and much less by cement geometry, while medial stress is consistently higher (indicating less stress shielding) with a thick/US mantle.

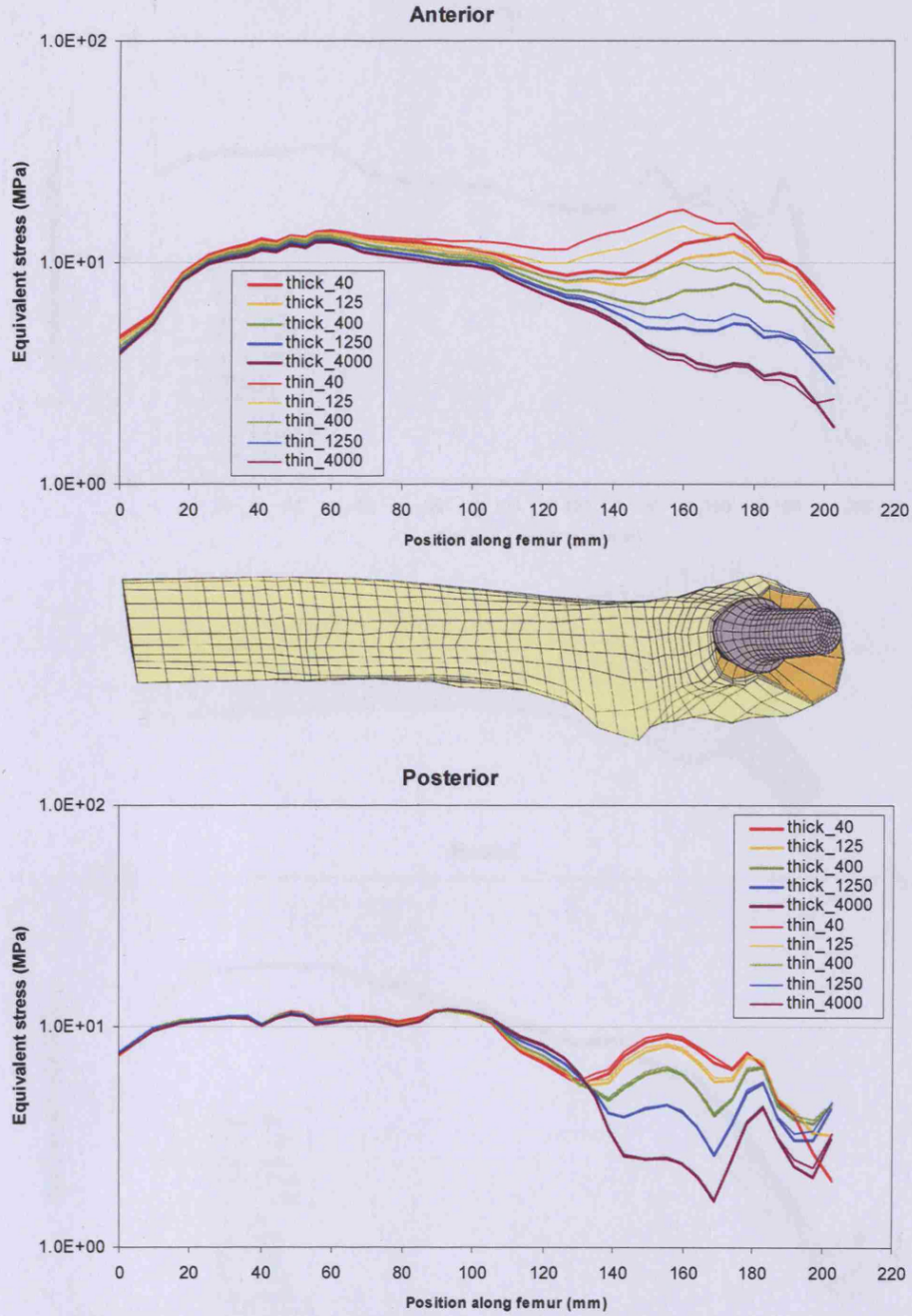

Figure 3.14. Equivalent stress plotted from distal to proximal along the midlines of the anterior and posterior aspects of the exterior surface of the femur. Coloured lines represent different cancellous bone moduli; thick and thin lines represent the use of thick/US and thin/UK cement mantles, respectively. Anteriorly, the thick/US mantle has lower stress proximally in all cases except for the most dense; posteriorly there is no discernible difference.

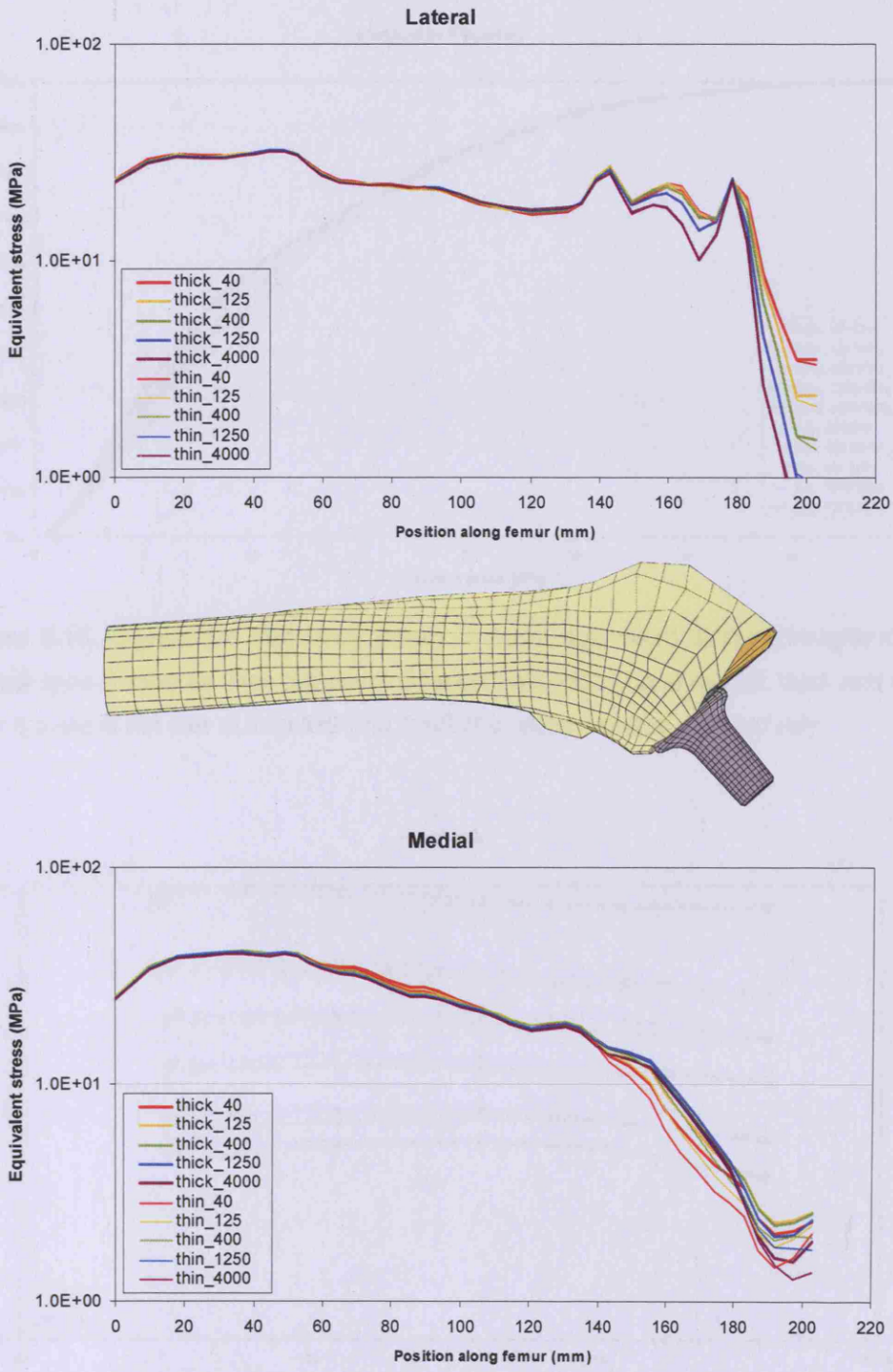

Figure 3.15. Equivalent stress plotted from distal to proximal along the midlines of the lateral and medial aspects of the exterior surface of the femur. Coloured lines represent different cancellous bone moduli; thick and thin lines represent the use of thick/US and thin/UK cement mantles, respectively. There is little difference on the lateral side; medially, the thin/UK has lower proximal stress in all cases.

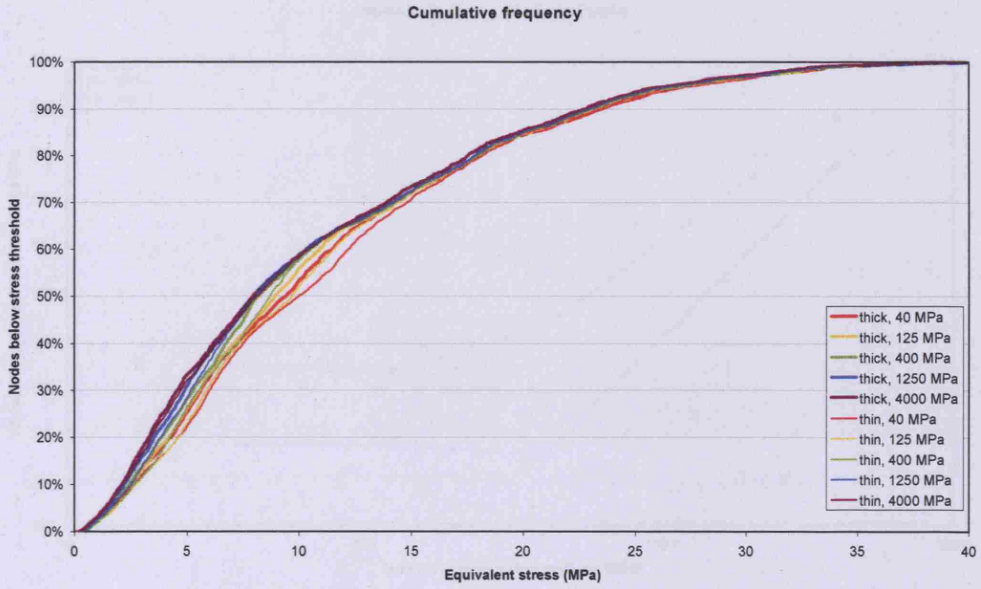

Figure 3.16. Cumulative frequency graph of nodal equivalent stress throughout all cortical bone. Coloured lines represent different cancellous bone moduli; thick and thin lines represent the use of thick/US and thin/UK cement mantles, respectively.

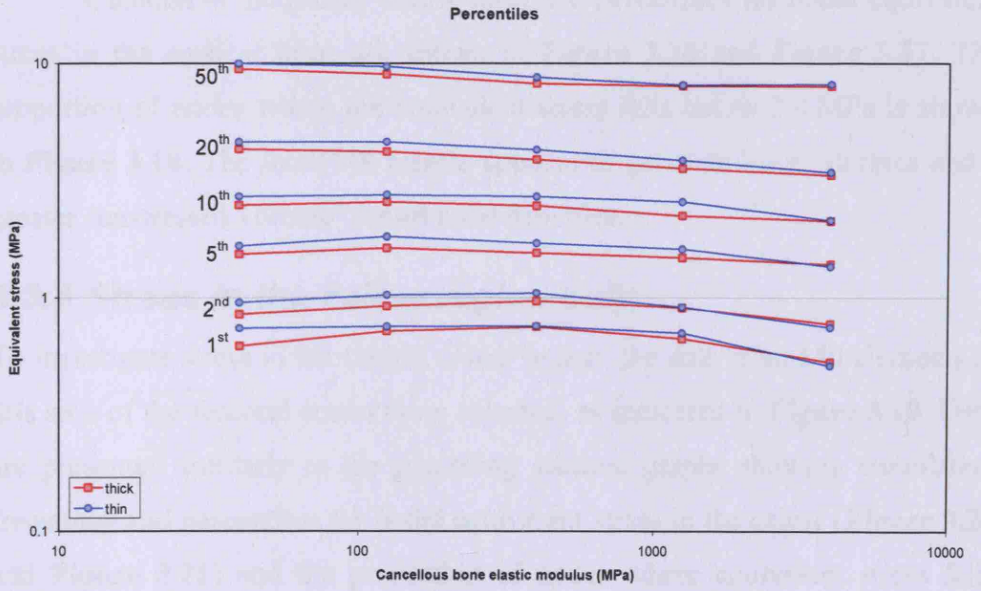

Figure 3.17. Percentiles of nodal equivalent stress in the cortical bone.

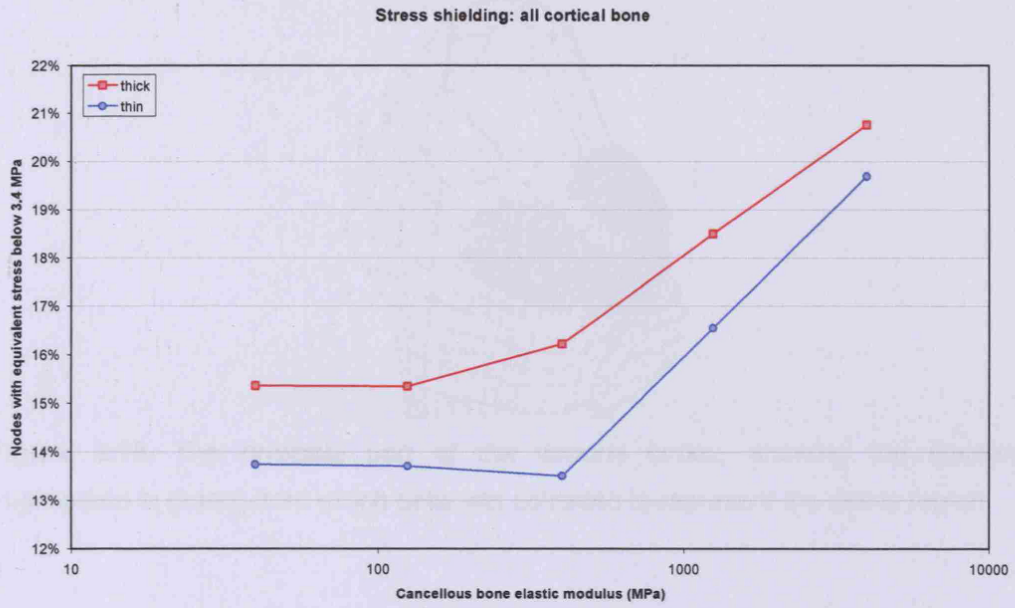

Figure 3.18. Proportion of nodes in the cortical bone where the equivalent stress falls below an approximate resorption threshold of 3.4 MPa. The thick/US mantle generates stress below this threshold in 5–20% more nodes.

Cumulative frequency distribution and percentiles for nodal equivalent stress in the cortical bone are shown in **Figure 3.16** and **Figure 3.17**. The proportion of nodes where the equivalent stress falls below 3.4 MPa is shown in **Figure 3.18**. The thick/US mantle appears to generate lower stresses and a greater 'unstressed volume' for all bone densities.

3.3.4 Stress in the calcar region only

To investigate stress in the critical calcar region, the data from 140 elements in this area of the femoral cortex were selected, as indicated in **Figure 3.19**. Data are presented similarly to the preceding section: graphs showing cumulative frequency and percentiles for nodal equivalent stress in the calcar (**Figure 3.20** and **Figure 3.21**) and the proportion of nodes where equivalent stress falls below 3.4 MPa (**Figure 3.22**). There is very little difference in stress between the different cement mantle thicknesses. The thin/UK mantle generates a greater 'unstressed volume' across all bone densities, indicating that the calcar region would experience less stress-shielding with the thick/US mantle.

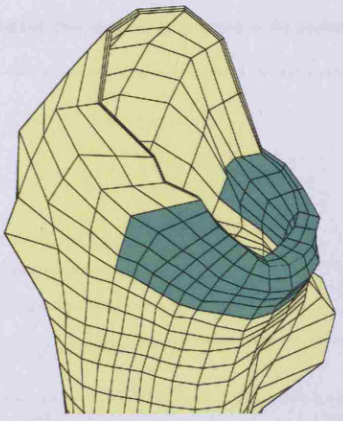

Figure 3.19. The proximal part of the femoral cortex, showing the elements (highlighted in green) from which data was collected to represent the calcar region.

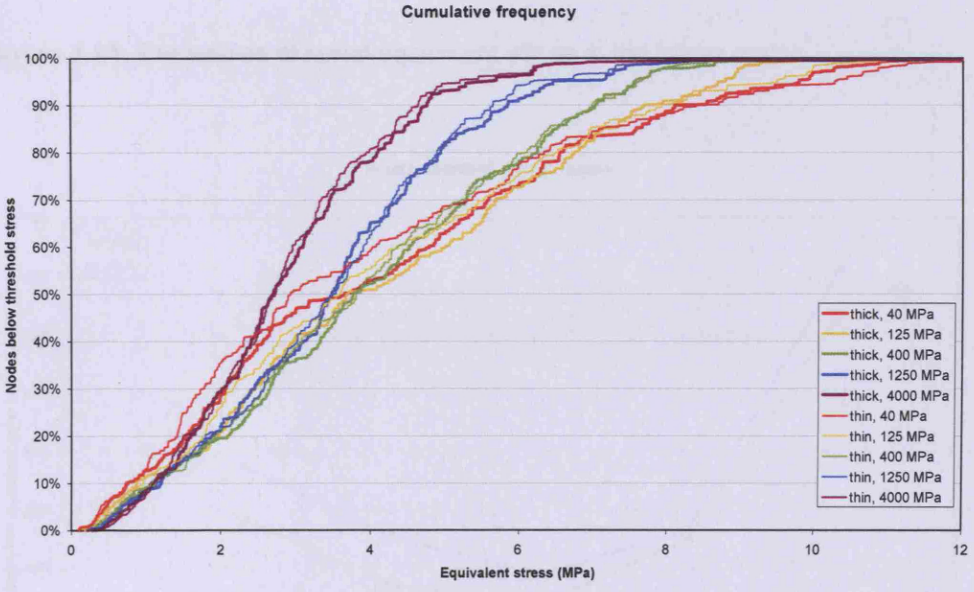

Figure 3.20. Cumulative frequency graph of nodal equivalent stress within the calcar region. Coloured lines represent different cancellous bone moduli; thick and thin lines represent the use of thick/US and thin/UK cement mantles, respectively.

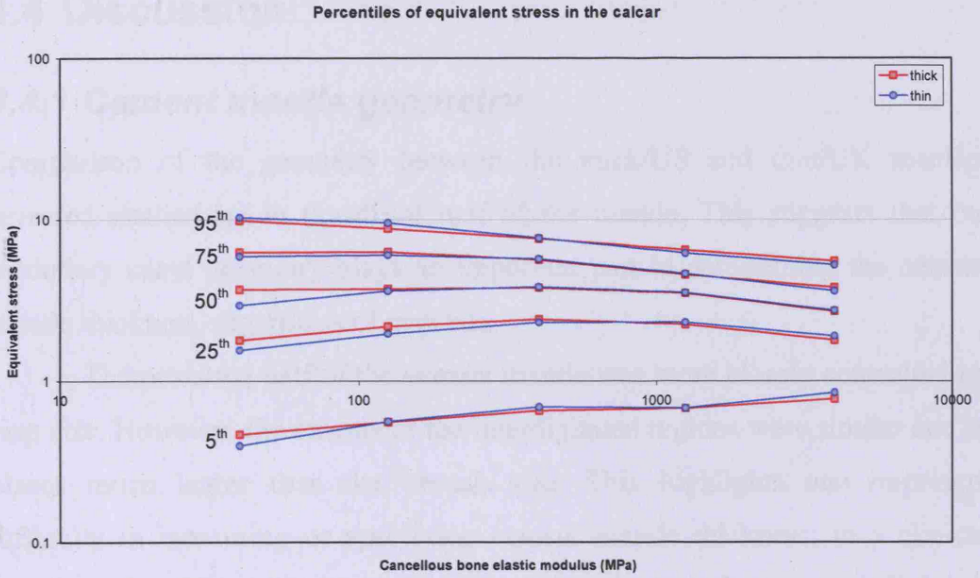

Figure 3.21. Percentiles of nodal equivalent stress in the calcar region.

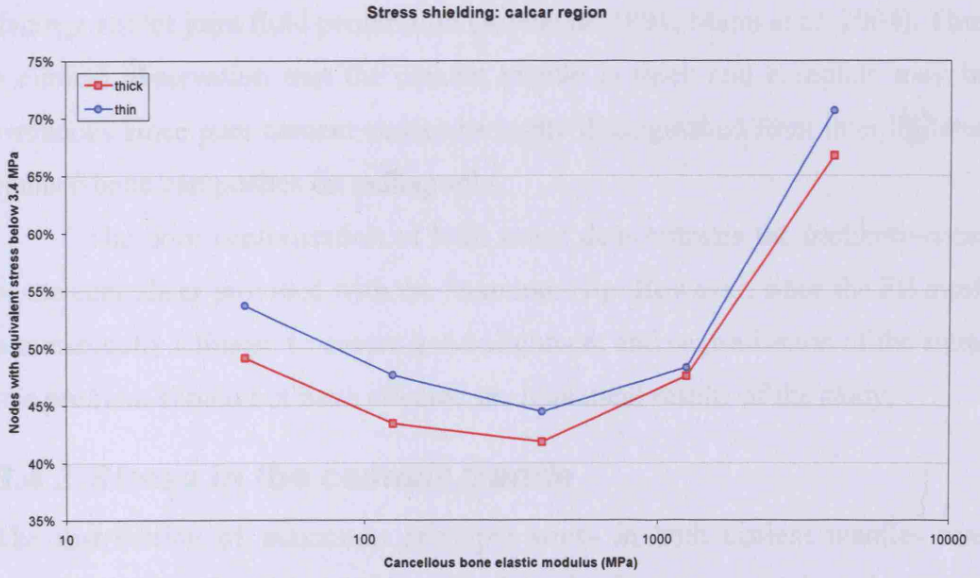

Figure 3.22. Proportion of nodes in the calcar region where the equivalent stress falls below an approximate resorption threshold of 3.4 MPa. The thin/UK mantle generates stress below this threshold in 2–10% more nodes.

3.4 Discussion

3.4.1 Cement mantle geometry

Comparison of the geometry between the thick/US and thin/UK mantles revealed similarities in the distal half of the mantle. This suggests that the medullary canal geometry plays an important part in determining the cement mantle thickness, regardless of rasp size.

The proximal half of the cement mantle was more closely controlled by rasp size. However, the extents of the interdigitated regions were similar and in places much larger than the broach size. This highlights one important difficulty in measuring or specifying cement mantle thickness: in a clinical situation, the thickness observed radiographically includes the interdigitated region which is often 10 mm thick or more, even though this region is inferior to pure bone cement in terms of mechanical properties and resistance to damage and/or joint fluid penetration (Jofe *et al.* 1991; Mann *et al.* 2004). Thus a clinical observation that the cement mantle is thick and complete may be erroneous since pure cement cannot be easily distinguished from interdigitated cement-bone composites on radiographs.

The poor centralisation of both stems demonstrates the ineffectiveness of the centraliser provided with the Stanmore Hip. However, since the FE mesh was manually adjusted to ensure good alignment and centralisation of the stem, this problem should not have affected the numerical results of the study.

3.4.2 Stress in the cement mantle

The distribution of maximum principal stress in both cement mantles was broadly similar. Stress levels along the lateral side were approximately double those seen along most of the medial side, representing the bending mode of loading applied to the femur. A much larger focal peak stress was observed in all cases posteromedially to the prosthesis tip, in radiographic zones V and XII. This is in agreement both with previous stress analyses and with clinical

observations of osteolysis in these regions (Kwak *et al.* 1979; Star *et al.* 1994; Ritter *et al.* 1999).

There was no difference between the magnitude of peak tensile stress in thick/US and thin/UK cement mantles for high bone density, whilst for low bone density the thin mantle experienced peak stress up to 7% higher.

The proportion of nodes in each cement mantle where the maximum principal stress exceeded the fatigue limit was 0.22–0.33%. There was hardly any difference between cement mantle thicknesses in this respect for normal cancellous bone density. Fewer nodes exceeded the fatigue limit in thin/UK mantles with very high bone density and in thick/US mantles with low bone density. Based on this result alone, it is not possible to favour one cement mantle thickness over the other.

Correlation of nodal maximum principal stresses between cement mantle thicknesses revealed that for nodes exceeding the fatigue limit of 8.3 MPa, the thin/UK mantle had consistently higher stresses. This suggests that the thinner mantle would fail sooner, in agreement with widely held current opinion in orthopaedics (Breusch and Malchau 2005).

3.4.3 Stress in the cortical bone

The equivalent stress in the femoral cortex was found to fall below the approximate resorption threshold of 3.4 MPa at 22–34% of nodes; low stresses were found around the proximal half of the implant, with the lowest occurring medially and laterally. This indicates a high likelihood of bone resorption due to stress shielding in all cases, with most bone loss expected proximally. The lateral minimum occurs only in the most proximal 20 mm of the greater trochanter, and is likely to be a result of the simplification of distributed muscle forces in this region to a single point load. The low stress in the medial calcar region is of most concern, since calcar atrophy due to stress shielding is a common problem thought to exacerbate the mechanism of prosthetic loosening by compromising the structural integrity of the bone-implant construct (Kroger *et al.* 1998; Venesmaa *et al.* 2003; Karachalios *et al.* 2004).

Stresses in the anterior, lateral, and posterior areas of the proximal femoral cortex were influenced much more by cancellous bone density than by cement mantle thickness. However, in the critical calcar region, consistently higher stress was achieved through the use of the thick/US mantle for all bone densities. This is likely to result from better transmission of load to the cortical bone by the removal of more of the interposing compliant cancellous bone.

Comparison of the proportion of nodes in the cortical bone where equivalent stress fell below an approximate resorption threshold indicated that the thin/UK mantle would lead to less resorption due to stress shielding. However, when this comparison was made only for nodes in the critical calcar region, the thick/US mantle appeared to lead to less bone resorption.

3.4.4 Limitations

Bone density

Our model represents the cancellous bone of the proximal femur as homogeneous and isotropic, and the geometry of the femur as identical in all cases. Cancellous bone varies considerably in density within one patient and is highly anisotropic, while increased anisotropy and geometric changes such as cortical expansion and thinning are often seen alongside reductions in bone density. However, it would be difficult to make meaningful comparisons of stress in the cortical bone if its geometry were to vary between models. Anisotropic properties and orientations for cancellous bone are currently difficult to ascertain except by the use of small scale, high resolution micro-CT-based models.

Interdigitation

Penetration of bone cement into cancellous bone varies with bone porosity, as does the stiffening effect of interdigitation; thus bone density would in practice affect both the geometry and the stiffness of interdigitated regions which are ignored in this study. Low bone density might be expected to lead to interdigitated regions which are both larger (due to increased permeability) and

relatively stiffer than the cancellous bone itself. If taken into account, this would be likely to reduce the differences in cement and cortical bone stresses between models with different cement mantle thicknesses and bone densities.

Linear-elastic stress analysis

In our linear-elastic stress analysis, only the initial state of stress is investigated, revealing none of the changes in stress or fixation which might occur over long periods of time as a result of time-dependent factors such as creep or stress relaxation in the cement, frictional slipping of the implant, or weakening of the cement through damage accumulation. Consequently, such a model provides a useful comparative tool for distinguishing between implant characteristics only in the case that the resulting stress distributions are very different and that these comparative results are unlikely to be significantly affected by long-term or time-dependent effects. In this study, the similarity between results for stress in the cement mantle is sufficient to justify further investigation of the effect of cement mantle thickness on stem fixation using a more refined model incorporating creep and frictional slipping. Subsidence and creep might also result in improved load transmission from implant collar to calcar, and hence increase compressive stress in the calcar over time.

Cement mantle thickness

Although every effort was made to use anatomically accurate cement mantle geometry, some idealisation was made just below the lateral collar. It was not possible to obtain reliable geometric data in this region from the section images and radiographs. As a result, this region is modelled as a uniformly thin cement mantle when in fact it should slightly flare to the lateral side just below the collar. However, this region is not highly stressed, and geometric inaccuracies here are unlikely to significantly affect remote stresses.

This study is concerned with thick, continuous cement mantles around a curved, collared prosthesis. Relevance to other types of femoral component is limited, since the geometry and resulting stress distributions may differ substantially. In particular, very thin, discontinuous cement mantles with large,

press-fit implants such as those commonly used in France are unlikely to fail through cement damage; other loading and failure mechanisms are thought to apply (Langlais *et al.* 2003).

3.5 Conclusions

The thin/UK and thick/US rasps generated cement mantles which were approximately 1 mm and 2.5 mm thick, respectively, in the proximal region and became more similar towards the distal end. This represents a clinically realistic alteration in cement geometry due to change in rasp size, but does not represent dramatically different cement mantle geometries. Hence, it is to be expected that the difference in stress between the two models is slight.

The thick/US mantle exhibited lower maximum principal stress in those regions of cement where the fatigue limit was exceeded, and more of the cortical bone in the calcar region exceeded the resorption threshold, indicating that the thick/US mantle should perform better clinically, both in terms of cement damage and resorption due to stress shielding. However, poor centralisation due to ineffective Stanmore Hip centralisers is likely to negate this effect.

Furthermore, time-dependent effects such as cement creep, implant subsidence and crack propagation are likely to influence the long term behaviour of each cement mantle significantly, particularly in light of the apparent similarities in stress levels found in this study. Thus it is necessary to include these effects in subsequent comparative studies. This will be addressed in later chapters of this thesis.

Variation in patient bone density strongly affected stress levels in the cortical bone and cement mantle. This effect was much greater than that of cement mantle thickness. However, it did not alter the basic conclusions drawn above.

Chapter 4

Fatigue testing

4.1 Introduction

4.1.1 Background

In the previous chapter, similar stress distributions were found around cement mantles of different thicknesses. However, the effect on cement cracking of mantle thickness due to broach size has not been investigated clinically, and *in vitro* studies relating to this issue have tended towards great simplification.

As discussed earlier, thin regions in the femoral cement mantle have been strongly associated with cracking (Jasty *et al.* 1991; Jasty *et al.* 1992; Kawate *et al.* 1998; Koster *et al.* 1999), and *in vitro* studies point to increased risk of the formation of through-thickness cracks in thin cement, although crack growth rates seem unrelated to cement thickness (Hertzler *et al.* 2002; Mann *et al.* 2004).

4.1.2 Aims and objectives

The study reported in this chapter investigates how cement mantle thickness, due to broach size and stem orientation, affects cement cracking around Stanmore Hip femoral components. This is achieved by fatigue testing of synthetic femurs containing Stanmore Hips with different cement thicknesses and stem orientations under a simulated cyclic stair-climbing load. In the next chapter, the results of this study will also be compared with those of corresponding finite element simulations of cement damage, for the purpose of validation of the finite element model.

4.1.3 Hypotheses

We hypothesised that, under a simulated stair-climbing load

(1) a thicker femoral cement mantle experiences fewer and shorter cracks;

(2) a well-centralised stem leads to fewer and shorter cement cracks.

4.2 Materials and methods

4.2.1 Experimental design

Three groups of implanted synthetic femurs were created with different cement mantle geometries for fatigue testing:

(1) those prepared with the larger US broach and good centralisation, 'thick/US' ($n = 5$);

(2) those prepared with the smaller UK broach and good centralisation, 'thin/UK' ($n = 5$); and

(3) those prepared with the UK broach with deliberate varus positioning to generate poor centralisation, 'varus/UK' ($n = 3$).

Power analysis based on the experimental data of Hertzler *et al.* (2002) had indicated that a group size of three would be sufficient to demonstrate statistically significant differences in crack length between groups.

4.2.2 Preparation of synthetic femurs

Thirteen synthetic femurs (Sawbones, Pacific Research Laboratories Inc., Vashon, USA) were prepared using methods resembling as closely as possible the standard surgical technique for the Stanmore Hip. Surgical templates were used to select the correct size and shape of implant and corresponding rasp size for the Sawbones. The 'medium' Sawbones used in this study were determined to require Stanmore Hip femoral components of the 'standard' shape, and size '2' in all cases. Power tools were used to perform the neck resection, broach and medullary reaming as the Sawbones proved extremely difficult to cut and ream using surgical hand tools. The medullary cavity was then widened by hand using rasps of ascending size, finishing with either the US-designed rasp

(thick/US group) or the UK-designed rasp (thin/UK and varus/UK groups), both of size '2'. Identical standard size-2 Stanmore femoral components were inserted in all cases.

4.2.3 Cementing technique

A 'third generation' cementing technique was used in all cases. Pre-chilled Refobacin Palacos-R bone cement (Biomet Europe BV, Dordrecht, The Netherlands) was vacuum-mixed and injected under pressure, using the Optivac mixing gun system (Biomet Europe), into the medullary cavity in a retrograde fashion. The powder and monomer components were mixed within a few minutes of removing from refrigeration at 5 °C. Injection into the medullary canal took place at 3–4 minutes from the start of mixing, and stem insertion at 6–8 minutes when the cement reached a doughy phase.

4.2.4 Insertion and centralisation

Stem insertion was performed using a custom insertion rig to control the degree of centralisation. For the 'well-centralised' groups (thick/US and thin/UK), the femoral component was clamped in place on the loading cross-head of a universal testing machine (Hounsfield H10KM, Hounsfield Test Equipment Ltd., Redhill, UK) with the implant shaft oriented in a vertical position. Using proximal and distal spacers to ensure adequate centralisation, the machine was used to lower the implant into the empty medullary canal of the prepared Sawbone. Held in position by the implant, the Sawbone was then cast in place using a potting metal alloy to hold it in alignment with the implant. Once the potting metal had set, the implant could then be raised and lowered freely using the machine loading head, whilst remaining well centralised. The centralisers were then removed to reduce defects due to air entrapment or turbulence in the cement flow during stem insertion. Cement was injected to fill the medullary cavity. The stem was inserted at a speed of 1000 mm/min, reducing to 10 mm/min as it came to within a few millimetres of its final position. As the stem came to rest with its collar in contact with the calcar, the reaction force

was allowed to reach approximately 100 N before the machine was stopped and intermittently advanced at 1 mm/min. This allowed the reaction force to be maintained at a level of around 100 N until the cement had cured. The load was then released and the potting metal was melted away.

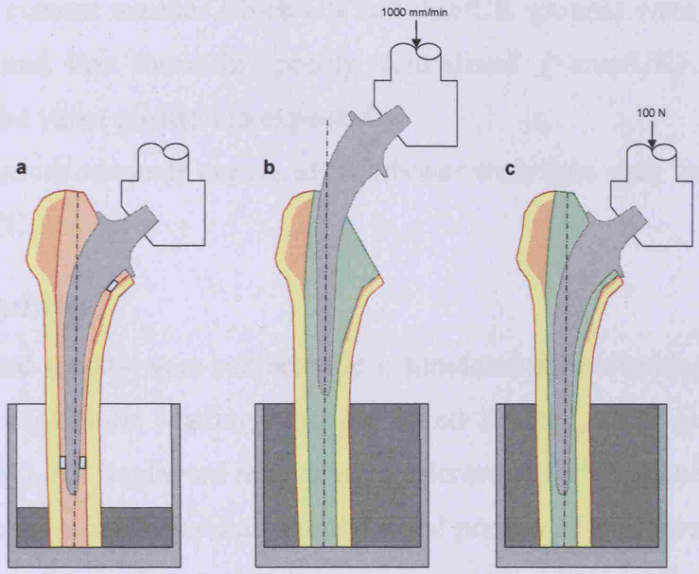

Figure 4.1. Schematic of the insertion process, showing (a) potting metal poured around the synthetic femur while it is held upright by the clamped prosthesis and centralisers; (b) the stem raised and the medullary canal filled with bone cement before insertion of the prosthesis without centralisers at 1000 mm/min; (c) the stem held in position with a force of approximately 100 N.

For the 'poorly-centralised' group (varus/UK), a similar method was used for insertion except that no centralising spacers were used, and the Sawbone was cast in such a position that the stem was oriented in varus, with the distal tip almost touching the inside of the cortex on the lateral side. After cement injection and stem insertion, the resulting cement mantle was thus very thin in this region. This amounts to a varus orientation of around 0.4 degrees, which is limited by the lateral cortical contact, representative of poor insertion into a well-aligned broach. The clinical scenario of a poorly-aligned broach

with cortical penetration could lead to greater stem misalignment, which is not investigated here.

Radiographs were taken of each implanted Sawbone in the anterior-posterior and lateral directions, giving an indication of the cement mantle geometry. These were inspected visually to confirm that the nominally 'well centralised' cement mantles (thick/US and thin/UK groups) were indeed well centralised and that those in 'poorly centralised' (varus/UK) group were oriented in the varus position as expected.

To ensure adequate curing, all Sawbones were then aged for 24 hours in water at 37 °C.

4.2.5 Loading

The implanted femurs were subjected to a simulated stair-climbing load, using a six-station hydraulic loading machine ('Red Rocket', RDP Howden Ltd., Southam, UK). All implanted femurs were oriented at 15° of adduction and 15° of flexion relative to the vertical, and the distal portion of the femoral shaft cast in place using the potting metal. A sinusoidal vertical load was applied to the head of each implant, simulating the orientation of the hip joint contact force during stair-climbing observed by Bergmann (2001a). The load was varied sinusoidally between 0.4 and 4.0 kN for four million cycles at 3 Hz.

Bergman's data show peak hip joint forces during stair climbing of around 2.0 kN. However, pilot studies for our experiment were run at peak loads of 2.0, 3.0 and 4.0 kN, and significant cement cracking after several million cycles was only observable in the highest load case. It was therefore decided that, for the purposes of crack initiation and measurement, a 4.0 kN load was necessary.

4.2.6 Sectioning and analysis

After loading, the femurs were sectioned at 5 mm intervals, using a water-cooled, diamond-coated saw to minimise surface damage. The sections were

then stained with a red dye penetrant and developer (Flawfinder, Rocol, Leeds, UK) to facilitate crack identification and measurement.

Image analysis software (KS300, Carl Zeiss, Oberkochen, Germany) was used to measure cement thickness and crack lengths under a confocal microscope. Cement thickness was measured radially at eight 45° intervals per section, as indicated in **Figure 4.2**. Cracks were measured and their locations categorised into the same 45° sectors. It was also noted whether any crack was contiguous with macropores or with the stem-cement and/or bone-cement interfaces.

Kolmogorov-Smirnoff tests indicated that the data were not normally distributed. Mann-Whitney U-tests were used for all statistical analysis relating to cement mantle thickness and crack length, and Chi-square tests for crack numbers.

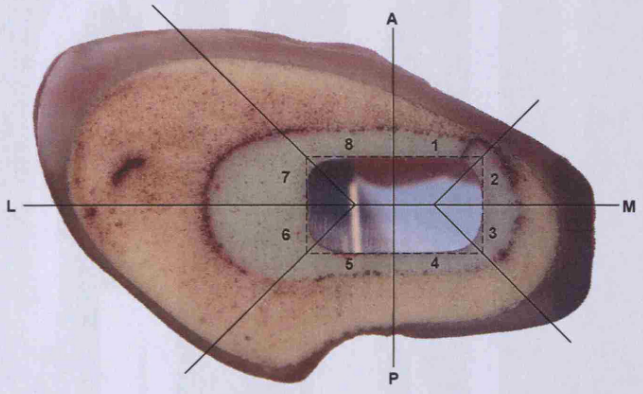

Figure 4.2. Section through a thick/US cement mantle showing the eight 45° sectors (1–8) into which cracks were categorised. Cement mantle thickness was measured at the dividing lines between sectors and at the location of any crack.

4.3 Results

4.3.1 Cement mantle thickness

Upon inspection of the radiographs, one of the femurs in the thick/US group was found to have a very thin medial cement mantle. This is thought to have

arisen due to overloading of the stem during insertion. Subsequent crack analyses after loading revealed that this cement mantle had experienced very extensive damage, especially in the thin regions. Since it was (a) not felt to be representative of a thick/US mantle, and (b) likely to have been damaged or highly stressed by the release of the high insertion load, it was decided that this femur should be excluded from all statistical analyses.

The other mantles were compared by group to ensure that cement thickness was well controlled. Radiographs showed reasonably uniform cement thickness representative of the thick/US and thin/UK groups, and very thin cement was confirmed at the tip of the stems in the varus/UK group. Representative radiographs are shown in **Figure 4.3**.

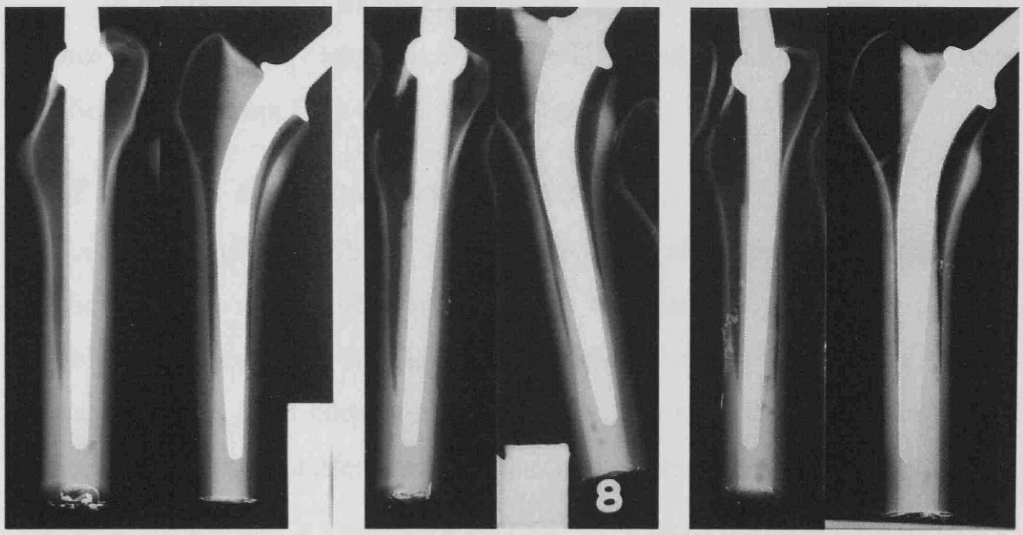

Figure 4.3. 'Lateral' and 'anteroposterior' radiographs of the synthetic femurs, showing (left to right) the thick/US, thin/UK, and varus/UK cement mantles.

In the medial half of the proximal third of the cement mantle, the median cement thickness measurements for the thick/US, thin/UK and varus/UK groups were 2.2 mm, 1.5 mm and 1.3 mm, respectively. Thick/US and thin/UK groups were significantly different ($p = 0.004$), as were thin/UK and varus/UK groups ($p = 0.01$). See **Figure 4.4**.

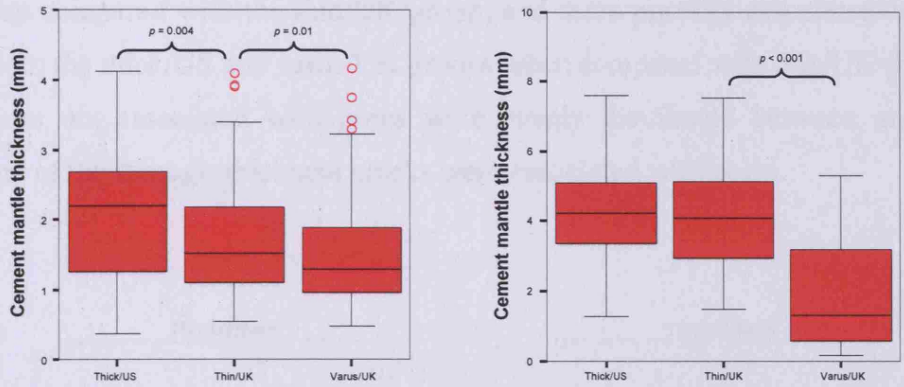

Figure 4.4. Box and whisker plots of cement mantle thickness measurements compared by group, in the medial half of the proximal third (left) and the lateral half of the distal third (right) of the cement mantle.

In the lateral half of the distal third, median thicknesses were 4.2 mm, 4.1 mm and 1.3 mm, respectively. Thin/UK and varus/UK groups were significantly different ($p < 0.001$). See **Figure 4.4**.

4.3.2 Spatial distribution of cracks

Cracks were widely distributed in all sectors and along the full length of the prosthesis. There was no obvious difference between groups in terms of crack distribution, as indicated in **Figure 4.5**. Although many of the very longest cracks originated from corners of the implant, they were not associated with a particular axial or circumferential position in the cement mantle.

4.3.3 Crack numbers and locations

Chi-square tests were used to examine the null hypothesis of equal numbers of cracks expected per femur in each group, as shown in **Table 4.1**. Similar chi-square tests were performed on the thick/US and thin/UK groups only and the thin/UK and varus/UK groups only (not shown). Numbers of cracks per femur between thick/US and thin/UK groups was not significantly different from the expected even distribution. The numbers of cracks contiguous with the stem-cement and/or bone-cement interfaces across groups did not differ significantly from the expected even distribution. There were more cracks in the varus/UK

group compared with the thin/UK group, and more porosity-associated cracks in both the thick/US and varus/UK groups when compared with thin/UK group. Cracks not associated with pores were evenly distributed between groups. None of the through-thickness cracks were associated with pores.

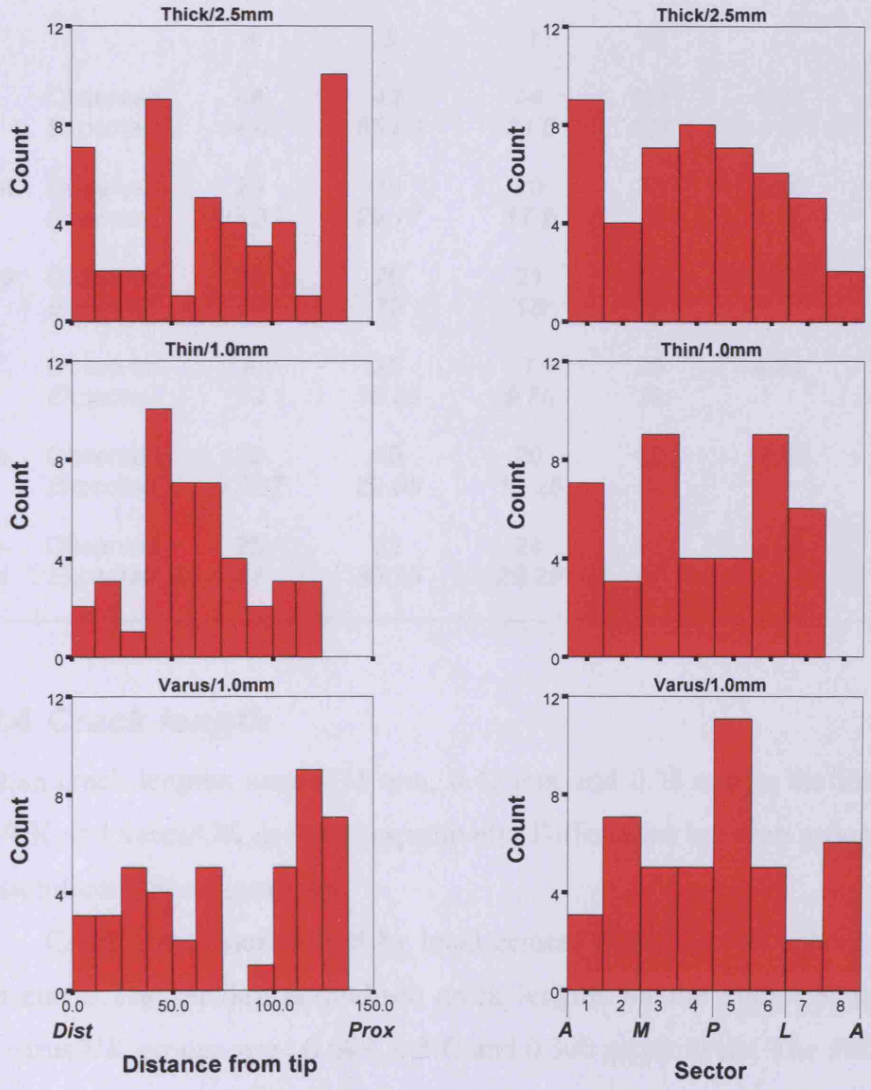

Figure 4.5. Histograms showing axial (left) and circumferential (right) crack distributions. Cracks appear to be widely and randomly distributed, with no clear trends or obvious differences between the groups.

Table 4.1. Crack frequencies in each group of *n* femurs. The rows represent all cracks (All), cracks associated with stem-cement (Stem) and bone-cement (Bone) interfaces, full-thickness cracks (Full), and cracks associated (Pore) and not associated (Non-pore) with pores. Chi-square tests examine the null hypothesis of the same number of cracks per femur expected in each group.

Cracks in group		Thick/US	Thin/UK	Varus/UK	Total	Chi-square	Sig.
n		*4*	*5*	*3*	*12*		
All	Observed	48	42	44	134	6.97	$p<0.05$
	Expected	*44.67*	*55.83*	*33.5*	*134*		
Stem	Observed	20	30	20	70	0.85	*NS*
	Expected	*23.33*	*29.17*	*17.5*	*70*		
Bone	Observed	23	28	21	72	0.675	*NS*
	Expected	*24*	*30*	*18*	*72*		
Full	Observed	9	23	7	39	4.81	*NS*
	Expected	*13*	*16.25*	*9.75*	*39*		
Pore	Observed	23	10	20	53	11.66	$p<0.01$
	Expected	*17.67*	*22.08*	*13.25*	*53*		
Non-pore	Observed	25	32	24	81	0.93	*NS*
	Expected	*27*	*33.75*	*20.25*	*81*		

4.3.4 Crack length

Median crack lengths were 0.18 mm, 0.42 mm and 0.38 mm in the thick/US, thin/UK and varus/UK groups, respectively. Differences between groups were not significant. See **Figure 4.6**.

Crack length normalised by local cement thickness was calculated for each crack. The median normalised crack lengths for the thick/US, thin/UK and varus/UK groups were 0.089, 0.302 and 0.300 respectively. The difference between thick/US and thin/UK groups was highly significant ($p = 0.002$), as shown in **Figure 4.6**.

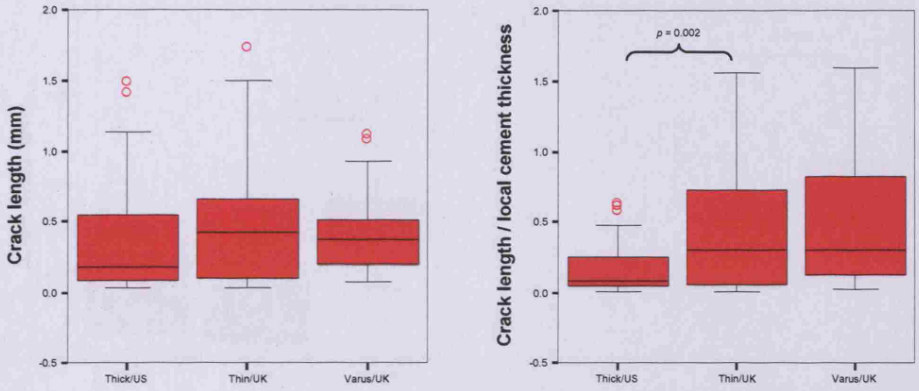

Figure 4.6. Box and whisker plots showing crack length (left) and normalised crack length (right) for each group.

4.3.5 Cracks in the distal mantle

In the cement surrounding only the distal 4 cm of the stem, median crack lengths were 0.19 mm, 0.07 mm and 0.38 mm in the thick/US, thin/UK and varus/UK groups, respectively. The differences between the thin/UK and varus/UK groups was significant ($p = 0.015$). Crack length normalised by local cement thickness was also calculated for each crack in the distal 4 cm of the mantle. The median normalised crack lengths for the thick/US, thin/UK and varus/UK groups were 0.093, 0.012 and 0.419 respectively. The difference between the thin/UK and varus/UK groups was significant ($p = 0.02$). See **Figure 4.7**.

For the thin/UK and varus/UK groups, cracks occurring in the distal 4 cm of the mantle are counted in **Table 4.2**. A chi-square test, examining the null hypothesis of equal numbers of cracks expected per femur, indicated that the poorly-centralised stem has more cement cracks than expected ($p < 0.05$).

4.3.6 Cracks in thin cement regions

Across all groups, the median length of cracks found in cement less than 1 mm thick was 0.51 mm. Thicker cement had a median crack length of 0.20 mm. This difference was significant ($p = 0.005$), as indicated in **Figure 4.8**.

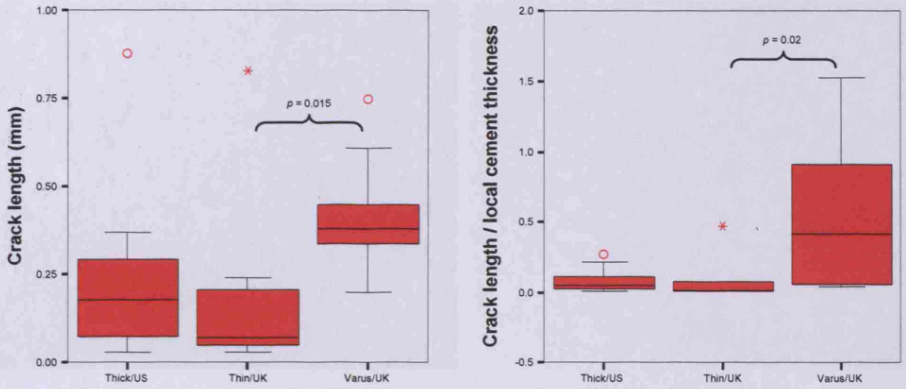

Figure 4.7. Box and whisker plots showing crack length (left) and normalised crack length (right), in the cement mantle around the distal 4 cm of the stem, for each group.

Table 4.2. Crack frequencies in distal 4 cm of the mantle, for the well- and poorly-centralised groups of *n* femurs. Chi-square test examines the null hypothesis of equal numbers of cracks expected per femur.

Cracks in group		**Thin/UK**	**Varus/UK**	**Total**	**Chi-square**	**Sig.**
n		*5*	*3*	*8*		
Cracks	Observed	7	11	18	4.28	$p < 0.05$
	Expected	*11.25*	*6.75*	*18*		

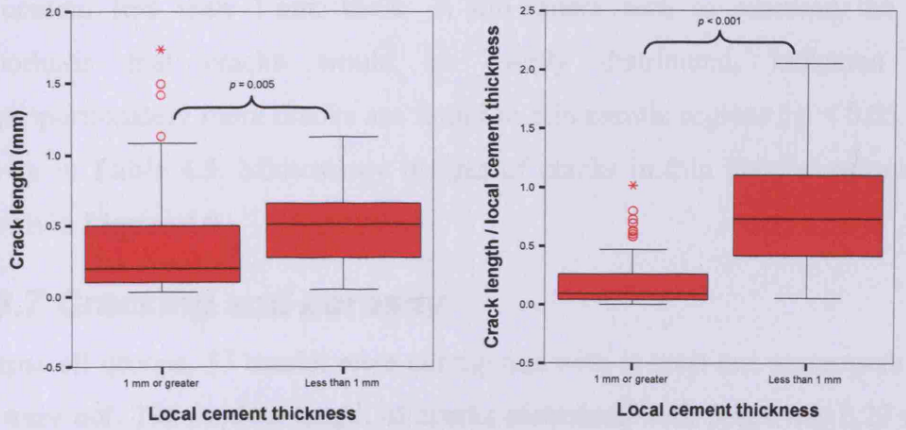

Figure 4.8. Box and whisker plots showing crack length (left) and normalised crack length (right), in cement locally measured as thick (1 mm or greater) and thin (less than 1 mm).

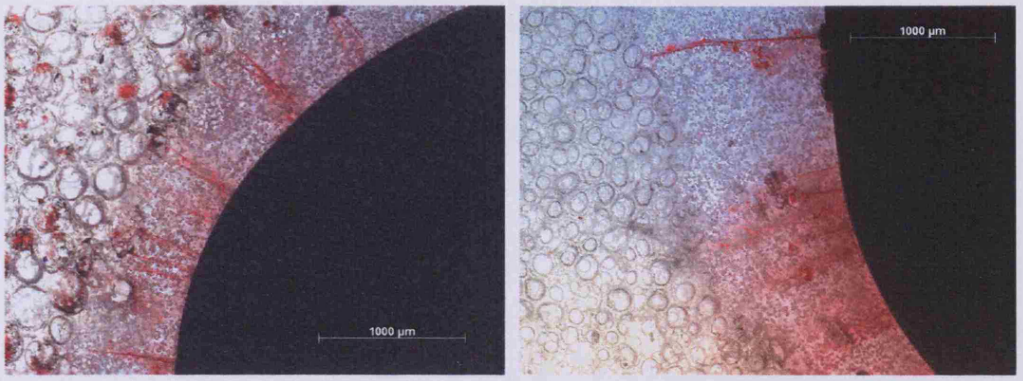

Figure 4.9. Cracks stained with dye penetrant and viewed under a microscope, showing many cracks, including full-thickness cracks, in thin mantle regions.

Table 4.3. Crack frequencies in cement locally measured as thick or thin. Chi-square test examines the null hypothesis of even crack distribution.

Cement thickness		< 1 mm	≥ 1 mm	Total	Chi-square	Sig.
Thickness measurements		176	1159	1335		
Cracks	Observed	34	100	134	17.40	$p < 0.01$
	Expected	*17.67*	*116.33*	*134*		

Cement thickness measurements of less than 1 mm comprised 13 percent of all thickness measurements, while 25 percent of all cracks occurred in cement less than 1 mm thick. A chi-square test, to examine the null hypothesis that cracks would be evenly distributed, indicated that disproportionately more cracks are found in thin mantle regions ($p < 0.05$), as shown in **Table 4.3**. Microscopy images of cracks in thin mantle regions are shown in **Figure 4.9**.

4.3.7 Cracking and porosity

Across all groups, 53 cracks were contiguous with at least one macropore and 81 were not. The median length of cracks associated with pores was 0.27 mm. Cracks not associated with pores had a median length of 0.55 mm. The difference between these categories was significant ($p < 0.001$). Crack length

normalised by local cement thickness was also significantly different between these two categories ($p < 0.001$), with cracks associated and not associated with pores having median normalised crack lengths of 0.144 and 0.332, respectively. See **Figure 4.10**.

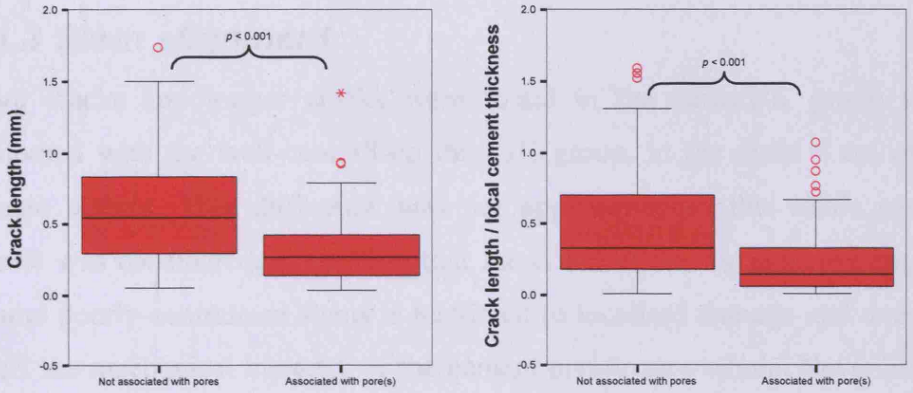

Figure 4.10. Box and whisker plots showing crack length (left) and normalised crack length (right) for cracks associated and not associated with macroporosity.

4.4 Discussion

4.4.1 Cement mantle thickness

The primary aim of this study was to investigate the effect of cement mantle thickness on cracking of the cement mantle. Significant differences in the proximal medial cement mantle thickness between the thick/US and thin/UK groups confirmed that cement thickness was effectively controlled by rasp size, within a clinically realistic range. Significant differences in the distal lateral thickness between the well- and poorly-centralised groups confirmed that cement thickness was effectively controlled by stem orientation.

4.4.2 Broach size

Although there was no significant difference between thick/US and thin/UK groups in terms of absolute crack length, when crack length was normalised by

locally-measured cement thickness the thick/US mantle had relatively shorter cracks, and this was significant. This concurs with the simpler torsional fatigue test findings of Hertzler *et al.* (2002) that crack growth is independent of cement thickness but that failure occurs sooner in thin mantles since the crack has less distance to travel.

4.4.3 Stem alignment

More cracks and longer cracks were found in the varus/UK group when compared with the well-centralised thin/UK group, in the distal 4 cm of the cement mantle. This difference was not apparent when the whole cement mantle was considered, suggesting that the effect of thin or defective regions around poorly-centralised stems is restricted to localised damage and does not affect the mechanical integrity of the cement mantle as a whole. Nevertheless, this is an important finding given that local cracking may be associated with lysis and failure, as indicated in the effective joint space scenario.

4.4.4 Local cement thickness

Significantly longer and proportionately more cracks were found in thin mantle regions, in agreement with clinical findings (Jasty *et al.* 1991; Jasty *et al.* 1992; Kawate *et al.* 1998; Koster *et al.* 1999). Rasp size alone did not have this effect, suggesting that control over local cement mantle thickness is more important than broach size in minimizing the risk of fatigue damage to the cement mantle. Good surgical technique, including the right choice of surgical approach and the use of effective centralisers where appropriate, are therefore likely to be of far greater clinical significance than design alterations to the surgical tooling.

4.4.5 Porosity

Whilst there was a significant difference between groups in terms of crack numbers, this difference is explained by the differing numbers of cracks associated with pores. We did not measure porosity levels directly, but it is conceivable that the thicker mantle might have experienced higher levels of

porosity, possibly due to lower pressurisation of the cement during insertion: pressurisation is known to increase strength (Guidoni and Vallo 2002) and fatigue resistance (Dunne *et al.* 2003; Freitag and Cannon 1977) by reducing porosity.

Nonetheless, cracks associated with pores were significantly shorter, did not traverse the full thickness of the cement, and generally followed a trajectory that was less straight than that of cracks remote from pores. This supports the viewpoint that pores either inhibit crack growth by crack-blunting and crack path deviation (Janssen *et al.* 2005b) or initiate cracks which are not particularly detrimental as they do not grow far. In either case, it is unlikely that differing levels of porosity between our experimental groups would have dramatically altered the mechanical integrity of the cement mantles.

4.4.6 Crack distribution

Cracks in all groups were widely and randomly scattered, and although many cracks appeared to originate at corners of the prosthesis, there was no obvious pattern to the distribution of cracks. In contrast, highly localised and extensive damage has been observed around sharp-cornered prostheses (Stolk *et al.* 2003a; Hertzler *et al.* 2002). It is likely that our choice of the Stanmore Hip – a smooth, rounded, clinically successful implant without major stress concentrators – renders comparison of crack distributions difficult due to the low level and diffuse nature of damage generated.

4.4.7 Limitations

The loading configuration used in this study was based on a peak stair climbing load. However, the magnitude of loading was double the physiological level and the combination of forces and constraints highly simplified to facilitate mechanical testing. These compromises were deemed necessary for two reasons. First, for technical and logistical reasons, periods of testing longer than several million cycles were not possible using hydraulic loading machinery available, necessitating the high load. This was the only way to

ensure sufficient measurable cracking of the cement for statistical analysis. Second, complex loading configurations including simulated muscle forces are difficult to apply, and have been attempted for gait loading (Britton *et al.* 2003; Cristofolini *et al.* 1995) but not for a stair-climbing setup.

In the next chapter, we describe the simulation of this experiment using a finite element method including damage accumulation. Such a model should facilitate the simulation of more realistic and complex loads, including muscle forces.

Chapter 5

Creep and damage accumulation

5.1 Introduction

In the previous chapter, fatigue testing was performed on synthetic femurs containing Stanmore Hips implanted into cement mantles of different thicknesses. Loading conditions represented a highly simplified approximation of a stair-climbing load. More appropriate, physiologically informed loading is difficult to apply experimentally, but may be easily applied to a finite element model. In Chapter 3, finite element models with different cement thicknesses were loaded with more physiological forces, but linear elastic stress analysis alone was not sufficient to allow us to differentiate between cement mantle thicknesses; creep and subsidence could alter these results significantly.

In this chapter, we use existing models for creep, damage accumulation and friction to model the material behaviour and interfacial characteristics of Palacos-R bone cement around a Stanmore Hip stem. Initially, a simple, axisymmetric finite element model is used to assess whether an existing creep algorithm and friction formulation adequately represents the subsidence characteristics of a satin-finish stem in a Palacos-R cement mantle. A finite element simulation of the fatigue test described in the previous chapter is then performed to assess the validity of a damage accumulation algorithm combined with the same creep and friction parameters.

5.2 Materials and methods

5.2.1 Cement creep and damage behaviour algorithm

The material behaviour of bone cement was modelled using a finite element approach combined with a Maxwell creep model and a three-dimensional continuum damage mechanics model. These algorithms were described in detail by Stolk *et al.* (2004), and implemented as MARC subroutines written by Jan Stolk and extensively tested and validated for comparative preclinical implant testing (Stolk *et al.* 2003a; Stolk *et al.* 2007). A brief explanation follows, as summarised in **Figure 5.1**.

It would be computationally impractical to simulate millions of loading cycles individually. Instead, a quasi-static load is applied representing the peak load, and the laws determining creep and damage properties for bone cement are derived from cyclic testing. Each iteration timestep thus represents many load cycles, and is varied in order to ensure a stable solution at minimal computational cost.

Creep strain and damage tensors are monitored at each integration point, and both are set to zero at the start of analysis. At the beginning of each increment, the FE code assembles the stiffness matrix and calculates the stress and elastic strain at each integration point.

At each integration point, the equivalent creep strain increment $\Delta\varepsilon^{c}_{eq}$ during timestep Δn is calculated based on the equivalent stress σ_{eq} and the existing equivalent creep strain ε^{c}_{eq} after n cycles,

$$\Delta\varepsilon^{c}_{eq} = 7.985\times10^{-7} \cdot (n+\Delta n)^{0.4113 - 0.116 \log \sigma_{eq}} \cdot \sigma_{eq}^{1.9063} - \varepsilon^{c}_{eq} , \quad (5.1)$$

based on the experimental data of Verdonschot and Huiskes (1995). The incremental creep strain tensor $\Delta\varepsilon^{c}_{ij}$ is then scaled from the equivalent creep strain increment, based on the stress tensor σ_{ij} ,

$$\frac{\Delta\varepsilon^{c}_{ij}}{\Delta\varepsilon^{c}_{eq}} = \frac{\partial\sigma_{ij}}{\partial\sigma_{eq}} , \quad (5.2)$$

and the new creep strain tensor $\varepsilon^{c}_{ij\,(n+\Delta n)}$ is the sum of the old and incremental creep strain tensors,

$$\varepsilon^{c}_{ij\,(n+\Delta n)} = \varepsilon^{c}_{ij\,(n)} + \Delta\varepsilon^{c}_{ij} \ . \tag{5.3}$$

A creep timestep Δn^{c} is selected each iteration such that the equivalent creep strain increment cannot exceed 5% of the equivalent creep strain at any integration point.

Damage accumulation at each integration point is represented as tensor rotated to local principal stress axes, where only the trace values are nonzero. The incremental damage tensor ΔD_{ii} is calculated as

$$\Delta D_{ii} = \left(\frac{n_i+\Delta n_i}{N_{fi}}\right)^{3.92} - D_{ii} \ , \tag{5.4}$$

where D_{ii} is the total damage tensor, and where the number of cycles to failure N_{fi} is related to the corresponding principal stress σ_i by the S-N curve

$$N_{fi} = 10^{(37.8-\sigma_i)/4.736} \ , \tag{5.5}$$

provided that the principal stress is tensile. This was derived experimentally by Murphy and Prendergast (1999). The new damage tensor $D_{ii\,(n+\Delta n)}$ is the sum of the old and incremental damage tensors,

$$D_{ii\,(n+\Delta n)} = D_{ii\,(n)} + \Delta D_{ii} \ . \tag{5.6}$$

The trace values of the total damage tensor cannot exceed 1.0, and a damage-based timestep Δn^{d} is selected for each iteration such that the total damage at any integration point does not exceed this level. The smaller of the two timesteps, Δn^{c} and Δn^{d}, is used.

The stiffness matrix is unaffected by (micro)damage accumulation until one of the local principal damage values reaches a critical level of 0.75. Then, a (macro)crack forms, in the plane normal to the corresponding principal damage direction. Crack formation forces the material to behave anisotropically, reducing the elastic modulus and two shear moduli normal to the crack plane to almost zero. Whilst the local damage tensor is aligned with the changing principal stress axes, formation of the first crack fixes the first local

damage axis and the second crack fixes the second damage axis; three orthogonal cracks are possible at each integration point.

Once the creep strain and damage tensors and the stiffness matrix have been updated, the next iteration begins at time $n+\Delta n$. Iterations continue until the desired number of loading cycles has been reached.

Figure 5.1. Iteration scheme used in cement creep/damage simulation. Adapted from Stolk *et al.* (2004).

5.2.2 Creep and subsidence test

Six conically-tapered implants were manufactured, of length 100 mm, taper angle 8 degrees and distal diameter 10 mm. Four were fabricated from cobalt chromium (CoCrMo) alloy and two from surgical stainless steel. The CoCrMo implants were surface treated by Biomet UK using vapour-blasting to provide a 'satin finish' identical to that of the Stanmore Hip. The steel implants were

polished to give a smooth finish similar to that used by Verdonschot and Huiskes (1996b), on whose experimental setup this test is based. The satin CoCrMo and polished steel tapers had mean surface rugosities (R_a) of 174 (± 36) nm and 48 (± 14) nm respectively, measured at 24 locations per taper, using a 'Talysurf 10' profilometer (Taylor Hobson Ltd., Leicester, UK).

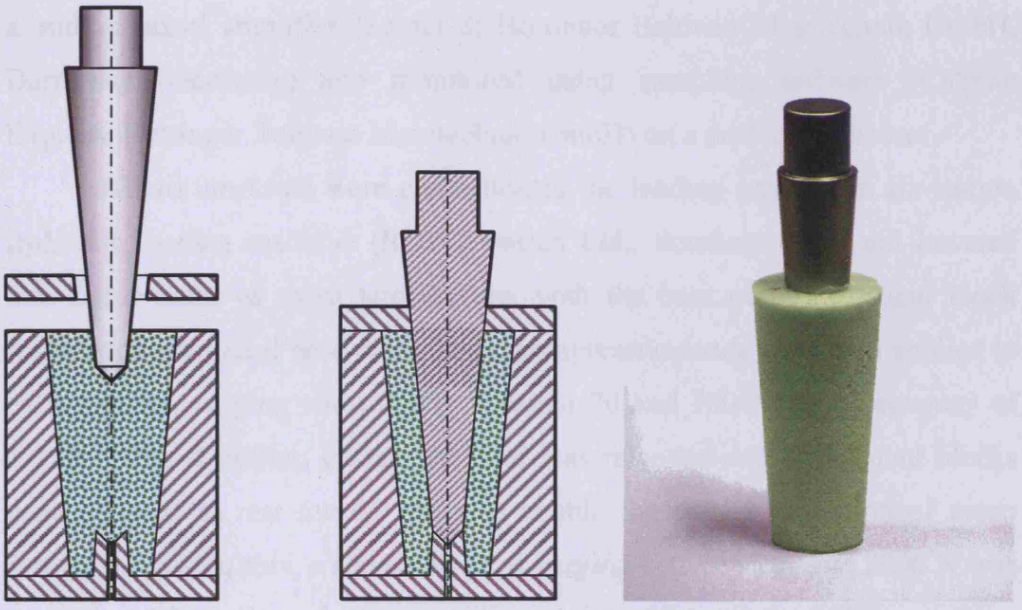

Figure 5.2. Fabrication of conical test samples, showing insertion of the tapered implant to the cement-filled mould casing (left) and the finished product (right).

Cement mantles with a uniform 10 mm thickness were cast around the implants from Palacos-R bone cement, using a 'third generation' mixing technique. The monomer and powder components were mixed within a few minutes of removing from refrigeration at 5°C. An Optivac mixing gun (Biomet, Inc., Warsaw, Indiana) was used to vacuum-mix and inject the cement, in a retrograde fashion, into a tapered steel casing coated with mould release agent. Once the casing was filled with cement, the conical implant was inserted by hand through a hole in the casing lid and pushed through the cement in an axial direction until it came to rest against the conical centralising notch in the base of the casing, as indicated in **Figure 5.2**. The insertion force

was maintained until the cement had cured. Afterwards, the casing was removed, leaving the implant embedded in a block of bone cement, as shown in **Figure 5.2**. This was then aged for 48 hours in water at 37 °C.

Displacement transducers with a 10 mm linear range were fixed between the implants and the base of the testing station, to measure the axial displacement of the implant, as shown in **Figure 5.3**. These were connected to a multi-channel amplifier (Spider-8; Hottinger Baldwin Messtechnik GmbH, Darmstadt, Germany) and monitored using sampling software (Catman Express; Hottinger Baldwin Messtechnik GmbH) on a desktop computer.

All six implants were connected to the loading heads of a six-station hydraulic loading machine (RDP Howden Ltd., Southam, UK) and lowered into saline baths at room temperature, with the base of each cement block resting against a steel base plate. Axial compressive loads were then applied to each implant, varying sinusoidally between 70 and 700 N, at a frequency of 1.0 Hz. After 4 million cycles, the load was removed and the cement blocks were allowed to rest for 48 hours to enable the partial relaxation of creep strains. Following this, a sinusoidal load varying between 200 and 2000 N was applied at 1.0 Hz for a further 4 million cycles. After another 48 hour resting period, a sinusoidal load of 300 to 3000 N was applied for 2 million cycles.

Figure 5.3. Instrumented test sample in saline bath. Loading head raised for clarity.

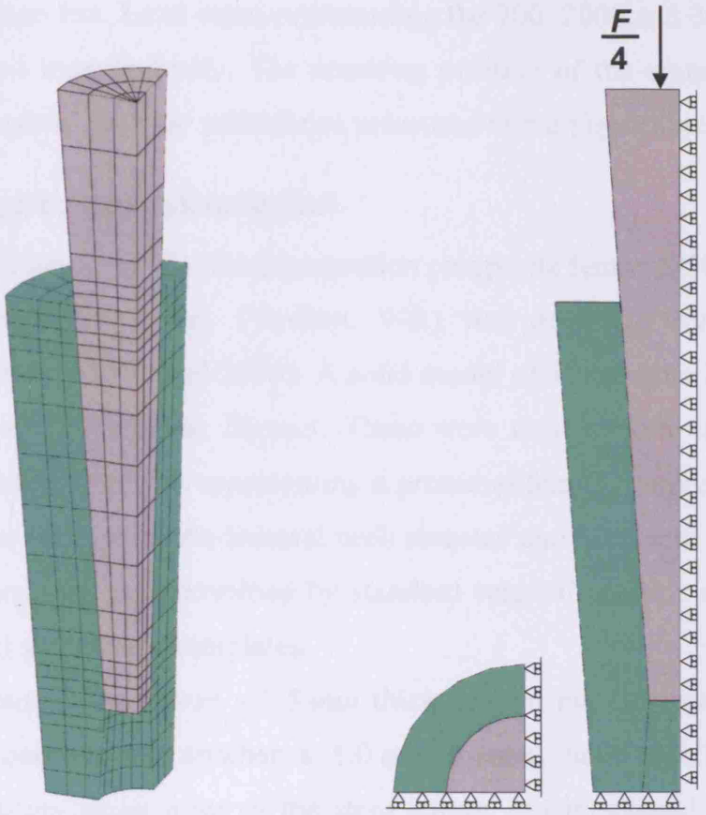

Figure 5.4. Finite element mesh of a quarter of the conical test sample (left), and a schematic of the boundary conditions applied (right).

5.2.3 Creep and subsidence simulation

A finite element mesh representing one quarter of the creep/subsidence test sample was constructed using 774 eight-noded linear brick elements. The Young's modulus for the metal implant and bone cement block were 220 GPa and 2.7 GPa respectively, and the Poisson's ratio was 0.3 for both materials. The bone cement material behaviour algorithm described above was used to simulate viscoelastic creep of the cement. The implant-cement interface was modelled with a stick-slip Coulomb friction formulation, using a friction coefficient of 0.25. Mesh geometry and simplified boundary conditions are shown in **Figure 5.4**.

A vertical compressive force was applied to nodes on the top surface of the taper, adding up to one quarter of the peak cyclic load applied in the

creep/subsidence test. Load cases representing the 700, 2000 and 3000 N loads were simulated independently. The resulting position of the metal taper over time was compared with the subsidence measured in the physical test.

5.2.4 Fatigue test simulation

An IGES solid model of the 'third generation composite femur #3306' made by Pacific Research Labs, Inc. (Vashon, WA) was acquired from the BEL repository (Papini and Zalzal 2003). A solid model of a Stanmore Hip femoral component was provided by Biomet. These were used to form the basis for three finite element meshes representing a proximal femur comprising cortical and cancellous bone, with the femoral neck resected and Stanmore Hip femoral components inserted as determined by standard surgical practice and with the aid of surgical stem sizing templates.

One model was given a 2.5 mm thick cement mantle surrounding the femoral component, and another a 1.0 mm mantle; both mantles were of uniform thickness along most of the stem length, but broadened near the tip due to the medullary canal geometry. A third model mimicked the 1.0 mm-thick mantle model, but the stem was tilted into varus, narrowing the lateral cement thickness to 0.1 mm near the stem tip. The cement layer surrounding the stem was three elements thick everywhere in all three models. Mesh structure and distribution of material properties are indicated in **Figure 5.5**.

Each mesh comprised of 4304 eight-noded brick elements with material properties assigned as in **Table 5.1**. All materials were considered isotropic and were representative of the properties of a 'third generation composite femur #3306' bone analogue (Pacific Research Labs, Inc.). The stem-cement interface was modelled as fully debonded, using a Coulomb stick-slip friction formulation with a friction coefficient of 0.25.

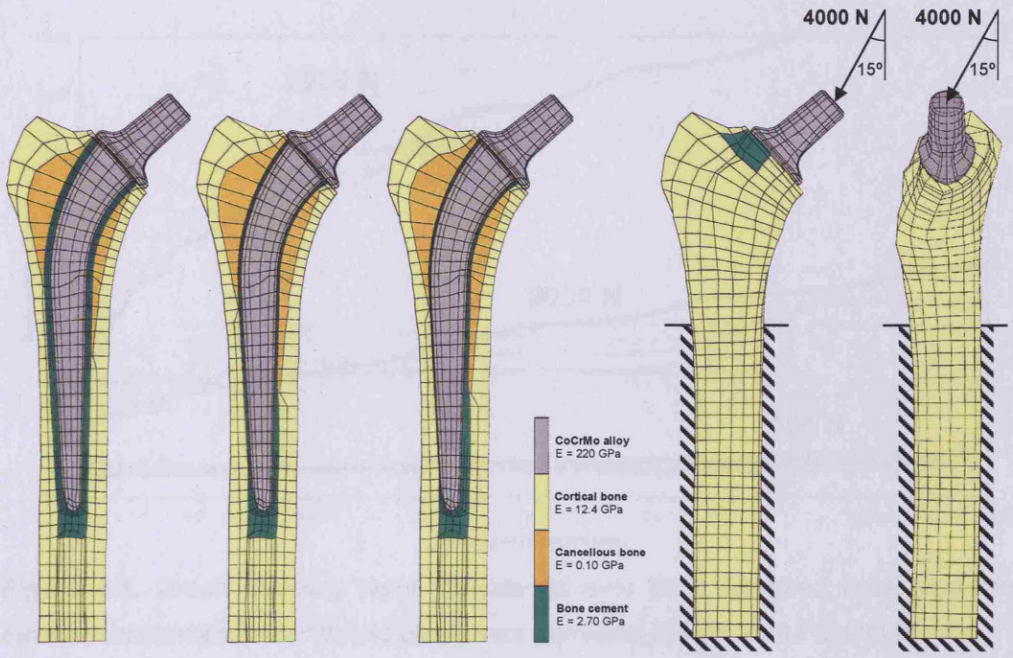

Figure 5.5. Finite element meshes of the implanted composite femur, showing (left to right) sections through the thick/2.5mm, thin/1.0mm and varus/1.0mm models, with material properties indicated, and frontal and lateral projections of the loading and boundary conditions applied.

Table 5.1. Numbers of elements of each material type in the three models.

Model	Number of elements in each material set			
	Cortical bone	Canc. bone	Bone cement	CoCr implant
Thick/2.5mm	1156	164	1640	1344
Thin/1.0mm	1086	234	1640	1344
Varus/1.0mm	1086	234	1640	1344

Creep strain and damage accumulation in the cement were simulated over 20 million cycles using the creep/damage subroutines described above. Load and boundary constraints were applied representing the loading setup of the fatigue test described in the previous chapter, as indicated in **Figure 5.5**.

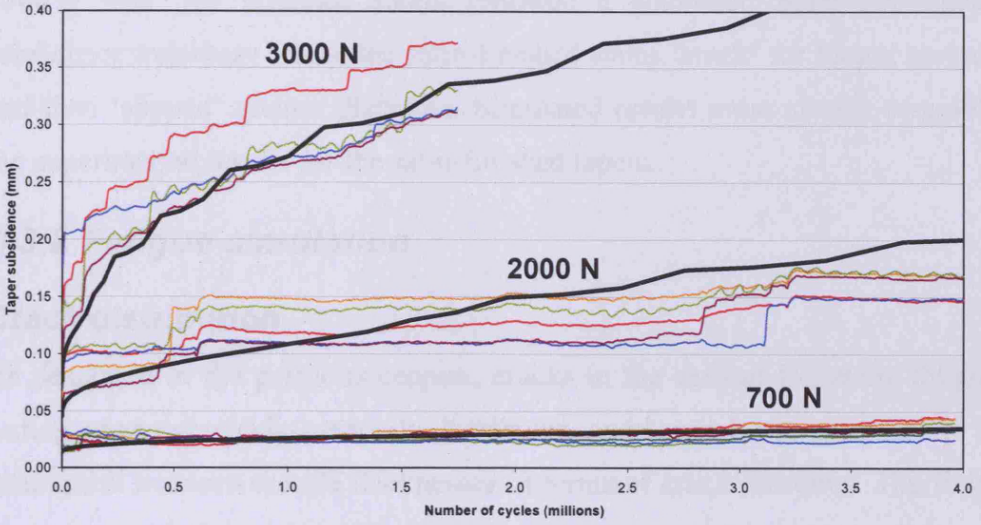

Figure 5.6. Graph showing taper subsidence over time. Coloured lines represent experimental measurements and black lines represent results from FE simulations.

5.3 Results

5.3.1 Creep and subsidence

Peak axial displacements under each of the three applied loads are plotted over time in **Figure 5.6**, for both the creep/subsidence experimental test samples and the finite element simulations. There is reasonable agreement between measured and computed results, simulated subsidence falling mostly within the range of the experimental data.

Subsidence appears to be predominantly through creep at 700 N, and predominantly through interfacial slipping at 3000 N. Under the 2000 N load, neither mechanism seems dominant, but the high sensitivity of subsidence rates to slight fluctuations (approximately ±5%) in the peak applied load indicates that this level of loading may represent a transition between 'sticking' and 'slipping' behaviour. The simulated results showed similar stick-slip characteristics to those measured experimentally.

Both the polished (shown in **Figure 5.6** as blue and purple lines) and satin-finish stems showed similar levels of subsidence. However, under the

3000 N load, the polished stems followed a smoother, more continuous subsidence trajectory whilst the satin-finished stems 'stuck' for longer periods and then 'slipped' greater distances. Simulated results more closely resemble the experimental results for the satin-finished tapers.

5.3.2 Fatigue simulation

Crack distribution

As described in the previous chapter, cracks in the cement following fatigue testing appeared widely randomly distributed, and hence it was not possible to distinguish between mantle thicknesses in terms of crack locations. The finite element simulations showed crack distributions which were much more consistent between different mantle thicknesses. Considering both the similarities seen between simulated crack locations and the scatter seen in fatigue test results, no direct comparison was possible between mantle thicknesses on the basis of crack location.

Through-thickness cracks were defined as collections of cracked integration points forming a continuous link between stem-cement and cement-bone interfaces. The locations of simulated through-thickness cracks corresponded to those of full-thickness cracks seen in some of the sections from the fatigue tests, shown in **Figure 5.7**. The variability in the locations of cracks seen in the fatigue test specimens prevented systematic comparison between finite element and experimental results. Nonetheless, close similarity in the locations of large and through-thickness cracks was observed between finite element simulations and some of the fatigue test specimens, as indicated in **Figure 5.7**.

Crack numbers and lengths

The total number of cracks occurring in each finite element simulation was recorded over time. This is shown in **Figure 5.8**, normalised by the total number of cracks possible (39360), i.e. the total number of cement elements (1640) multiplied by the number of integration points per element (8)

multiplied by the number of cracks possible per integration point (3). Since the cement mantles were all three elements (six integration points) thick, this quantity is effectively scaled to the cement mantle thickness. For comparison, the measured crack lengths reported in the previous chapter are presented in **Figure 5.9**, also normalised by cement mantle thickness.

These results show near-identical levels of cracking in the thin/1.0mm and varus/1.0mm simulations. Corresponding near-identical median normalised crack lengths are reported for the thin/UK and varus/UK fatigue test groups (0.302 and 0.300, respectively). The thick/2.5mm simulation exhibits a cracking level less than half that of the thin/1.0mm model. Median normalised crack length for the thick/US fatigue test group is around one third that of the thin/UK group (0.089 versus 0.302).

The normalised number of cement cracks multiplied by the total cement volume is also plotted for each model in **Figure 5.10**. This measure compensates for the different through-thickness mesh densities between models, and can therefore be compared to absolute crack lengths reported in the previous chapter. These are shown in **Figure 5.11**.

These results indicate similar levels of cracking in all three models, although slightly lower in the thick/2.5mm model over much of the simulation. Correspondingly, there is no significant difference between the three experimental groups in terms of crack length, although the thick/US group does have a lower median crack length.

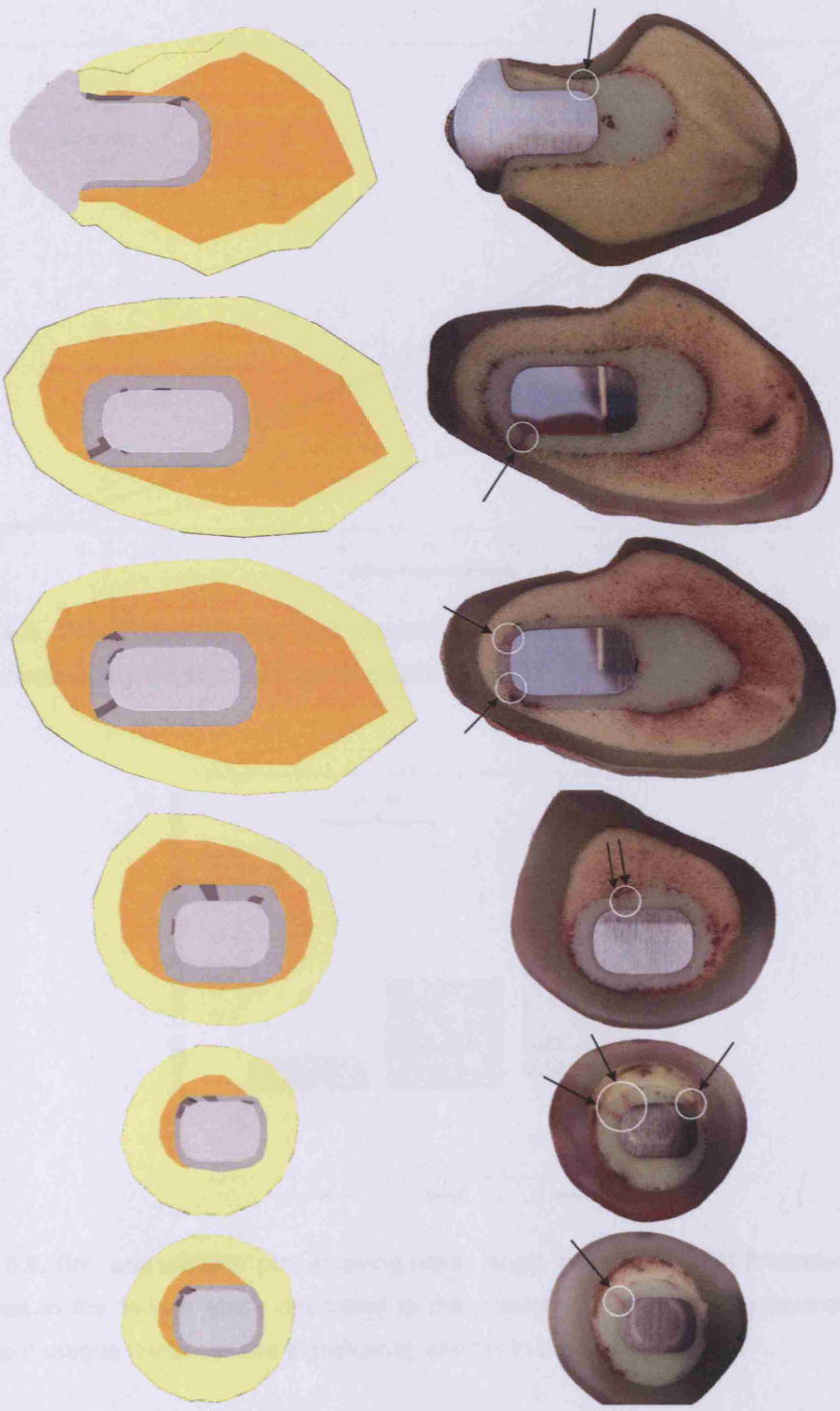

Figure 5.7. Some representative sections from the finite element simulation (left) after 20 million cycles, and the fatigue study described in the previous chapter (right). Cracked integration points are shown in dark grey. Arrows indicate full-thickness fatigue cracks.

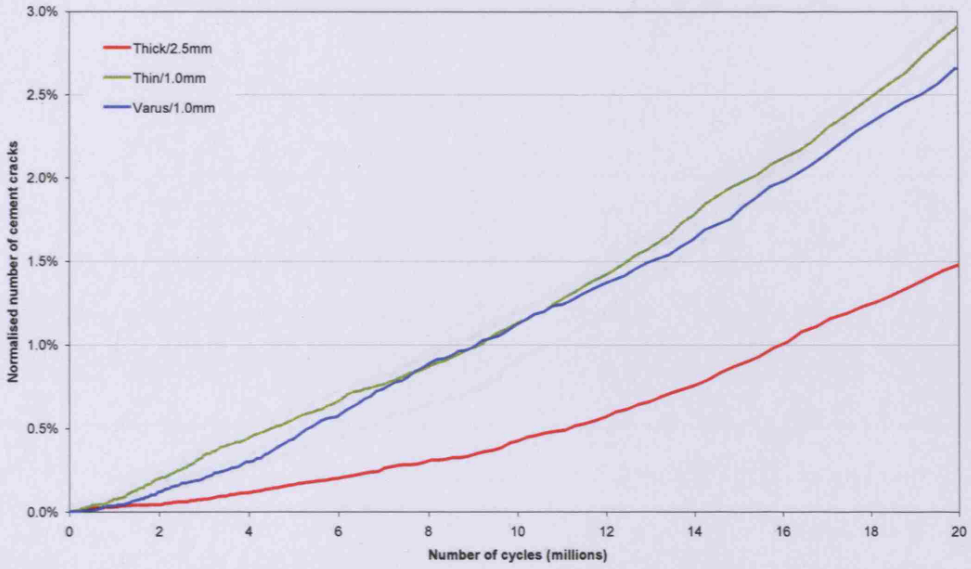

Figure 5.8. Graph showing the total number of cracks in each cement mantle over time, normalised by the total number of cracks possible.

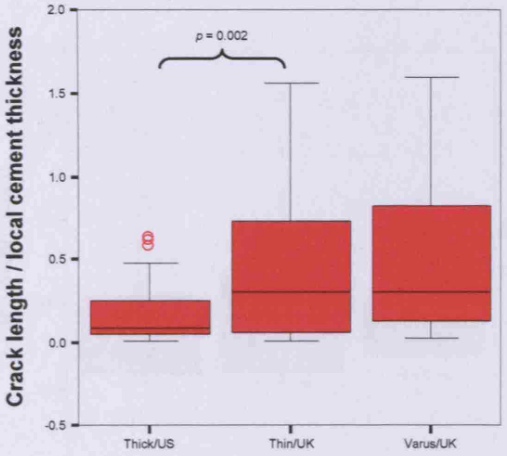

Figure 5.9. Box and whisker plot showing crack length per unit cement thickness, as measured in the fatigue study described in the previous chapter. Cracks normalised by cement mantle thickness are significantly shorter in the thick/US group.

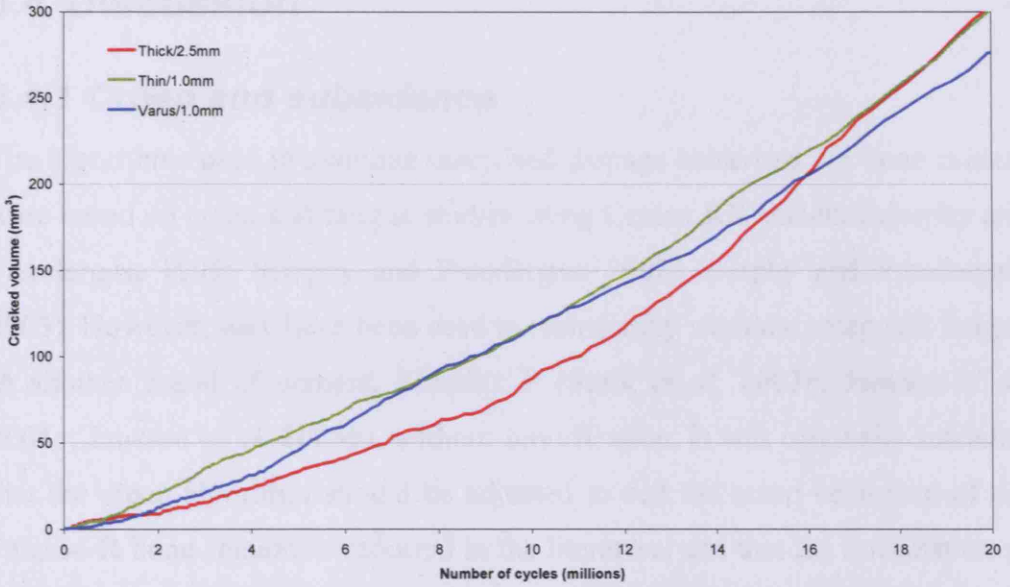

Figure 5.10. Graph showing the 'cracked volume' in each cement mantle over time, where cracked volume is the normalised crack number multiplied by the total cement volume.

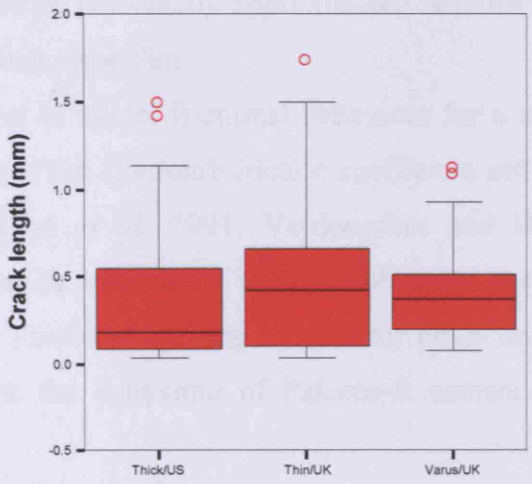

Figure 5.11. Box and whisker plot showing crack lengths from the fatigue test in the previous chapter, with no significant difference between thick/US, thin/UK and varus/UK groups.

5.4 Discussion

5.4.1 Creep and subsidence

The algorithms used to simulate creep and damage behaviour for bone cement were based on creep and fatigue studies using Cemex RX cement (Murphy and Prendergast 1999; Murphy and Prendergast 2002; Murphy and Prendergast 2003). However, they have been used to realistically simulate creep and fatigue in another brand of cement, Simplex P (Stolk *et al.* 2003b; Janssen *et al.* 2005c; Janssen *et al.* 2005b), without modification. It was originally intended that the creep algorithm should be adjusted to suit the creep behaviour of the Palacos-R bone cement as reported in the literature, and that the formulation of frictional behaviour for the satin-finished stem be informed, if necessary, by the experimental data. However, given the similarity between subsidence levels measured experimental and predicted computationally, it was decided that the creep and frictional behaviour of the Palacos-R bone cement around a Stanmore Hip could be reasonably approximated without modifications to the previously-used creep algorithm.

The decision to model frictional behaviour for a satin-finished cobalt-chrome stem using to the Coulomb friction coefficient established for polished steel implants (Mann *et al.* 1991; Verdonschot and Huiskes 1996b) was justified by the similar subsidence rates we observed for polished and satin-finished implants. Thus, the existing models for creep and interfacial friction adequately describe the behaviour of Palacos-R cement around a Stanmore Hip.

Cement blocks were re-used for each successive cyclic loading test, rather than replacement by fresh samples for every test. This was deemed acceptable since the measured subsidence at the end of each test (once the load had been reduced to zero) was a small fraction of that achieved within the first few cycles of the subsequent, more aggressive test. Therefore, the influence of the 700 N loading on the subsequent 2000 N test results, or of the 2000 N

loading on the 3000 N test results, is likely to be small. After each loading period, one cement block was removed, sectioned at 5 mm intervals and stained with dye penetrant to reveal cracks; none were found in any case.

5.4.2 Fatigue simulation

The finite element simulation correctly predicts similar cracking levels in all three mantles, and lower cracking levels in the thick/2.5mm mantle as a proportion of the cement volume, in agreement with experimental crack length measurements. This corroborates the finding that crack growth rates in torsional loading are independent of cement thickness but that cracks would therefore traverse a thin mantle sooner (Hertzler *et al.* 2002). Our model is loaded predominantly in torsion, since the rigid boundary constraint applied to the femur prevents significant bending. This was necessary to mimic the fatigue test setup, but more realistic boundary conditions including muscle loading are used in the next chapter. It is possible that more physiological loading including a significant bending component would lead to differing crack growth rates between cement mantles.

The diffuse nature of the cracking observed following fatigue testing prevented systematic comparison between experimental and computed results, although many of the larger and through-thickness cracks simulated could be identified on sections from the fatigue test specimens. The variability in experimental fatigue test results prevented differentiating between cement mantle thicknesses on the basis of crack distribution; such a comparison of simulated results was also impeded by the similarity of crack distributions between mantle thicknesses.

Stolk (2003a) records an underestimation of damage levels by his creep/damage algorithms, noting that the timescale appears to be out by factor of ten; our results concur with this: damage patterns simulated at 20 million cycles appear comparable to those measured after 4 million cycles of fatigue testing. Roques *et al.* (2004) suggest that the omission of residual cement stresses (arising from curing and thermal shrinkage) from the simulation may

account for this timescale error. Nevertheless, timescale notwithstanding, the reasonable comparative results of Stolk *et al.* (2003a; 2004; 2007) suggest that this model can be used for comparative purposes. However, it is worth bearing in mind that the data from Stolk *et al.* are based on very different prostheses with clinical outcomes ranging from excellent to disappointing, whilst our study is concerned with differences to the mantle of one clinically excellent prosthesis.

Porosity is also known to affect the fatigue behaviour of cement (Ishihara *et al.* 2000; Murphy and Prendergast 2002), but the principal difficulty in including porosity in a predictive fatigue model is that whilst the effect of porosity on tensile specimens is dramatic, physiological stresses and the resulting crack propagation in cement mantles are affected primarily by pore location rather than the level of porosity (Janssen *et al.* 2005c; Janssen *et al.* 2005b). Thus, a probabilistic/stochastic approach is required to take account of the many possible pore distributions (Jeffers *et al.* 2005a). Research into such a model is at an early stage, having been recently investigated by Jeffers *et al.* (2007a) for a simplistic two-dimensional model; such an approach is likely to be incorporated into future models as computational power allows. To do so would be beyond the scope of this study, but would allow variability in fatigue test results to be represented computationally. The method used in this study provides a reasonable comparative test (Stolk *et al.* 2003a; Stolk *et al.* 2004; Stolk *et al.* 2007) but would not reproduce this variability.

Crack propagation rates are known to be dependent on mesh density, finer mesh sizes encouraging faster crack growth at stress concentrators such as prosthesis corners where high stress gradients occur. However, the Stanmore Hip is a smooth-cornered implant without major stress concentrators, so this factor is unlikely to have any major impact on our results. Furthermore, the independently-developed creep/damage algorithms of both Stolk *et al.* (2003b) and Jeffers *et al.* (2003) show reliable crack growth rates in mesh sizes similar to those used in our study, which are also very close to those used in previous

studies (Stolk *et al.* 2003a; Stolk *et al.* 2004; Stolk *et al.* 2007). In fact, the only region of the cement mantle likely to have suffered exaggerated damage due to its higher mesh density is very thin lateral region near the stem tip in the varus/1.0mm model, where the elements approach a critical size expected to promote exaggerated cracking rates (Stolk *et al.* 2003b); we recorded very little damage in this region, suggesting that this is not a problem.

5.5 Conclusion

Finite element-based creep and damage algorithms have previously been shown to realistically simulate damage accumulation in cement mantles around the femoral components of hip replacements, enabling comparative preclinical testing. Although developed for another brand of cement, we have shown that an existing creep/damage model, combined with frictional parameters for polished stems, accurately predicts creep and subsidence for a satin-finish Stanmore Hip in a Palacos-R cement mantle. Furthermore, this model correctly predicts very similar levels of cracking in cement mantles of different thicknesses, as measured experimentally in the previous chapter. However, porosity and residual stress are omitted from this model, explaining why the high degree of variability in fatigue crack distribution is not simulated and why the timescale for crack propagation is inaccurate.

Chapter 6

Parametric damage simulation

6.1 Introduction

6.1.1 Loading configuration

In Chapters 4 and 5, we first measured and then simulated crack propagation in the cement mantles around Stanmore Hips under a loading configuration representative of a simplified stair-climbing load. This loading configuration had some major modifications to facilitate substantial, measurable damage within a reasonable timeframe and without damage to the synthetic femur: notably, an over-constrained proximal femur with only an exaggerated hip joint contact force applied. In the current chapter, a more physiologically relevant test setup is used, with a stair-climbing load incorporating muscle forces and more realistic bone material properties. We have thus far been concerned with stair-climbing loads only, since these are known to be particularly detrimental to the cement mantle (Stolk *et al.* 2002). In this chapter, we also consider gait loading for comparative purposes, since this comprises the majority of load cycles experienced by the cement mantle and has been widely used in other stress analyses and fatigue simulations of the cement mantle.

6.1.2 Debonding

The role of the interfacial bond between stem and cement upon implant fixation is poorly understood. Clinically, rough stems designed to remain bonded have tended to perform worse than smooth stems of similar geometry (Collis and Mohler 2002; Collis and Mohler 1998; Datir and Wynn-Jones

2005; Datir *et al.* 2006; Della Valle *et al.* 2005; Hinrichs *et al.* 2003), although some have performed well (Harris 1998). Debonding of the stem-cement interface has been observed by some to increase peak cement stress levels (Harrigan and Harris 1991; Verdonschot and Huiskes 1997b; Chang *et al.* 1998), whilst others have observed the opposite effect (Wheeler *et al.* 1997; Massin *et al.* 2003). It is likely that the effect of stem-cement debonding on the stress or damage sustained by the cement mantle is affected by a range of factors related to stem design, cement geometry and load configuration.

6.1.3 Collar

One such factor is the presence of absence of a collar. Contact between a collar and the medial calcar has been shown to increase bone stress and reduce cement stress proximally (Crowninshield *et al.* 1980; Lewis *et al.* 1984; Fagan and Lee 1986a; Prendergast and Taylor 1990; O'Connor *et al.* 1996). Whilst work in previous chapters has concerned the Stanmore Hip, a 'shape-closed' design, we shall also consider a modified collarless version of the Stanmore, representative of a double-tapered 'force-closed' design. This should delineate between those observations which apply specifically to stem designs equivalent to the Stanmore Hip and those which are also applicable to collarless types of stem design.

6.1.4 Objectives

The study described in this chapter aims to investigate the effects of cement mantle thickness and centralisation on damage to the cement mantle around a femoral component with or without a proximal collar, where the stem-cement interface is bonded or debonded, under simulated stair-climbing and gait loads. To estimate the likely effects of stem design and cement geometry on bone resorption due to stress-shielding, the stress in the medial calcar is also investigated under simulated gait loading.

6.2 Materials and methods

6.2.1 Mesh generation

Six finite element models were constructed based on solid models of a Stanmore Hip femoral component and a Standard Femur. Surgical size guide templates were used to ensure correct prosthesis size and alignment. Two models were developed with a 2.5 mm ('thick') and a 1.0 mm ('medium') cement mantle around the implant, and a third where the stem within the 1.0 mm mantle was tilted into varus, as explained in the previous chapter. Collarless versions of the 'thick/2.5 mm' and 'medium/1.0 mm' models were also generated. Lastly, a sixth model, with an oversized (size 3) Stanmore Hip in a 'thin' (0.5 mm) mantle was created. The main characteristics of each mesh are summarised in **Table 6.1**, and their respective stem and cement mantle geometries are indicated in **Figure 6.1**. The minimum cement element edge lengths were 0.49, 0.31, 0.15 and 0.09 mm in the thick/2.5 mm, medium/1.0 mm, thin/0.5 mm and varus/1.0 mm mantles, respectively. Maximum cement element size was 10.5 mm in all cases.

Table 6.1. Mesh properties for each finite element model

Model descriptor	Nominal cement thickness	Stem size	Number of elements of each material			
			CoCr stem	PMMA cement	Cancellous bone	Cortical bone
Thick/2.5mm	2.5 mm	2	1344	1640	164	1156
Thick/2.5mm without collar	2.5 mm	2	1296	1640	164	1156
Medium/1.0mm	1.0 mm	2	1344	1640	234	1086
Medium/1.0mm without collar	1.0 mm	2	1296	1640	234	1086
Varus/1.0mm	1.0 mm	2	1344	1640	234	1086
Thin/0.5mm	0.5 mm	3	1904	1640	164	1092

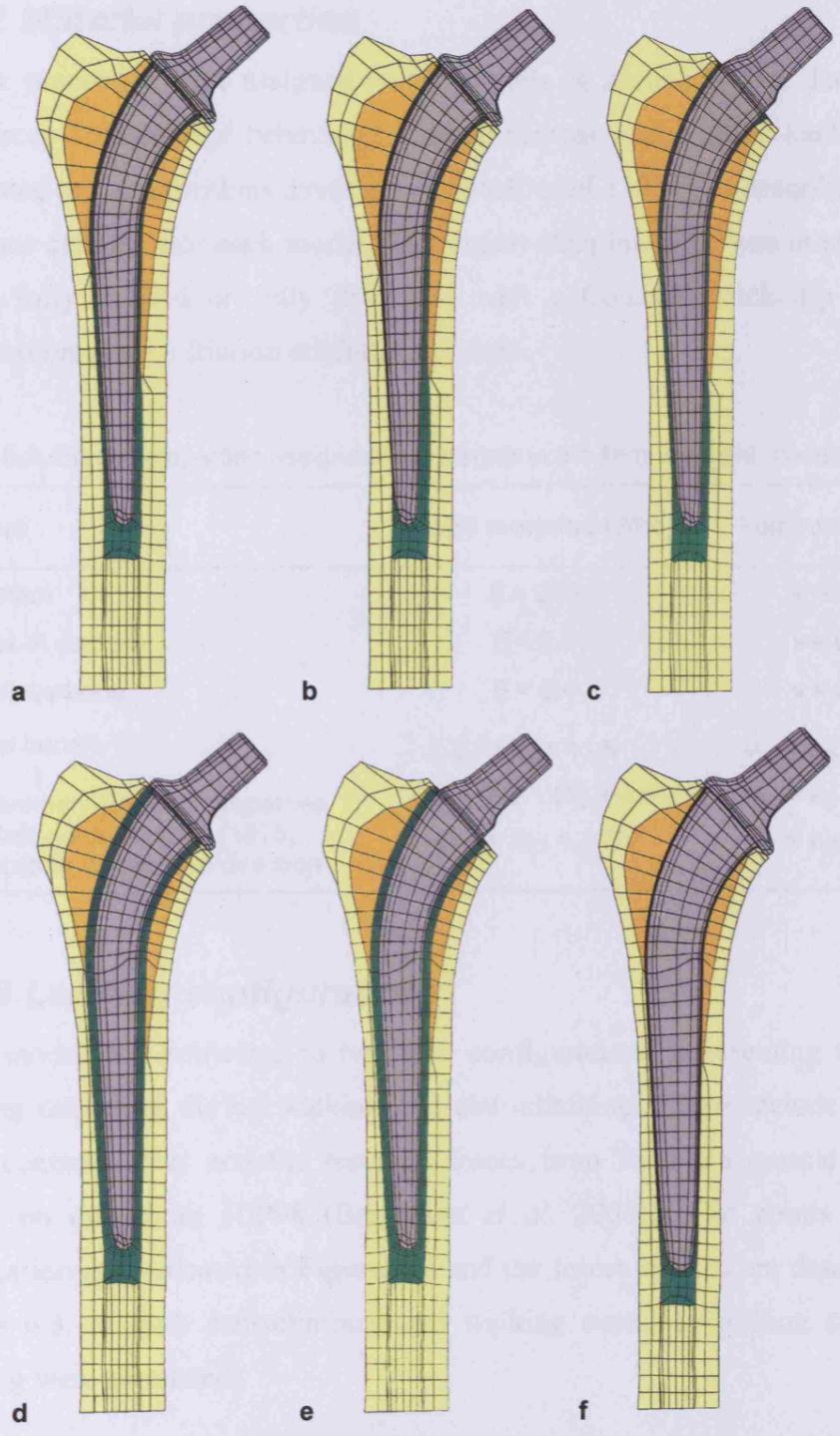

Figure 6.1. Sections through the finite element meshes, showing the different cement mantle and stem geometries. (a) Medium/1.0 mm; (b) Varus/1.0 mm; (c) Medium/ 1.0 mm without collar; (d) Thick/2.5 mm; (e) Thick/2.5 mm without collar; (f) Thin/0.5 mm.

6.2.2 Material properties

Elastic properties were assigned to the models as summarised in **Table 6.2**. The creep and damage behaviour of bone cement under cyclic loading was simulated using algorithms developed by Stolk *et al.* (2004), as described in the previous chapter. For each model, the cement-stem interface was modelled as either fully bonded or fully debonded with a Coulomb stick-slip friction formulation using a friction coefficient of 0.25.

Table 6.2. Elastic properties assigned to materials in the finite element models

Material	Elastic modulus (GPa)	Poisson's ratio
CoCr stem	$E = 220$	$v = 0.3$
Palacos-R cement	$E = 2.7$	$v = 0.3$
Cancellous bone	$E = 0.4$	$v = 0.3$
Cortical bone*	$E_1 = E_2 = 11.5$	$v_{12} = v_{21} = 0.58$
*Transversely-isotropic properties from Reilly and Burstein (1975). Third axis is longitudinal direction.	$E_3 = 17.0$ $G_{12} = 3.6$	$v_{13} = v_{23} = 0.31$
	$G_{13} = G_{23} = 3.28$	$v_{31} = v_{32} = 0.46$

6.2.3 Loading configurations

Each model was subjected to two load configurations representing the peak loading occurring during walking and stair-climbing. These include the hip joint contact forces and the resultant forces from the main muscle groups, based on data from HIP98 (Bergmann *et al.* 2001b). The points of load application are indicated in **Figure 6.2** and the forces applied are described in **Table 6.3**. In both stair-climbing and walking cases, 20 million cycles of loading were simulated.

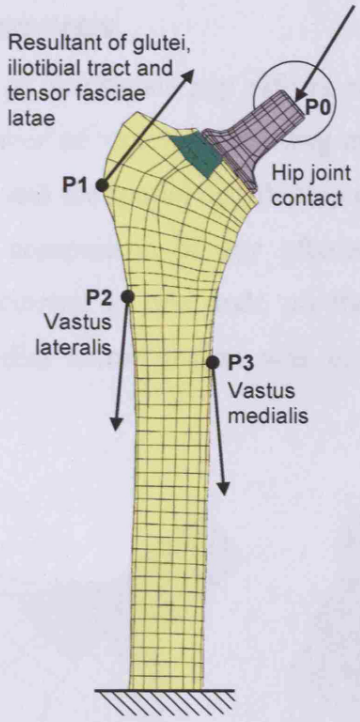

Figure 6.2. Schematic showing points of load application representing joint and muscle forces for stair-climbing and gait loads. Load magnitudes are indicated in **Table 6.3**.

Table 6.3. Joint and muscle forces applied during stair-climbing and walking loads, based on data from HIP98 (Bergmann *et al.* 2001b) for a patient weighing 750 N.

Description of force	Force component magnitudes (N)			Point of application*
	X (lateral)	Y (posterior)	Z (proximal)	
Stair-climbing				
Hip joint contact	444.8	454.5	-1772.3	P0
Glutei, iliotibial tract, tensor fasciae latae	-622.5	-222.0	579.8	P1
Vastus lateralis	16.5	-168.0	-1013.3	P2
Vastus medialis	66.0	-297.0	-2003.3	P3
Walking				
Hip joint contact	405.0	246.0	-1719.0	P0
Glutei, iliotibial tract, tensor fasciae latae	-485.3	-114.0	605.3	P1
Vastus lateralis	6.8	-138.8	-696.8	P2
Vastus medialis	0.0	0.0	0.0	P3

*See **Figure 6.2** for points of load application.

6.2.4 Outcome measures

The main measures used to investigate any effects on cement mantle integrity were the cumulative number of 'cracks' occurring at integration points in the cement mantle over time, and the spatial distribution of these cracks throughout the cement mantle. For comparison of any effects on stress-shielding, the equivalent (J_2) stress occurring at one node on the external surface of the cortical bone of the medial calcar region was considered, as indicated in **Figure 6.3**.

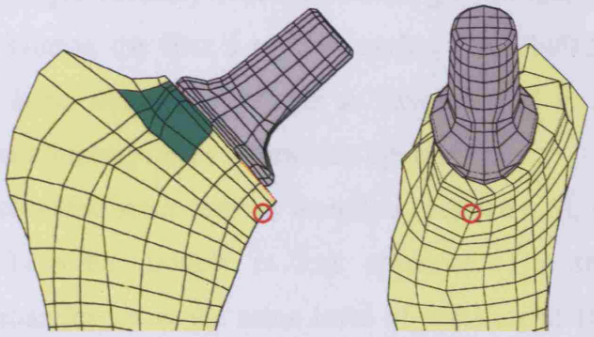

Figure 6.3. The proximal part of a finite element mesh, showing the surface node in the medial calcar region at which equivalent stress is compared for the purposes of comparing any likely effects on stress shielding. The location of this node and the local mesh geometry were the same across all models.

6.3 Results

The total numbers of cracks occurring at all integration points in the cement mantle, normalised by the total number of cracks possible (1640 elements × 8 integration points per element × 3 possible cracks per integration point), were computed for each model under a simulated stair-climbing load. Expressing cement damage thus, as a proportion of the whole mantle, enables comparison both between results and with other papers where cement cracks are expressed similarly. These are plotted against time for each of the models with a collar, with results generated using a bonded stem-cement interface shown in **Figure**

6.4 and those generated with a debonded stem-cement interface shown in **Figure 6.5**. Anterior and posterior halves of each cement mantle, showing the distribution of cracks, are shown for the bonded case in **Figure 6.6** and for the debonded case in **Figure 6.7**.

6.3.1 Cement mantle thickness

In the case of a bonded stem-cement interface (**Figure 6.4**), the thick/2.5mm and medium/1.0mm cement mantles experience near-identical levels of cracking, while the thin/0.5mm mantle has consistently more than twice as many cracks and approximately twice the crack growth rate over most of the simulation time. During the first 5 million cycles, the thin/0.5mm mantle has accumulated the same number of cracks as have formed in the thick/2.5mm and medium/1.0mm mantles after 20 million cycles.

With a debonded stem-cement interface (**Figure 6.5**), the difference in crack numbers between models is less apparent. The thick/2.5mm and medium/1.0mm mantles show the same level of cracking at 10 million cycles, while the thin/0.5mm mantle generates around 40 percent more cracks at this time point. Crack growth rates are similar, and it takes 14 million cycles for the number of cracks in the thin/0.5mm mantle (the most damaged) to reach those seen at 20 million cycles in the thick/2.5mm mantle (the least damaged).

In the cement mantles with a bonded stem-cement interface (**Figure 6.6**), cracks are numerous and widely distributed, predominantly in the distal half of the mantle, and are more concentrated around corners of the implant and at its tip. Damage to the thin/1.0mm mantle is noticeably more extensive. In cement mantles with a debonded stem-cement interface (**Figure 6.7**), cracks are concentrated at the prosthesis tip but elsewhere appear sparsely scattered, mainly in the distal half of the mantle.

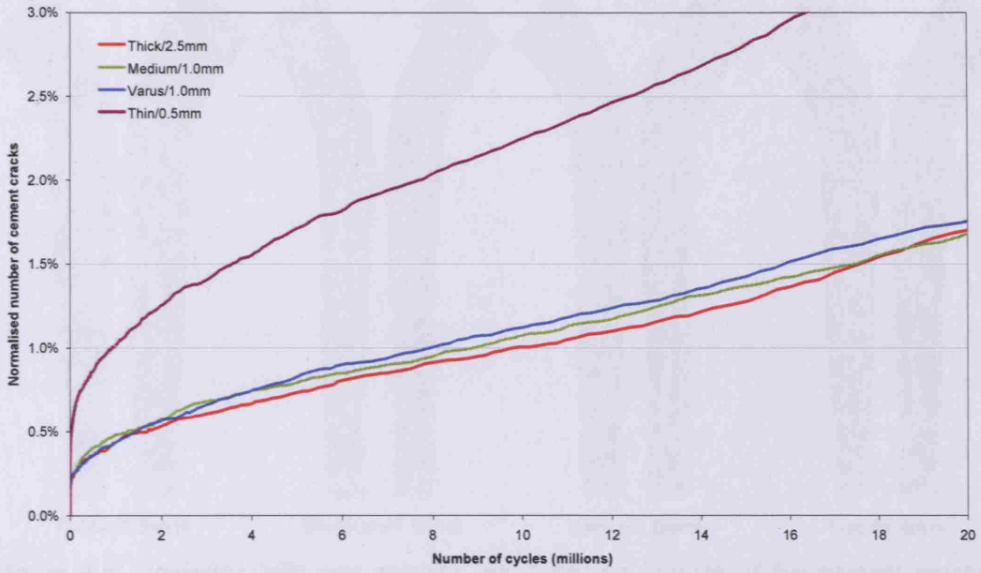

Figure 6.4. Graph showing the 'normalised number of cement cracks' (total number of cracked integration points normalised by the total number possible) over time for each cement mantle, around collared prostheses with a bonded stem-cement interface.

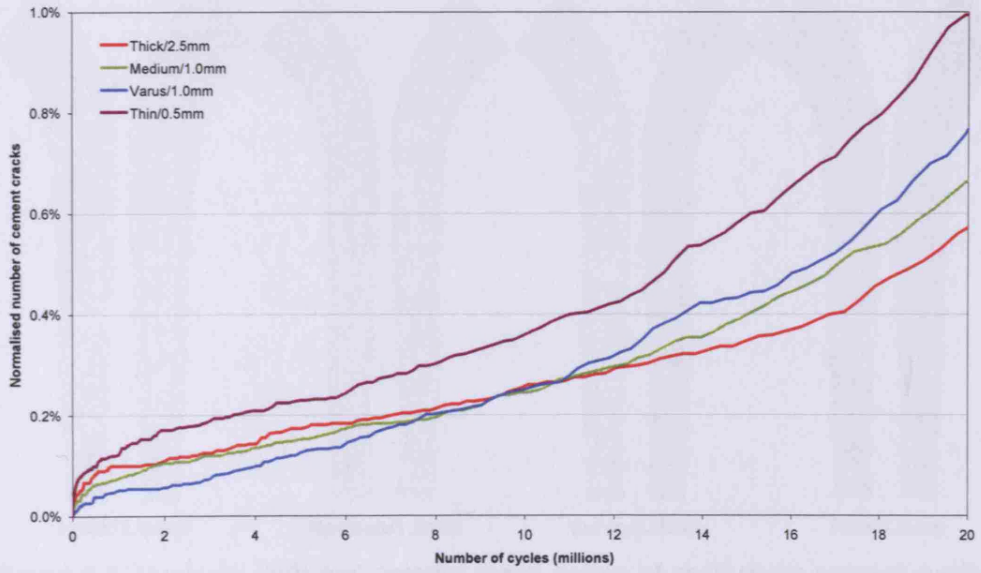

Figure 6.5. Graph showing the 'normalised number of cement cracks' (total number of cracked integration points normalised by the total number possible) over time for each cement mantle, around collared prostheses with a debonded stem-cement interface.

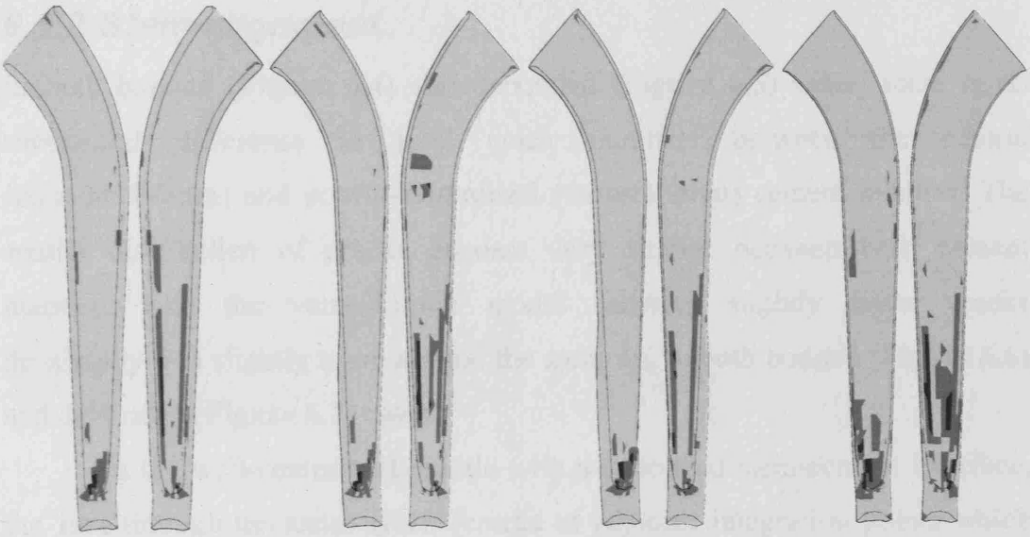

Figure 6.6. Posterior (left) and anterior (right) halves of each of the cement mantles around the collared prostheses with a bonded stem-cement interface, showing the distribution of cracks after 20 million cycles.

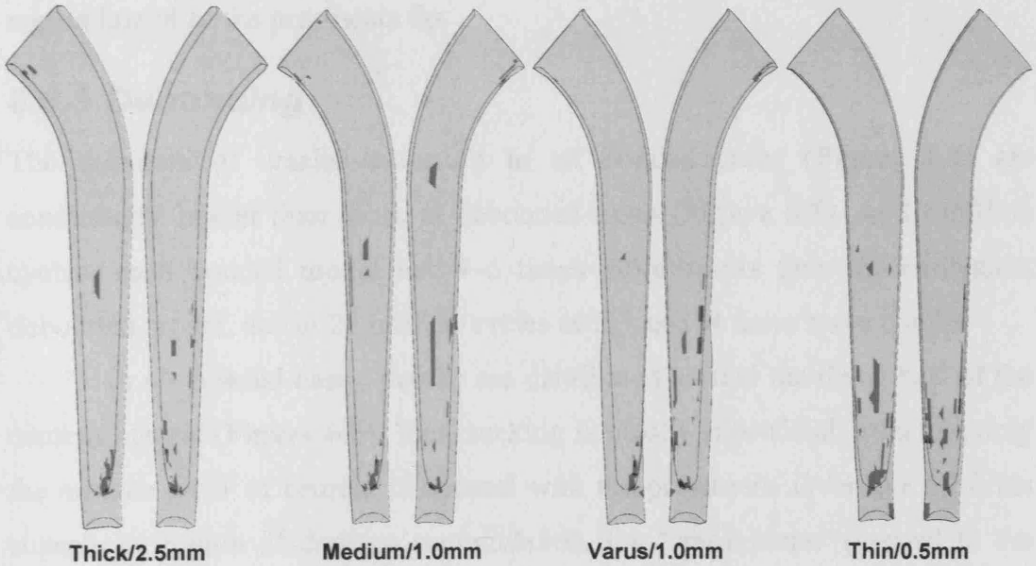

Figure 6.7. Posterior (left) and anterior (right) halves of each of the cement mantles around the collared prostheses with a debonded stem-cement interface, showing the distribution of cracks after 20 million cycles.

6.3.2 Stem alignment

In both bonded (**Figure 6.4**) and debonded (**Figure 6.5**) cases, there is no substantial difference in total crack numbers between the central (medium/1.0mm) and poorly-centralised (varus/1.0mm) cement mantles. The spatial distribution of cracks appears very similar between both cement mantles, with the varus/1.0mm model showing slightly fewer cracks proximally and slightly more around the stem tip, in both bonded (**Figure 6.6**) and debonded (**Figure 6.7**) cases.

In the well-centralised mantle with a debonded stem-cement interface, the first through-thickness crack (cracks at adjacent integration points which bridge the stem-cement and cement-bone interfaces) occurs after 15.4 million cycles. This is located medially, around one-third of the way up the stem from the distal end. A further through-thickness crack occurs at 17.1 million cycles at the anteromedial corner, just below the collar. In the varus-positioned model, the first through-thickness crack occurs after 8.6 million cycles, in the very thin region lateral to the prosthesis tip.

6.3.3 Debonding

The numbers of cracks occurring in all bonded cases (**Figure 6.4**) are consistently higher than those in debonded cases (**Figure 6.5**). At 10 million cycles, each bonded model has 4–6 times more cracks than the equivalent debonded model, and at 20 million cycles each has 3–4 times more cracks.

In all bonded cases, cracks are distributed around the distal half of the cement mantle (**Figure 6.6**). The cracking is mostly superficial, affecting only the surface layer of cement in contact with the prosthesis. Over much of this superficial region of damage accumulation, the 'crack plane' (normal to the first component of the local damage tensor) is nearly parallel to the stem-cement interface.

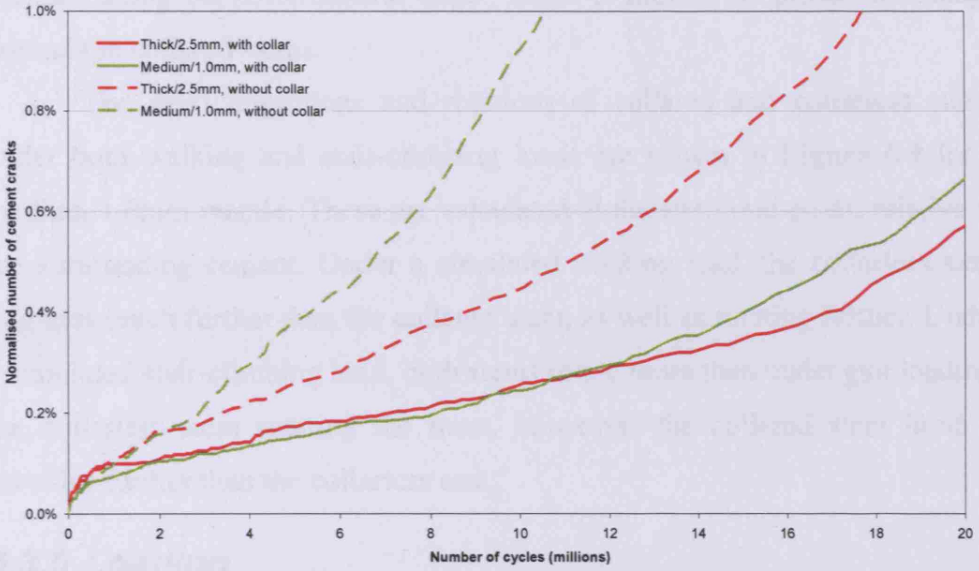

Figure 6.8. Graph showing the 'normalised number of cement cracks' (total number of cracked integration points normalised by the total number possible) over time for the thick/2.5mm and medium/1.0mm cement mantles around prostheses with and without a collar.

6.3.4 Collar

The normalised numbers of cement cracks in the thick/2.5mm and medium/1.0mm mantles, around debonded prostheses both with and without a collar, are shown over time under a stair-climbing load in **Figure 6.8**. The collarless prosthesis generates more cracks in both cement mantle thicknesses. After 10 million cycles, the thick/2.5mm and medium/1.0mm mantles have each accumulated the same number of cracks around a collared prosthesis, while around collarless prostheses the medium/1.0mm mantle has twice as many cracks as the thick/2.5mm mantle, and four times the crack growth rate.

The distribution of cracks in each of these cement mantles is indicated in **Figure 6.10**. Collared and collarless prostheses generate nearly identical crack distributions in the distal half of the mantle. In the proximal half, both mantles have extensive cracking around the collarless stem, including a long

fracture along its posterolateral edge. There is almost no proximal damage around the collared stems.

The axial migrations and rotations of collared and collarless stems under both walking and stair-climbing loads are shown in **Figure 6.9** for a medium/1.0mm mantle. These are calculated at the stem mid-point, relative to the surrounding cement. Under a simulated walking load, the collarless stem migrates much further than the collared stem, as well as rotating further. Under a simulated stair-climbing load, both stems rotate more than under gait loading, the collarless stem rotating the most. However, the collared stem initially subsides further than the collarless one.

6.3.5 Loading

Crack distribution in the debonded thick/2.5mm and medium/1.0mm mantles around prostheses with and without a collar are shown after 20 million cycles of simulated stair-climbing load in **Figure 6.10** and after 20 million cycles of simulated gait load in **Figure 6.11**. Under gait loading, there is almost no cracking anywhere except for around the tip of collared prostheses; collarless stems generate some additional proximal damage, but this is much less pronounced than under the stair-climbing load.

The total number of cracks is plotted over time for the medium/1.0mm mantle with collared and collarless, bonded and debonded stems, under both stair-climbing and gait loads, in **Figure 6.12**. The steep increase in cracking around the debonded collarless stem was the only instance where the total crack number results generated under a stair-climbing load showed a substantial qualitative difference from those generated by gait loading. In all other cases, crack numbers were typically 2–4 times greater under a stair-climbing load than under gait loading, but demonstrated similar comparative behaviour between cement mantle thicknesses and stem geometries. For simplicity, the crack results from gait loading are not explored further in this chapter.

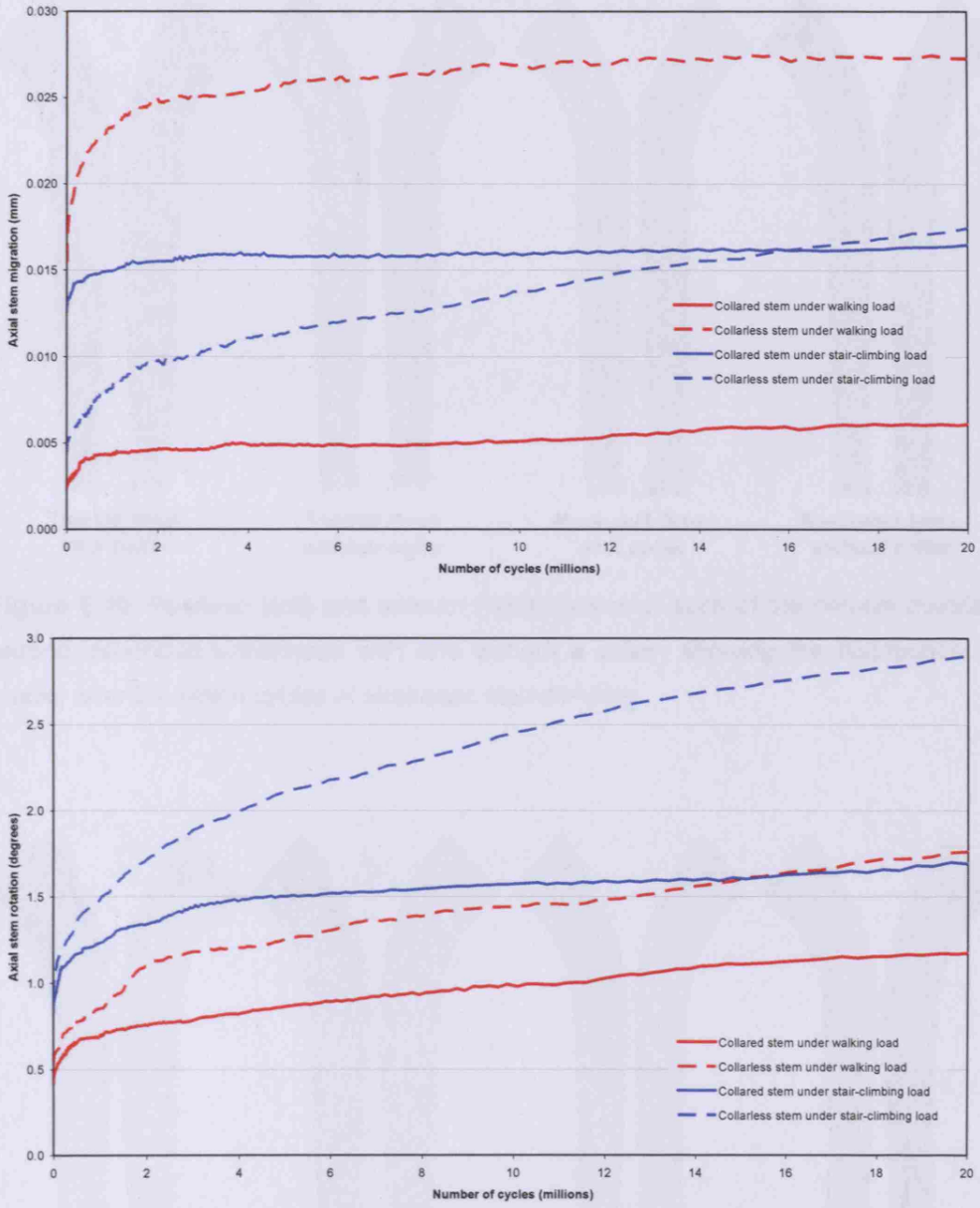

Figure 6.9. Graphs showing the axial migration and rotation of the mid-shaft of collared and collarless stems, relative to the surrounding cement, under simulated gait and stair-climbing loads. Results are shown for the medium/1.0mm cement mantle.

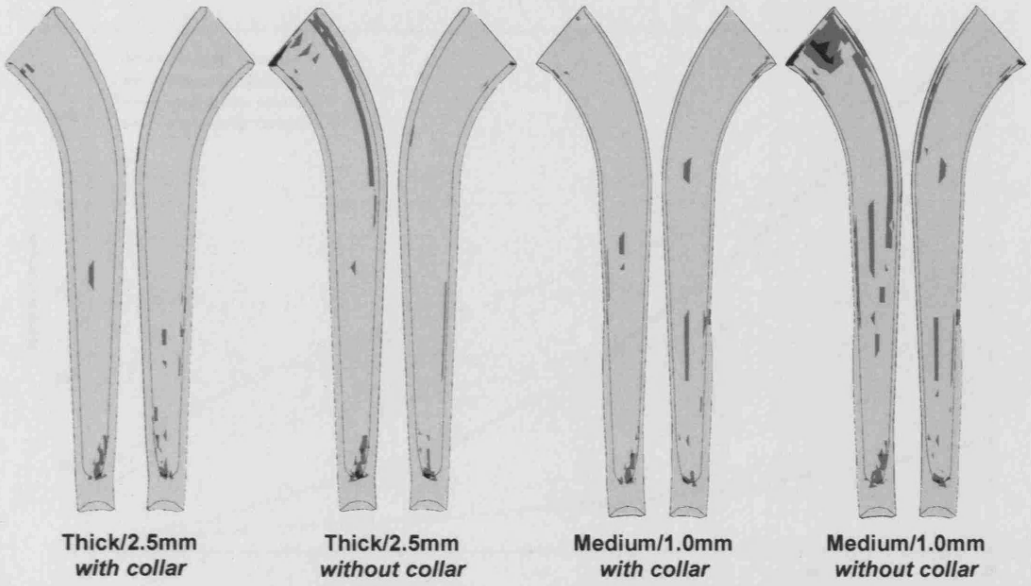

Figure 6.10. Posterior (left) and anterior (right) halves of each of the cement mantles around debonded prostheses with and without a collar, showing the distribution of cracks after 20 million cycles of simulated stair-climbing.

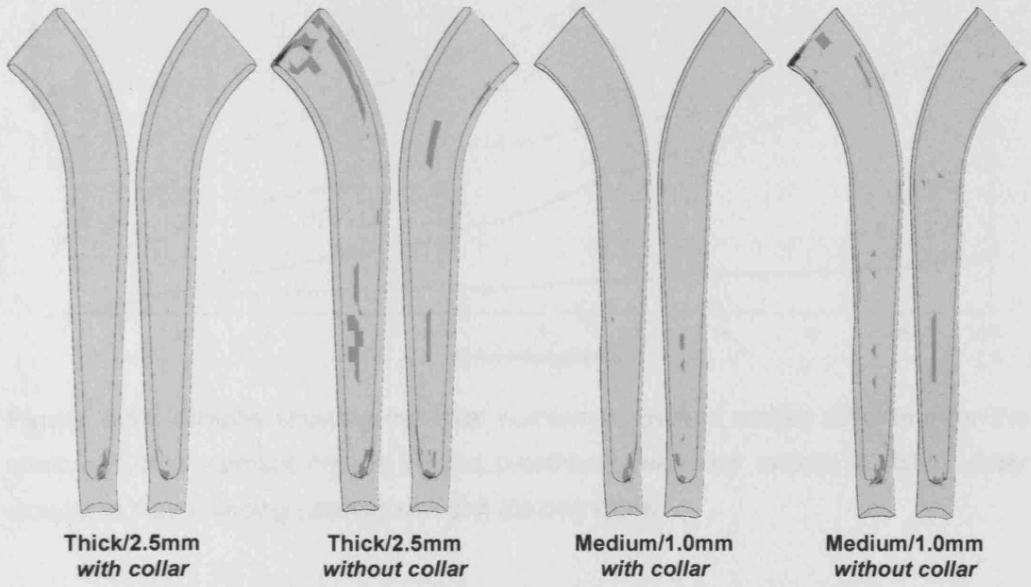

Figure 6.11. Posterior (left) and anterior (right) halves of each of the cement mantles around debonded prostheses with and without a collar, showing the distribution of cracks after 20 million cycles of simulated gait.

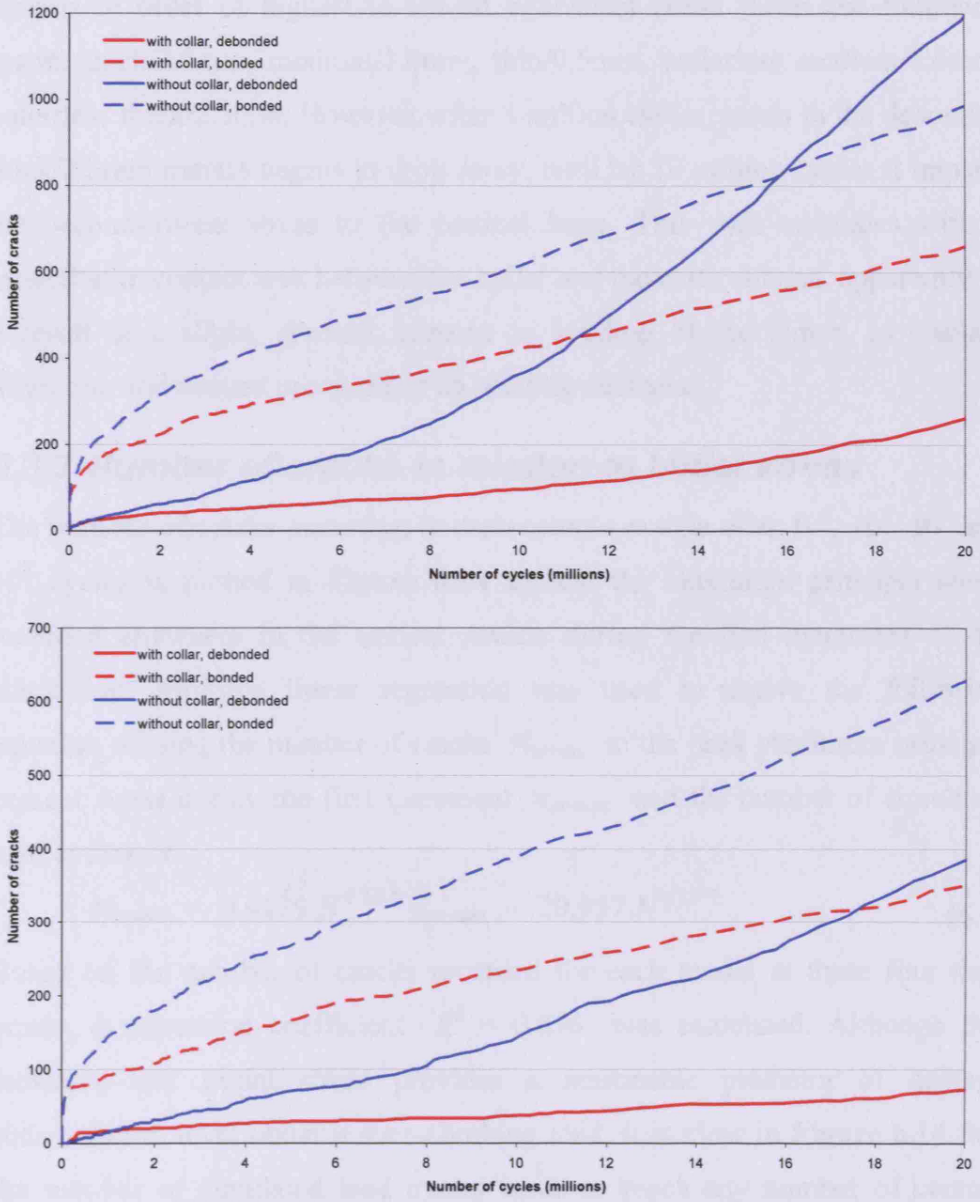

Figure 6.12. Graphs showing the total number of cement cracks over time for the medium/1.0mm cement mantle around prostheses with and without a collar, under simulated stair-climbing (above) and gait (below) loads.

6.3.6 Stress in the medial calcar

At the node indicated in **Figure 6.3**, equivalent stress over time is shown for the bonded and debonded cases in **Figure 6.13**. In both cases, ranking the

models in order of highest to lowest equivalent stress yields the following result: thick/2.5mm, medium/1.0mm, thin/0.5mm, collarless medium/1.0mm, collarless thick/2.5mm. However, after 3 million cycles, stress in the debonded thick/2.5mm mantle begins to drop away, until by 10 million cycles it imparts the second-lowest stress to the cortical bone. This shift coincides with a reduction in contact area between the collar and the cortical bone, apparently as a result of a slight, gradual increase in bending of the femur, as implant migration and cement creep affect its bending stiffness.

6.3.7 Number of cracks in relation to initial stress

The number of cracks occurring in each cement mantle after 10^4, 10^5, 10^6 and 10^7 cycles is plotted in **Figure 6.14** against the maximum principal stress recorded anywhere in the cement mantle during the first increment of the simulation. Multiple linear regression was used to derive the following equation relating the number of cracks N_{cracks} to the peak maximum principal cement stress during the first increment $\sigma_{\text{pr-max}}$ and the number of simulated load cycles N.

$$N_{\text{cracks}} = 0.4179\, N^{0.2109}\, \hat{\sigma}_{\text{pr-max}} - 20.957\, N^{0.1377} \tag{6.1}$$

Based on the number of cracks recorded for each model at these four time points, a regression coefficient $R^2 = 0.856$ was calculated. Although this indicates that initial stress provides a reasonable predictor of damage accumulation level under a stair-climbing load, it is clear in **Figure 6.14** that the number of simulated load cycles taken to reach any number of cement cracks upwards of 100 cracks may differ from the prediction by up to an order or magnitude. Furthermore, goodness of fit is worse ($R^2 = 0.771$) for the data at 10^7 cycles only, indicating that simulated cracking levels diverge further from predicted levels as the simulation progresses.

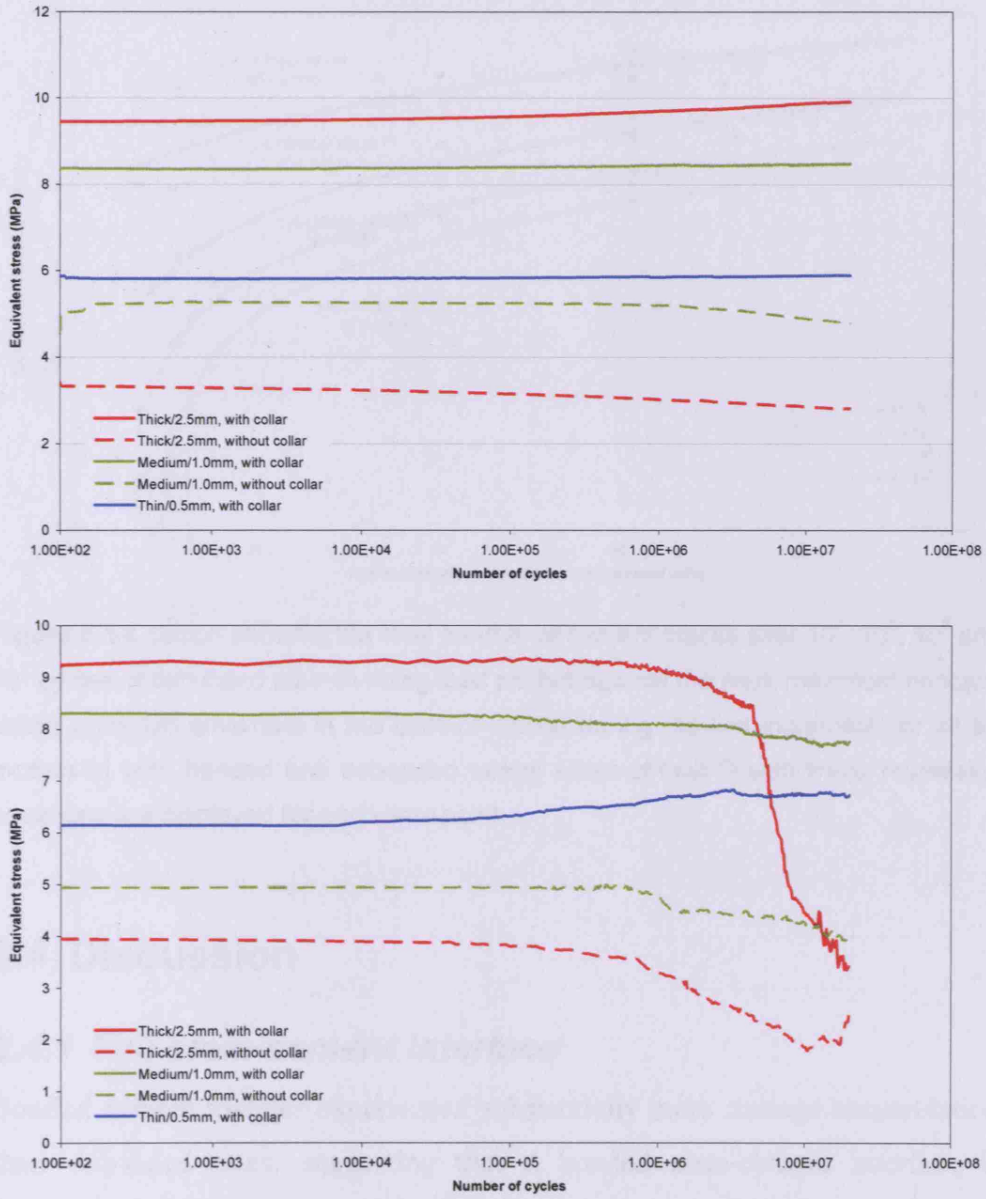

Figure 6.13. Graphs showing the equivalent (J_2) stress at a node in the medial calcar, around bonded (above) and debonded (below) prostheses, under a simulated gait load.

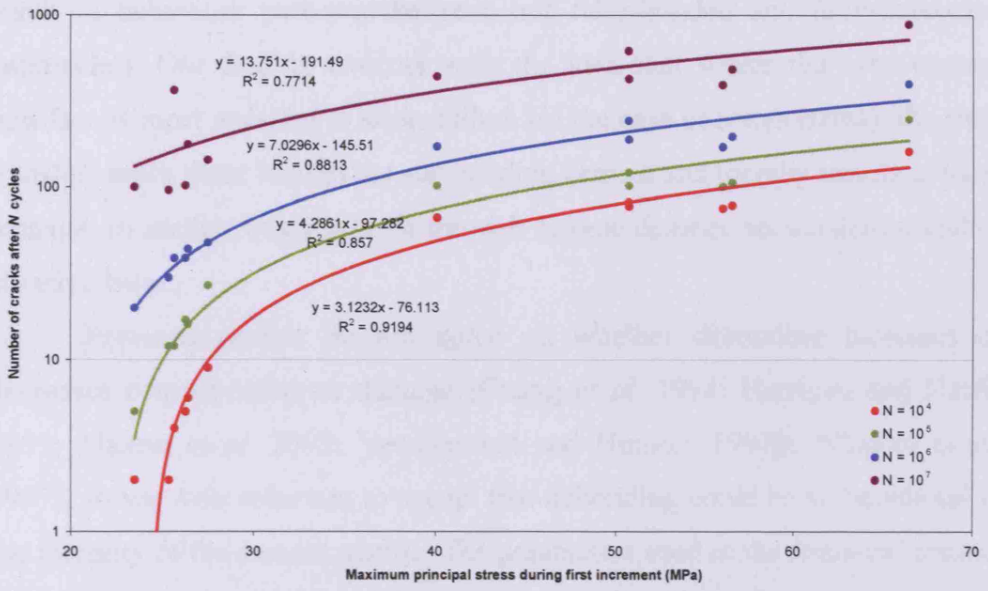

Figure 6.14. Graph showing the total number of cement cracks after 10^4, 10^5, 10^6 and 10^7 cycles of simulated stair-climbing load plotted against the peak maximum principal stress recorded anywhere in the cement mantle during the first increment, for all six models in both bonded and debonded cases. Lines-of-best-fit with linear regression equations are displayed for each time point.

6.4 Discussion

6.4.1 The stem-cement interface

Bonded cement mantles experienced substantially more damage accumulation than debonded ones, suggesting that a bonded stem-cement interface is detrimental to the integrity of the cement mantle. The distribution of cracks in bonded cement mantles – predominantly in the superficial layer of elements closest to the stem, in the distal half of the mantle – appears to represent the debonding process itself, suggesting that debonding is evident, even when the stem-cement interface is explicitly modelled as bonded. This indicates that the debonding process (or, at least, partial debonding) is inevitable. We did not attempt to simulate the debonding process itself using a fatigue failure criterion for stem-cement interfacial gap-elements, although this might be expected to

result in behaviour part-way between our fully-bonded and fully-debonded approaches. Our finding concurs with the idea that where the stem-cement interface is most resistant to shear failure (in the case of rough stems), the stem transfers more shear load to the surrounding cement and thereby results in local damage. In reality, this might be through fatigue damage accumulation and/or abrasive wear.

Previous studies do not agree on whether debonding increases or decreases cement stress or damage (Chang *et al.* 1998; Harrigan and Harris 1991; Massin *et al.* 2003; Verdonschot and Huiskes 1997b; Wheeler *et al.* 1997), so we were reluctant to accept that debonding could be so beneficial to the integrity of the cement mantle. The parameters used in the frictional contact formulation (such as the type of friction model, friction coefficient, and surface modelling and detection parameters) were varied to ensure that they did not have a confounding effect on the model behaviour. In fact, few parameters had a significant effect on the results except for the coefficient of friction (varied from 0.2 to 0.5): in debonded cases, a lower coefficient of friction resulted in less cement cracking, suggesting that for an optimal surface finish, the smoother the better.

Clinical data suggest that, all other factors being equal, a smooth-finished femoral component performs better than a rough one (Collis and Mohler 2002; Collis and Mohler 1998; Datir and Wynn-Jones 2005; Datir *et al.* 2006; Della Valle *et al.* 2005; Hinrichs *et al.* 2003). We suggest that the higher level of damage around stems that remain bonded may account for this difference.

From the engineer's perspective, it is essential that future finite element models of femoral cement mantles take account of the debonding process, as their behaviour around bonded and debonded stem-cement interfaces differs substantially. Recent progressive debonding models based on interfacial fatigue damage have begun to address this issue (Damron *et al.* 2006).

6.4.2 Cement mantle thickness

Variation in the cement mantle thickness, within a clinically-realistic range based on the femoral broach sizes supplied with the Stanmore Hip, did not contribute significantly to crack formation in the femoral cement mantles around debonded Stanmore Hip prostheses. This suggests that the overall cement mantle thickness, often cited as a critical factor affecting implant survival, may in fact be less important than previously thought, around smooth, collared prostheses. This reinforces the findings reported in Chapter 3. Hence, we conclude that global cement thickness, as determined by femoral broach size, does not play an important role in the fatigue life of cement mantles around smooth, collared femoral prostheses such as the Stanmore Hip.

In the case of bonded stems, a thin mantle around an oversized prosthesis was found to be most damaging, although for a smooth stem, this may simply reflect the more rapid process of debonding at the stem-cement interface in this case, in which case the debonded model might be more pertinent. In the case of a rough stem designed not to debond, our results indicate that a very thin cement mantle would be expected to fail much sooner.

Whilst thick cement is widely thought to be optimal for implant survival, the large femoral components inserted with line-to-line reaming which are favoured in France enjoy excellent clinical results despite their very thin or discontinuous cement mantles – the so-called 'French paradox' (Langlais *et al.* 2003; Skinner *et al.* 2003). Our results for debonded stems suggest that the large prosthesis with a thin mantle performs similarly to a smaller prosthesis with a thick mantle, in terms of proportional damage, in agreement with an earlier, torsionally-loaded, two-dimensional study (Janssen *et al.* 2007). In our simulation, the relatively small differences in normalised crack numbers between different cement mantle thicknesses are comparable to those observed between several clinically excellent femoral components under a less severe loading regime (Stolk *et al.* 2007).

In reality, other factors not considered in this study are likely to influence the effect of cement mantle thickness on cement cracking. Microcracks due to the thermal shrinkage of curing interdigitated cement around the bone trabeculae (Race *et al.* 2003) may have a more detrimental effect on thin cement. Greater and more rapid thermal shrinkage of curing thick cement may adversely affect the mechanical integrity of local thin regions. Conversely, inserting large, press-fit implants may have a toughening effect on thin cement regions due to pressurising and extrusion of the cement and may also reduce cement stress due to more direct load transmission to bone (Langlais *et al.* 2003). These factors are not yet well understood and would need to be better characterised before they could be incorporated into finite element studies.

6.4.3 Centralisation

Although there was no difference in total crack numbers between well-centralised and varus stems, the damage in the varus case was weighted towards the tip and very thin lateral region of the cement mantle, with a corresponding reduction in proximal damage. It took nearly half the number of load cycles for a full-thickness crack to form near the tip of the varus stem, compared with the well-centralised stem. This confirms that a locally thin mantle region due to stem misalignment may be damaging, but suggests that it should not affect implant stability via fatigue failure of the cement mantle; rather, an osteolytic pathway is implied, where full-thickness cracks can extend the effective joint space, exuding synovial fluid and articular wear particles, and hence causing localised lytic lesions in the surrounding bone (Schmalzried *et al.* 1992a).

6.4.4 Collarless prostheses

Prostheses without a collar generated significantly more cement cracking, located in the proximal part of the cement mantle. This is representative of the differing method of load transmission through collared and collarless stems:

since collarless stems are freer to subside within the cement mantle, the proximal cement is prized open by the rotation and axial subsidence of the stem. In fact, our migration results suggest that rotation of the stem limits subsidence, and vice versa. Either migration mode (rotation or subsidence) would tighten the taper-lock holding the stem within the cement, stabilising the stem and thus limiting the other migration mode. Stair-climbing leads to predominantly rotary migration, compared with gait, which leads to predominantly distal migration. This is attributable to the higher posterior component of the hip joint contact force during stair-climbing, contributing axial torque to the stem shaft. This explains the high level of proximal damage around the corners of collarless stems under stair-climbing loads. Collarless stems are designed to impart hoop stress to the cortical bone, but this would clearly affect the cement, too. In the case of collarless stems, our results demonstrate that, contrary to our findings for collared prostheses, cement mantle thickness is critical to cement damage, and a thick mantle is therefore advisable, particularly in the proximal part of the femur.

The geometry of each cement mantle was idealised to provide a uniform thickness over much of the mantle, for comparative purposes. The proximal lateral part of the mantle, above the implant shoulder should in fact flare out from the implant, to enable insertion of the prosthesis through the reamed medullary canal. In prostheses with a collar, this region of the mantle experiences very low levels of stress and its precise geometry is unlikely to have any significant bearing on the results. However, for collarless stems, many of the cracks are located in this region. Furthermore, clinically successful collarless designs such as the Exeter Hip are broader in the mediolateral dimension at the implant shoulder, which contributes to its torsional and axial stability within the cement. Therefore, it would be inappropriate to conclude on the basis of our results that collarless stems experience more damage, as we used a modified Stanmore Hip, rather than a purpose-designed, clinically successful collarless stem. Nonetheless, the increased proximal damage and its

sensitivity to cement mantle thickness are important distinguishing characteristics of collarless from collared stems, and highlight the different approaches required for their design and usage.

6.4.5 Stress shielding

Our results indicate that, in the case of a collared stem, a thicker mantle imparts the most stress to the cortical bone in the medial calcar region. The reduction in stress seen over time in the thickest mantle in the debonded case seems to have arisen as a result of changing load orientation due to progressive bending of the femur through cement creep. This is a consequence of the sustained cyclic loading scenario presented in this study: in reality, no prosthesis would be continuously dynamically loaded, as the patient would undergo long 'resting' periods of relative inactivity, meaning that the femur would not deform through creep, relative to the applied joint contact load. However, our results indicate that any of the cement mantle thicknesses investigated around collared prostheses would lead to adequate loading of the calcar region, sustaining equivalent stresses of at least that estimated in Chapter 3 (3.4 MPa) to prevent loss of bone stock due to stress shielding.

6.4.6 Initial cement stress as a predictor of cracking

We attempted a post-hoc 'prediction' of total crack numbers based on the peak maximum principal cement stress during the first increment of the simulation, but this proved to be progressively less accurate as the simulation time progressed. This indicates that the simulation of non-linear damage accumulation over a large number of cycles is justified, as this process cannot be reliably estimated via a simple stress analysis such as that reported in Chapter 3.

6.4.7 Limitations

In some respects, this study was simplistic, neglecting to take into account cancellous bone anisotropy or bone density, and assuming 'average' patient mass and gait characteristics. However, some idealisation is necessary for any

study, and our finite element models are at least comparable with those used in similar studies reported in the literature, and should be adequate to deliver the objectives. The results from Chapter 3 suggest that bone density should have a significant effect on stress and damage in the cement mantle, but would be unlikely to alter the qualitative results of our comparative study.

Jeffers *et al.* (2007b) simulated ultimate fatigue failure (fracture) of the cement mantle, leading to stem instability, as an endpoint in comparative tests of two collarless prostheses. While this is a useful comparative test, it was not feasible in the current study, for two reasons. First, the Stanmore Hip, around which these analyses are based, is more stable than the Exeter Hip due to its collar, and should experience lower and more stable crack growth; second, the algorithms we used, developed by Stolk *et al.*, tend to under-estimate damage while those developed by Jeffers *et al.* tend to over-estimate it, leading to cement fracture within fewer load cycles (Jeffers 2007). The decision was made to restrict the analyses to 20 million load cycles in order to conserve file space, and none of the cement mantles in our study failed within this time frame. If cement fracture occurs when around 10 percent of the cement mantle has failed (Jeffers *et al.* 2007b), it would have taken many more cycles of our simulation to reach this level, as we only observed around 0.5 to 1.0 percent cement failure around debonded, collared stems after 20 million cycles.

Finally, the actual number of cycles simulated in such a comparative study is, to some extent, immaterial since it does not translate directly into a particular proportion of an implant's lifetime in years. The frequency of loading cycles detrimental to the cement mantle will vary from patient to patient, depending on age, weight, and respective levels of each different type of activity. Furthermore, periods during which the prosthetic joint remains unloaded would allow cement creep strains to relax, reducing the beneficial stress-relaxation effect which a sustained cyclic loading regime would allow. Thus, infrequent bursts of activity in the patient are likely to be more damaging than the sustained cyclic loading applied in this study.

6.5 Conclusions

A bonded stem-cement interface is detrimental to the mechanical integrity of the cement mantle, leading to increased cement damage. Even 'perfectly bonded' rough stems will still partially debond through cracking of the bulk cement, which would be more detrimental to implant fixation than the debonding of a smooth stem. This greater level of damage around bonded stems would account for their comparably poor clinical outcomes.

The mechanical integrity of the cement mantle around smooth, collared prostheses does not depend significantly on overall cement mantle thickness or stem alignment, although poor alignment can lead to increased local cement damage in thin mantle regions, which may lead to local osteolysis. This confirms the importance of correct centralisation, but does not agree with the received wisdom that a thick mantle is necessarily better. The 'French paradox' of clinically successful stems with thin cement mantles does not appear to be so paradoxical after all.

However, both rough stems designed not to debond and collarless stems designed to subside within the cement mantle do require a thick cement mantle to reduce the risk of excessive cement damage.

A smooth, collared prosthesis such as the Stanmore Hip loads the calcar region adequately, sustaining sufficient stresses in the cortical bone as to prevent loss of bone stock due to stress shielding.

Simulation of bone cement creep and non-linear damage accumulation over a large number of cycles is justified, as this process cannot be reliably estimated via a simple stress analysis.

Chapter 7

General discussion

Does cement mantle thickness really matter? To address the question posed in the title of this thesis, the cement mantle thickness around femoral components has been considered both in terms of its global or average thickness, as determined by the broach size and resulting reamed canal geometry relative to the stem, and the local cement thickness, determined by stem alignment as influenced by surgical technique.

My first study (Chapter 2) investigated the effect of surgical approach on the quality of cement mantles around Stanmore Hips, and found that a posterior approach provided a more even cement mantle with fewer deficiencies when compared with an anterolateral approach. This could account for the Swedish Hip Arthroplasty Register's hitherto unexplained finding that a posterior approach poses a significantly lower revision risk than an anterolateral approach (Malchau and Herberts 1998). Thus, we may infer that poor control of cement mantle thickness and/or continuity is a factor both (*a*) significantly influenced by surgical technique and (*b*) significantly influencing implant survival. In this sense, cement mantle thickness certainly does seem to matter. Surgeons should be aware of this, using effective centralisation where appropriate, particularly when approaching the hip via an anterolateral incision.

Finite element stress analysis was performed, as reported in Chapter 3, for cement mantles around Stanmore Hips generated using two different broach sizes, to determine the effect of the resulting cement thickness on stress in the cement and cortical bone. Lower cancellous bone density proved detrimental to the cement mantle, generating higher peak cement stresses. Whilst bone

density had a strong effect on cement and bone stresses, it did not qualitatively alter the influence of cement mantle thickness on these parameters. The results suggest that thick cement is preferable for increasing bone stress (to minimise bone loss through stress shielding) and minimising cement stress (to increase fatigue life), but the differences observed were sufficiently slight that the time-dependent processes of creep and damage of the cement and subsidence of the stem could be expected to substantially influence the result. Hence, it was decided that further investigation of this topic was warranted, using a more sophisticated model which would incorporate these factors. Results from the parametric damage simulation study (Chapter 6), where this more complex model is used, confirm that while stress analysis alone can provide an indication of likely damage accumulation, this prediction becomes progressively less accurate for greater numbers of load cycles.

Fatigue testing of cement mantles around Stanmore Hip femoral components in synthetic femurs was reported in Chapter 4. The results concur with the torsional test finding that absolute crack length is independent of cement thickness and therefore that thin mantles would fail sooner (Hertzler *et al.* 2002). Varus stem alignment (resulting in cement deficiency lateral to the tip) does not affect overall crack lengths but does increase the numbers and lengths of cracks in the distal part of mantle. This supports the assumption that failure of poorly-centralised stems progresses through an osteolytic rather than a fracture pathway: thin mantle regions may experience large cracks sooner, which extend the effective joint space, allowing synovium and wear debris to reach the bone and provoke an inflammatory response which weakens the cement-bone construct; but in the absence of a biological response, these cracks are unlikely to result in earlier mechanical failure. Significantly longer and proportionately more cracks were found in sub-millimetre thin mantle regions, as clinical findings would suggest (Jasty *et al.* 1991; Jasty *et al.* 1992; Kawate *et al.* 1998; Koster *et al.* 1999). This emphasises the importance of the surgeon's control over local cement thickness by ensuring adequate

centralisation, in contrast to reamed canal size which does not seem to influence cement cracking. Surgical technique and the use of effective centralisers where appropriate are therefore of far greater clinical significance than design alterations to the surgical tooling. The loading and constraints applied in my study represented a highly simplified stair-climbing load, over-constrained in order to ensure measurable cracking within a reasonable time frame and to prevent fracture of the synthetic femurs. Nonetheless, the test is an improvement on the idealised, simple torsional loading previously employed for investigating the effects of cement mantle thickness, and is justifiable for comparative purposes to distinguish between different cement mantle geometries. That such loading was required to achieve measurable cracking levels demonstrates efficacy and good design of the Stanmore Hip.

The following study (Chapter 5) sought to simulate computationally the fatigue experiments reported in the previous chapter, using creep and damage accumulation algorithms (Stolk *et al.* 2004), so that a more realistic loading scenario could be later applied to a numerical model. Creep and subsidence behaviour for Palacos-R bone cement and satin-finished stems were realistically simulated, confirming that this model would also be applicable to a Stanmore Hip. Finite element simulation of the experimental fatigue test reported in Chapter 4 generated similar cracking rates in cement mantles of different thicknesses, in agreement with the experimental data. Larger and through-thickness cracks, occurring mainly at corners of the prosthesis, were located similarly to those seen in fatigue test specimens.

The final study (Chapter 6) was a finite element investigation of cement mantles of differing thickness and stem alignment, around prostheses with and without collars, using the same creep and damage algorithm to describe bone cement behaviour. Physiologically-informed gait and stair-climbing loads were simulated, providing data of greater clinical relevance than the preceding study. Bonded stem-cement interfaces caused substantially greater superficial damage to the cement mantle, suggesting that the debonding process is inevitable and

that prostheses roughened to promote stem-cement bonding would be most damaging to the cement; this would account for their poor clinical outcomes (Collis and Mohler 2002; Collis and Mohler 1998; Datir and Wynn-Jones 2005; Datir *et al.* 2006; Della Valle *et al.* 2005; Hinrichs *et al.* 2003). Cement damage around smooth, collared prostheses did not depend on overall cement mantle thickness or stem alignment, although poor alignment does lead to increased local cement damage in thin mantle regions, facilitating local osteolysis. This confirms the importance of correct centralisation, but does not agree with the received wisdom that a thick mantle is necessarily better. The 'French paradox' of clinically successful stems with thin cement mantles does not appear to be so paradoxical, after all. This study reinforces the previous findings (Chapters 3–5) that cement damage is not affected by mantle thickness, but limits this finding to smooth, collared prostheses; it was shown that rough, collared stems (designed not to debond) and smooth, collarless stems (designed to subside within the cement mantle) both require a thick cement mantle to reduce the risk of excessive cement damage, in agreement with the findings of others (Estok *et al.* 1997; Fisher *et al.* 1997; Lee *et al.* 1993; Schmolz *et al.* 2000; Ayers and Mann 2003).

One of the limitations of this and many other finite element studies involving bone cement is a simplistic disregard for the variability and complexity in its material behaviour. The distributions of porosity and residual stresses within the cement could be expected to influence its cracking behaviour; neglect of these properties may account for the diffuse and more rapid damage observed in the fatigue test, in comparison with simulations. More sophisticated algorithms and simulation methods including stochastic/probabilistic approaches to porosity distribution and other geometric parameters are currently under investigation (Jeffers *et al.* 2007a); these could be incorporated into future models as computational power allows.

The algorithms used here assume that bone cement is homogeneous. Thin cement regions may potentially be weaker due to the more rapid curing

and contraction of the surrounding thick cement regions; conversely, thin mantles may be toughened by a pressurisation/extrusion process during stem insertion. It is likely that future FE-based models for bone cement behaviour will incorporate insertion (fluid dynamics) and/or curing (thermal) simulations prior to the loading simulation, in order to ascertain the distribution of material properties and residual stresses in the cement. More work would be needed to understand these processes.

Cement thickness was not varied as a continuous parameter, and only one form of stem misalignment was investigated (varus stem orientation is thought to be most detrimental (Kobayashi and Terayama 1992)). However, the similarity in both observed and simulated cracking rates between these cases implies that more in-depth study of the effects of cement thickness on survival of Stanmore Hip stems is unlikely to discriminate further.

Two of the most prevalent and detrimental load cycles were applied to the hip during damage accumulation simulations: stair-climbing (including a larger axial torque component which leads to relatively more axial rotation of the prosthesis) and gait (which leads to relatively more axial stem subsidence). The damage simulation did not take into account any interaction between the two types of load and migration. To address this issue, Stolk *et al.* (2007) arbitrarily used a 1:9 ratio of stair-climbing to gait cycles. However, since gait and stair climbing did not produce qualitatively different comparative results, use of such a method would be unlikely to shed any further light on the issue of cement mantle thickness.

To conclude, the key findings of this project can be summarised as follows:

(1) The posterolateral approach to the hip results in more neutral stem alignment, more uniform cement mantle thickness and fewer cement mantle deficiencies when compared with the anterolateral approach.

(2) Poor stem alignment increases fatigue crack concentrations near the stem tip, increasing the risk of osteolysis and aseptic loosening.

(3) Thin cement regions of less than 1 mm experience higher crack concentrations and longer cracks, and effective centralisation should be used to minimise this risk.

(4) Debonding is inevitable, and rough stems designed not to debond are most damaging to the cement.

(5) Thick cement mantles are required around rough or collarless stems, to minimise the risk of cement damage and stem loosening.

(6) Cement thickness, determined by femoral broach size, does not significantly influence the levels of cement stress or cracking around smooth, collared stems such as the Stanmore Hip. For this type of prosthesis, cement mantle thickness is less important than previously thought.

7.1 Further work

One of the main areas that would benefit future finite element studies of this nature is the enhancement of simulations to incorporate more complex material and interfacial behaviour which are grossly idealised in current models. Factors to be included in future models should include (*a*) stochastic/probabilistic approaches to cement porosity distribution, implant positioning, and bone geometric and material properties; (*b*) thermal and fluid modelling of the curing process to ensure realistic levels of porosity and shrinkage stresses prior to the simulation of fatigue loading; (*c*) interfacial debonding behaviour to enable stem-cement debonding and cement cracking to be simulated together; (*d*) finite element-based interfacial wear models, similar to those currently in use for the joint bearing surfaces, to model the processes of debonding, subsidence and micromotion in terms of abrasive wear.

Material behaviour of interdigitated cement-bone composites is poorly understood. Investigation of the relationship between cancellous bone density and the mechanical properties of the resulting cement-bone composite would allow more realistic representation of the mechanical properties of the cement mantle in finite element simulations. This would also have applications in patient-specific finite element models where likely cement mantle properties can be assumed based on current CT-derived bone density values.

The material properties of bone cement are likely to be influenced by the thickness of the mantle, since thicker regions would cure and contract sooner, potentially exposing thinner regions to tensile forces and expelled monomer vapour, and thus reducing their density and mechanical integrity. This topic warrants further investigation.

List of references

Anthony, P. P., Gie, G. A., Howie, C. R., and Ling, R. S. (1990) Localised endosteal bone lysis in relation to the femoral components of cemented total hip arthroplasties. *J Bone Joint Surg Br* **72,** 971-979.

Armstrong, M. S., Spencer, R. F., Cunningham, J. L., Gheduzzi, S., Miles, A. W., and Learmonth, I. D. (2002) Mechanical characteristics of antibiotic-laden bone cement. *Acta Orthop Scand* **73,** 688-690.

Arnold, J. C. and Venditti, N. P. (2001) Effects of environment on the creep properties of a poly(ethylmethacrylate) based bone cement. *J Mater Sci Mater Med* **12,** 707-717.

Ashman, R. B. and Rho, J. Y. (1988) Elastic modulus of trabecular bone material. *J Biomech* **21,** 177-181.

Aspenberg, P. and van der Vis, H. (1998) Migration, particles, and fluid pressure. A discussion of causes of prosthetic loosening. *Clin Orthop Relat Res* **352,** 75-80.

Ayers, D. C. and Mann, K. A. (2003) The importance of proximal cement filling of the calcar region: a biomechanical justification. *J Arthroplasty* **18,** 103-109.

Baleani, M., Cristofolini, L., Minari, C., and Toni, A. (2003) Fatigue strength of PMMA bone cement mixed with gentamicin and barium sulphate vs pure PMMA. *Proc Inst Mech Eng [H]* **217,** 9-12.

Baleani, M., Cristofolini, L., and Toni, A. (2001) Temperature and ageing condition effects on the characterization of acrylic bone cement. *Proc Inst Mech Eng [H]* **215,** 113-118.

Barber, T. C., Roger, D. J., Goodman, S. B., and Schurman, D. J. (1996) Early outcome of total hip arthroplasty using the direct lateral vs the posterior surgical approach. *Orthopedics* **19,** 873-875.

Bauer, R., Kerschbaumer, F., Poisel, S., and Oberthaler, W. (1979) The transgluteal approach to the hip joint. *Arch Orthop Trauma Surg* **95,** 47-49.

Beaule, P. E., Campbell, P., Mirra, J., Hooper, J. C., and Schmalzried, T. P. (2001) Osteolysis in a cementless, second generation metal-on-metal hip replacement. *Clin Orthop Relat Res* **386,** 159-165.

Berger, R. A., Seel, M. J., Wood, K., Evans, R., D'Antonio, J., and Rubash, H. E. (1997) Effect of a centralizing device on cement mantle deficiencies and initial prosthetic alignment in total hip arthroplasty. *J Arthroplasty* **12,** 434-443.

Bergmann, G., Deuretzbacher, G., Heller, M., Graichen, F., Rohlmann, A., Strauss, J., and Duda, G. N. (2001a) Hip contact forces and gait patterns from routine activities. *J Biomech* **34,** 859-871.

Bergmann, G., Heller, M., and Duda, G. N. (2001b) Preclinical testing of cemented hip replacement implants: Pre-Normative Research for a European Standard. In: *HIP98*, Free University, Berlin.

Berry, D. J., von Knoch, M., Schleck, C. D., and Harmsen, W. S. (2005) Effect of femoral head diameter and operative approach on risk of dislocation after primary total hip arthroplasty. *J Bone Joint Surg Am* **87,** 2456-2463.

Bischoff, R., Dunlap, J., Carpenter, L., DeMouy, E., and Barrack, R. (1994) Heterotopic ossification following uncemented total hip arthroplasty. Effect of the operative approach. *J Arthroplasty* **9,** 641-644.

Bishop, N. E., Ferguson, S. J., and Tepic, S. (1996) Porosity reduction in bone cement at the cement-stem interface. *J Bone Joint Surg Br* **78,** 349-356.

Bos, J. C., Stoeckart, R., Klooswijk, A. I., van Linge, B., and Bahadoer, R. (1994) The surgical anatomy of the superior gluteal nerve and anatomical radiologic bases of the direct lateral approach to the hip. *Surg Radiol Anat* **16,** 253-258.

Bowditch, M. and Villar, R. (2001) Is titanium so bad? Medium-term outcome of cemented titanium stems. *J Bone Joint Surg Br* **83,** 680-685.

Bozic, K. J., Katz, P., Cisternas, M., Ono, L., Ries, M. D., and Showstack, J. (2005) Hospital resource utilization for primary and revision total hip arthroplasty. *J Bone Joint Surg Am* **87,** 570-576.

Bragdon, C. R., Biggs, S. A., Mulroy, W. F., and Harris, W. H. (1995) Defects in the cement mantle: A fatal flaw in cemented femoral stems for THR. *Trans Orthop Res Soc* **20,** 710.

Breusch, S. J., Lukoschek, M., Kreutzer, J., Brocai, D., and Gruen, T. A. (2001) Dependency of cement mantle thickness on femoral stem design and centralizer. *J Arthroplasty* **16,** 648-657.

Breusch, S. J. and Malchau, H. (2005) Operative Steps: Femur. In: *The Well-Cemented Total Hip Arthroplasty: Theory and Practice*, pp. 28-36. Springer Berlin Heidelberg.

Britton, J. R., Walsh, L. A., and Prendergast, P. J. (2003) Mechanical simulation of muscle loading on the proximal femur: analysis of cemented femoral component migration with and without muscle loading. *Clin Biomech* **18,** 637-646.

Brown, T. D., Pedersen, D. R., Radin, E. L., and Rose, R. M. (1988) Global mechanical consequences of reduced cement/bone coupling rigidity in proximal femoral arthroplasty: a three-dimensional finite element analysis. *J Biomech* **21,** 115-129.

Cannestra, V. P., Berger, R. A., Quigley, L. R., Jacobs, J. J., Rosenberg, A. G., and Galante, J. O. (2000) Hybrid total hip arthroplasty with a precoated offset stem. Four to nine-year results. *J Bone Joint Surg Am* **82,** 1291-1299.

Caruana, J., Mannan, K., Sanghrajka, A. P., Higgs, D., Briggs, T. W. R., and Blunn, G. W. (2006) Choice of femoral cement mantle thickness based on initial stress. *J Bone Joint Surg Br* **88-B,** 71.

Chang, P. B., Mann, K. A., and Bartel, D. L. (1998) Cemented femoral stem performance. Effects of proximal bonding, geometry, and neck length. *Clin Orthop Relat Res* **355,** 57-69.

Charnley, J. (1961) Arthroplasty of the hip. A new operation. *Lancet* **1,** 1129-1132.

Charnley, J. (1972) The long-term results of low-friction arthroplasty of the hip performed as a primary intervention. *J Bone Joint Surg Br* **54,** 61-76.

Charnley, J. (1979) *Low Friction Arthroplasty of the Hip: Theory and Practice.* Springer-Verlag: New York.

Cheal, E. J., Spector, M., and Hayes, W. C. (1992) Role of loads and prosthesis material properties on the mechanics of the proximal femur after total hip arthroplasty. *J Orthop Res* **10,** 405-422.

Chwirut, D. J. (1984) Long-term compressive creep deformation and damage in acrylic bone cements. *J Biomed Mater Res* **18,** 25-37.

Collis, D. K. and Mohler, C. G. (1998) Loosening rates and bone lysis with rough finished and polished stems. *Clin Orthop Relat Res* **355,** 113-122.

Collis, D. K. and Mohler, C. G. (2002) Comparison of clinical outcomes in total hip arthroplasty using rough and polished cemented stems with essentially the same geometry. *J Bone Joint Surg Am* **84-A,** 586-592.

Crawford, R. W., Psychoyios, V., Gie, G. A., Ling, R. S., and Murray, D. W. (1999) Incomplete cement mantles in the sagittal femoral plane: an anatomical explanation. *Acta Orthop Scand* **70,** 596-598.

Cristofolini, L., Viceconti, M., Toni, A., and Giunti, A. (1995) Influence of thigh muscles on the axial strains in a proximal femur during early stance in gait. *J Biomech* **28,** 617-624.

Crowninshield, R. D., Brand, R. A., Johnston, R. C., and Milroy, J. C. (1980) An analysis of femoral component stem design in total hip arthroplasty. *J Bone Joint Surg Am* **62,** 68-78.

Dall, D. M., Miles, A. W., and Juby, G. (1986) Accelerated polymerization of acrylic bone cement using preheated implants. *Clin Orthop Relat Res* **211,** 148-150.

Damron, L. A., Kim, D. G., and Mann, K. A. (2006) Fatigue debonding of the roughened stem-cement interface: effects of surface roughness and stem heating conditions. *J Biomed Mater Res B Appl Biomater* **78,** 181-188.

Datir, S. P., Kurta, I. C., and Wynn-Jones, C. H. (2006) Ten-year survivorship of rough-surfaced femoral stem with geometry similar to Charnley femoral stem. *J Arthroplasty* **21,** 392-397.

Datir, S. P. and Wynn-Jones, C. H. (2005) Staged bilateral total hip arthroplasty using rough and smooth surface femoral stems with similar design: 10-year survivorship of 48 cases. *Acta Orthop* **76,** 809-814.

Davies, J. P. and Harris, W. H. (1992) The effect of the addition of methylene blue on the fatigue strength of Simplex P bone-cement. *J Appl Biomater* **3,** 81-85.

Della Valle, A. G., Zoppi, A., Peterson, M. G., and Salvati, E. A. (2005) A rough surface finish adversely affects the survivorship of a cemented femoral stem. *Clin Orthop Relat Res* **436,** 158-163.

Dixon, M. C., Scott, R. D., Schai, P. A., and Stamos, V. (2004) A simple capsulorrhaphy in a posterior approach for total hip arthroplasty. *J Arthroplasty* **19,** 373-376.

Dowd, J. E., Cha, C. W., Trakru, S., Kim, S. Y., Yang, I. H., and Rubash, H. E. (1998) Failure of total hip arthroplasty with a precoated prosthesis. 4- to 11-year results. *Clin Orthop Relat Res* **355,** 123-136.

Downing, N. D., Clark, D. I., Hutchinson, J. W., Colclough, K., and Howard, P. W. (2001) Hip abductor strength following total hip arthroplasty: a prospective comparison of the posterior and lateral approach in 100 patients. *Acta Orthop Scand* **72,** 215-220.

Dunne, N. J. and Orr, J. F. (1998) Flow characteristics of curing polymethyl methacrylate bone cement. *Proc Inst Mech Eng [H]* **212,** 199-207.

Dunne, N. J. and Orr, J. F. (2001) Influence of mixing techniques on the physical properties of acrylic bone cement. *Biomaterials* **22,** 1819-1826.

Dunne, N. J., Orr, J. F., Mushipe, M. T., and Eveleigh, R. J. (2003) The relationship between porosity and fatigue characteristics of bone cements. *Biomaterials* **24,** 239-245.

Ebramzadeh, E., Normand, P. L., Sangiorgio, S. N., Llinas, A., Gruen, T. A., McKellop, H. A., and Sarmiento, A. (2003) Long-term radiographic changes in cemented total hip arthroplasty with six designs of femoral components. *Biomaterials* **24,** 3351-3363.

Ebramzadeh, E., Sarmiento, A., McKellop, H. A., Llinas, A., and Gogan, W. (1994) The cement mantle in total hip arthroplasty. Analysis of long-term radiographic results. *J Bone Joint Surg Am* **76,** 77-87.

Egund, N., Lidgren, L., and Onnerfalt, R. (1990) Improved positioning of the femoral stem with a centralizing device. *Acta Orthop Scand* **61,** 236-239.

Espehaug, B., Furnes, O., Havelin, L. I., Engesaeter, L. B., and Vollset, S. E. (2002) The type of cement and failure of total hip replacements. *J Bone Joint Surg Br* **84,** 832-838.

Estok, D. M. and Harris, W. H. (1994) Long-term results of cemented femoral revision surgery using second-generation techniques. An average 11.7-year follow-up evaluation. *Clin Orthop Relat Res* **299,** 190-202.

Estok, D. M. and Harris, W. H. (2000) A stem design change to reduce peak cement strains at the tip of cemented total hip arthroplasty. *J Arthroplasty* **15,** 584-589.

Estok, D. M., Orr, T. E., and Harris, W. H. (1997) Factors affecting cement strains near the tip of a cemented femoral component. *J Arthroplasty* **12,** 40-48.

Fagan, M. J. and Lee, A. J. (1986a) Role of the collar on the femoral stem of cemented total hip replacements. *J Biomed Eng* **8,** 295-304.

Fagan, M. J. and Lee, A. J. C. (1986b) Materials Selection in the Design of the Femoral Component of Cemented Total Hip Replacement. *Clin Mater* **1,** 151-167.

Fender, D., van der Meulen, J. H., and Gregg, P. J. (2003) Relationship between outcome and annual surgical experience for the charnley total hip replacement. Results from a regional hip register. *J Bone Joint Surg Br* **85,** 187-190.

Fisher, D. A., Tsang, A. C., Paydar, N., Milionis, S., and Turner, C. H. (1997) Cement-mantle thickness affects cement strains in total hip replacement. *J Biomech* **30,** 1173-1177.

Fornasier, V., Wright, J., and Seligman, J. (1991) The histomorphologic and morphometric study of asymptomatic hip arthroplasty. A postmortem study. *Clin Orthop Relat Res* **271,** 272-282.

Freitag, T. A. and Cannon, S. L. (1977) Fracture characteristics of acrylic bone cements. II. Fatigue. *J Biomed Mater Res* **11,** 609-624.

Fritsch, E., Rupp, S., and Kaltenkirchen, N. (1996) Does vacuum-mixing improve the fatigue properties of high-viscosity poly(methyl-methacrylate) (PMMA) bone cement? Comparison between two different evacuation methods. *Arch Orthop Trauma Surg* **115,** 131-135.

Frndak, P. A., Mallory, T. H., and Lombardi, A. V. (1993) Translateral surgical approach to the hip. The abductor muscle "split". *Clin Orthop Relat Res* **295,** 135-141.

Galante, J. O. (1980) Causes of fractures of the femoral component in total hip replacement. *J Bone Joint Surg Am* **62,** 670-673.

Gammer, W. (1985) A modified lateroanterior approach in operations for hip arthroplasty. *Clin Orthop Relat Res* **199,** 169-172.

Gerritsma-Bleeker, C. L., Deutman, R., Mulder, T. J., and Steinberg, J. D. (2000) The Stanmore total hip replacement. A 22-year follow-up. *J Bone Joint Surg Br* **82,** 97-102.

Gibson, A. (1950) Posterior exposure of the hip joint. *J Bone Joint Surg Br* **32-B,** 183-186.

Gluck, T. (1890) Die Invaginationsmethode der Osteo-und Arthroplastik. *Berl Klin Wochenschr* **33,** 752-757.

Glyn-Jones, S., Alfaro-Adrian, J., Murray, D. W., and Gill, H. S. (2006) The influence of surgical approach on cemented stem stability: an RSA study. *Clin Orthop Relat Res* **448,** 87-91.

Goldberg, B. A., al Habbal, G., Noble, P. C., Paravic, M., Liebs, T. R., and Tullos, H. S. (1998) Proximal and distal femoral centralizers in modern cemented hip arthroplasty. *Clin Orthop Relat Res* **349,** 163-173.

Goldring, S. R., Jasty, M., Roelke, M. S., Rourke, C. M., Bringhurst, F. R., and Harris, W. H. (1986) Formation of a synovial-like membrane at the bone-cement interface. Its role in bone resorption and implant loosening after total hip replacement. *Arthritis Rheum* **29,** 836-842.

Gore, D. R., Murray, M. P., Sepic, S. B., and Gardner, G. M. (1982) Anterolateral compared to posterior approach in total hip arthroplasty: differences in component positioning, hip strength, and hip motion. *Clin Orthop Relat Res* **165,** 180-187.

Graham, J., Pruitt, L. A., Ries, M. D., and Gundiah, N. (2000) Fracture and fatigue properties of acrylic bone cement: the effects of mixing method, sterilization treatment, and molecular weight. *J Arthroplasty* **15,** 1028-1035.

Grossmann, P., Braun, M., and Becker, W. (1994) [Dislocation following total hip endoprosthesis. Association with surgical approach and other factors]. *Z Orthop Ihre Grenzgeb* **132,** 521-526.

Gruen, T. A., McNeice, G. M., and Amstutz, H. C. (1979) "Modes of failure" of cemented stem-type femoral components: a radiographic analysis of loosening. *Clin Orthop Relat Res* **141,** 17-27.

Guidoni, G. and Vallo, C. I. (2002) Influence of pressurization on flexural strength distributions of PMMA-based bone cements. *J Mater Sci Mater Med* **13,** 1077-1081.

Haboush, E. J. (1953) A new operation for arthroplasty of the hip based on biomechanics, photoelasticity, fast-setting dental acrylic, and other considerations. *Bull Hosp Joint Dis* **14,** 242-277.

Hailey, J. L., Turner, I. G., and Miles, A. W. (1994) An in vitro study of the effect of environment and storage time on the fracture properties of bone cement. *Clin Mater* **16,** 211-216.

Hallam, P., Haddad, F., and Cobb, J. (2004) Pain in the well-fixed, aseptic titanium hip replacement. The role of corrosion. *J Bone Joint Surg Br* **86,** 27-30.

Hansen, D. and Jensen, J. S. (1990) Prechilling and vacuum mixing not suitable for all bone cements. Handling characteristics and exotherms of bone cements. *J Arthroplasty* **5,** 287-290.

Hanson, P. B. and Walker, R. H. (1995) Total hip arthroplasty cemented femoral component distal stem centralizer. Effect on stem centralization and cement mantle. *J Arthroplasty* **10,** 683-688.

Hardinge, K. (1982) The direct lateral approach to the hip. *J Bone Joint Surg Br* **64,** 17-19.

Harper, E. J. and Bonfield, W. (2000) Tensile characteristics of ten commercial acrylic bone cements. *J Biomed Mater Res* **53,** 605-616.

Harper, E. J., Braden, M., Bonfield, W., Dingeldein, E., and Wahlig, H. (1997) Influence of sterilization upon a range of properties of experimental bone cements. *J Mater Sci Mater Med* **8,** 849-853.

Harrigan, T. P. and Harris, W. H. (1991) A three-dimensional non-linear finite element study of the effect of cement-prosthesis debonding in cemented femoral total hip components. *J Biomech* **24,** 1047-1058.

Harris, W. H. (1967) A new lateral approach to the hip joint. *J Bone Joint Surg Am* **49,** 891-898.

Harris, W. H. (1975) A new approach to total hip replacement without osteotomy of the greater trochanter. *Clin Orthop Relat Res* **106,** 19-26.

Harris, W. H. (1992) Will stress shielding limit the longevity of cemented femoral components of total hip replacement? *Clin Orthop Relat Res* **274,** 120-123.

Harris, W. H. (1998) Long-term results of cemented femoral stems with roughened precoated surfaces. *Clin Orthop Relat Res* **355,** 137-143.

Hashemi-Nejad, A., Birch, N. C., and Goddard, N. J. (1994) Current attitudes to cementing techniques in British hip surgery. *Ann R Coll Surg Engl* **76,** 396-400.

Havelin, L. I., Espehaug, B., Vollset, S. E., and Engesaeter, L. B. (1995) The effect of the type of cement on early revision of Charnley total hip prostheses. A review of eight thousand five hundred and seventy-nine primary arthroplasties from the Norwegian Arthroplasty Register. *J Bone Joint Surg Am* **77,** 1543-1550.

Hedia, H. S., Barton, D. C., Fisher, J., and Elmidany, T. T. (1996) A method for shape optimization of a hip prosthesis to maximize the fatigue life of the cement. *Med Eng Phys* **18,** 647-654.

Hedley, A. K., Hendren, D. H., and Mead, L. P. (1990) A posterior approach to the hip joint with complete posterior capsular and muscular repair. *J Arthroplasty* **5 Suppl,** S57-S66.

Hedlundh, U., Hybbinette, C. H., and Fredin, H. (1995) Influence of surgical approach on dislocations after Charnley hip arthroplasty. *J Arthroplasty* **10,** 609-614.

Herberts, P., Kärrholm, J., and Garellick, G. (2005) Årsrapport 2004. *Nationalregistret för höftledsplastiker i Sverige.*

Herberts, P. and Malchau, H. (1998) Årsrapport 1997. *Nationalregistret för höftledsplastiker i Sverige.*

Hertzler, J., Miller, M. A., and Mann, K. A. (2002) Fatigue crack growth rate does not depend on mantle thickness: an idealized cemented stem construct under torsional loading. *J Orthop Res* **20,** 676-682.

Hinrichs, F., Kuhl, M., Boudriot, U., and Griss, P. (2003) A comparative clinical outcome evaluation of smooth (10-13 year results) versus rough surface finish (5-8

year results) in an otherwise identically designed cemented titanium alloy stem. *Arch Orthop Trauma Surg* **123,** 268-272.

Hirakawa, K., Jacobs, J. J., Urban, R., and Saito, T. (2004) Mechanisms of failure of total hip replacements: lessons learned from retrieval studies. *Clin Orthop Relat Res* **420,** 10-17.

Holm, N. J. (1977) The modulus of elasticity and flexural strength of some acrylic bone cements. *Acta Orthop Scand* **48,** 436-442.

Holm, N. J. (1980) The relaxation of some acrylic bone cements. *Acta Orthop Scand* **51,** 727-731.

Hovelius, L., Hussenius, A., and Thorling, J. (1977) Posterior versus lateral approach for hip arthroplasty. *Acta Orthop Scand* **48,** 47-51.

Hughes, K. F., Ries, M. D., and Pruitt, L. A. (2003) Structural degradation of acrylic bone cements due to in vivo and simulated aging. *J Biomed Mater Res A* **65,** 126-135.

Huiskes, R. and Boeklagen, R. (1989) Mathematical shape optimization of hip prosthesis design. *J Biomech* **22,** 793-804.

Huiskes, R., Verdonschot, N., and Nivbrant, B. (1998) Migration, stem shape, and surface finish in cemented total hip arthroplasty. *Clin Orthop Relat Res* **355,** 103-112.

Huiskes, R. and Vroemen, W. (1986) A standardized finite element model for routine comparative evaluations of femoral hip prostheses. *Acta Orthop Belg* **52,** 258-261.

Huiskes, R., Weinans, H., and van Rietbergen, B. (1992) The relationship between stress shielding and bone resorption around total hip stems and the effects of flexible materials. *Clin Orthop Relat Res* **274,** 124-134.

Iesaka, K., Jaffe, W. L., and Kummer, F. J. (2003) Effects of preheating of hip prostheses on the stem-cement interface. *J Bone Joint Surg Am* **85-A,** 421-427.

Ishihara, S., McEvily, A. J., Goshima, T., Kanekasu, K., and Nara, T. (2000) On fatigue lifetimes and fatigue crack growth behavior of bone cement. *J Mater Sci Mater Med* **11,** 661-666.

Janssen, D., Aquarius, R., Stolk, J., and Verdonschot, N. (2005a) Finite-element analysis of failure of the Capital Hip designs. *J Bone Joint Surg Br* **87,** 1561-1567.

Janssen, D., Aquarius, R., Stolk, J., and Verdonschot, N. (2005b) The contradictory effects of pores on fatigue cracking of bone cement. *J Biomed Mater Res [B]* **74,** 747-753.

Janssen, D., Stolk, J., and Verdonschot, N. (2005c) Why would cement porosity reduction be clinically irrelevant, while experimental data show the contrary. *J Orthop Res* **23,** 691-697.

Janssen, D., van Aken, J., Scheerlinck, T., and Verdonschot, N. (2007) The "French paradox" exposed: a finite element analysis of cement philosophy on implant stability and crack formation in the cement mantle. *Trans Orthop Res Soc* **32,** 280.

Jasty, M., Jiranek, W., and Harris, W. H. (1992) Acrylic fragmentation in total hip replacements and its biological consequences. *Clin Orthop Relat Res* **285,** 116-128.

Jasty, M., Maloney, W. J., Bragdon, C. R., Haire, T. C., and Harris, W. H. (1990) Histomorphological studies of the long-term skeletal responses to well fixed cemented femoral components. *J Bone Joint Surg Am* **72,** 1220-1229.

Jasty, M., Maloney, W. J., Bragdon, C. R., O'Connor, D. O., Haire, T. C., and Harris, W. H. (1991) The initiation of failure in cemented femoral components of hip arthroplasties. *J Bone Joint Surg Br* **73,** 551-558.

Jeffers, J. R., Browne, M., Lennon, A. B., Prendergast, P. J., and Taylor, M. (2007a) Cement mantle fatigue failure in total hip replacement: Experimental and computational testing. *J Biomech* **40,** 1525-1533.

Jeffers, J. R., Browne, M., Roques, A., and Taylor, M. (2005a) On the importance of considering porosity when simulating the fatigue of bone cement. *J Biomech Eng* **127,** 563-570.

Jeffers, J. R., Browne, M., and Taylor, M. (2005b) Damage accumulation, fatigue and creep behaviour of vacuum mixed bone cement. *Biomaterials* **26,** 5532-5541.

Jeffers, J. R. and Taylor, M. (2003) Mesh considerations for adaptive finite element analyses of cement failure in total hip replacement. *Summer Bioengineering Conference* 729.

Jeffers, J. R. T. (2007) *Private communication.*

Jeffers, J. R. T., Browne, M., Wroblewski, B. M., Isaac, G. H., and Taylor, M. (2007b) Loosening of two contemporary stem designs by cement mantle fatigue in hip arthroplasty. *Trans Orthop Res Soc* **32,** 1740.

Jergesen, H. E. and Karlen, J. W. (2002) Clinical outcome in total hip arthroplasty using a cemented titanium femoral prosthesis. *J Arthroplasty* **17,** 592-599.

Jofe, M. H., Takeuchi, T., and Hayes, W. C. (1991) Compressive behavior of human bone-cement composites. *J Arthroplasty* **6,** 213-219.

Johnsson, R., Hallin, E., Nordstrom, B., and Lidgren, L. (1981) Modified technique in the dorsal approach in total hip arthroplasty. *Arch Orthop Trauma Surg* **99,** 43-45.

Johnston, R. C., Fitzgerald, R. H., Jr., Harris, W. H., Poss, R., Muller, M. E., and Sledge, C. B. (1990) Clinical and radiographic evaluation of total hip replacement. A standard system of terminology for reporting results. *J Bone Joint Surg Am* **72,** 161-168.

Jolles, B. M. and Bogoch, E. R. (2004) Surgical approach for total hip arthroplasty: direct lateral or posterior? *J Rheumatol* **31,** 1790-1796.

Joshi, R. P., Eftekhar, N. S., McMahon, D. J., and Nercessian, O. A. (1998) Osteolysis after Charnley primary low-friction arthroplasty. A comparison of two matched paired groups. *J Bone Joint Surg Br* **80,** 585-590.

Kaneko, T. S., Bell, J. S., Pejcic, M. R., Tehranzadeh, J., and Keyak, J. H. (2004) Mechanical properties, density and quantitative CT scan data of trabecular bone with and without metastases. *J Biomech* **37,** 523-530.

Karachalios, T., Tsatsaronis, C., Efraimis, G., Papadelis, P., Lyritis, G., and Diakoumopoulos, G. (2004) The long-term clinical relevance of calcar atrophy caused by stress shielding in total hip arthroplasty: a 10-year, prospective, randomized study. *J Arthroplasty* **19,** 469-475.

Kärrholm, J., Garellick, G., and Herberts, P. (2006) Årsrapport 2005. *Nationalregistret för höftledsplastiker i Sverige.*

Katoozian, H. and Davy, D. T. (2000) Effects of loading conditions and objective function on three-dimensional shape optimization of femoral components of hip endoprostheses. *Med Eng Phys* **22,** 243-251.

Katz, J. N., Losina, E., Barrett, J., Phillips, C. B., Mahomed, N. N., Lew, R. A., Guadagnoli, E., Harris, W. H., Poss, R., and Baron, J. A. (2001) Association between hospital and surgeon procedure volume and outcomes of total hip replacement in the United States medicare population. *J Bone Joint Surg Am* **83-A,** 1622-1629.

Kawate, K., Maloney, W. J., Bragdon, C. R., Biggs, S. A., Jasty, M., and Harris, W. H. (1998) Importance of a thin cement mantle. Autopsy studies of eight hips. *Clin Orthop Relat Res* **355,** 70-76.

Kawate, K., Ohmura, T., Hiyoshi, N., Natsume, Y., Teranishi, T., and Tamai, S. (1999) Thin cement mantle and osteolysis with a precoated stem. *Clin Orthop Relat Res* **365,** 124-129.

Kawate, K., Ohmura, T., Nakajima, H., and Takakura, Y. (2001) Distal cement mantle thickness with a triangular distal centralizer inserted into the stem tip in cemented total hip arthroplasty. *J Arthroplasty* **16,** 998-1003.

Kawate, K., Yajima, H., Tomita, Y., Sugimoto, K., Ohmura, T., Hiyoshi, N., and Takakura, Y. (2003) Four-angle radiographic assessment of cement mantle thickness in cemented total hip arthroplasty. *J Arthroplasty* **18,** 914-919.

Keggi, K. J., Huo, M. H., and Zatorski, L. E. (1993) Anterior approach to total hip replacement: surgical technique and clinical results of our first one thousand cases using non-cemented prostheses. *Yale J Biol Med* **66,** 243-256.

Kleemann, R. U., Heller, M. O., Stoeckle, U., Taylor, W. R., and Duda, G. N. (2003) THA loading arising from increased femoral anteversion and offset may lead to critical cement stresses. *J Orthop Res* **21,** 767-774.

Kobayashi, S., Saito, N., Horiuchi, H., Iorio, R., and Takaoka, K. (2000) Poor bone quality or hip structure as risk factors affecting survival of total-hip arthroplasty. *Lancet* **355,** 1499-1504.

Kobayashi, S., Takaoka, K., Saito, N., and Hisa, K. (1997) Factors affecting aseptic failure of fixation after primary Charnley total hip arthroplasty. Multivariate survival analysis. *J Bone Joint Surg Am* **79,** 1618-1627.

Kobayashi, S. and Terayama, K. (1992) Factors influencing survivorship of the femoral component after primary low-friction hip arthroplasty. *J Arthroplasty* **7 Suppl,** 327-338.

Kon, H. (1981) [A study on the mechanical properties of bone cement (methylmethacrylate) and its strength alteration in vivo (author's transl)]. *Nippon Seikeigeka Gakkai Zasshi* **55,** 71-83.

Koster, G., Willert, H., and Buchhorn, G. H. (1999) Endoscopy of the femoral canal in revision arthroplasty of the hip.A new method for improving the operative technique and analysis of implant failure. *Arch Orthop Trauma Surg* **119,** 245-252.

Kroger, H., Venesmaa, P., Jurvelin, J., Miettinen, H., Suomalainen, O., and Alhava, E. (1998) Bone density at the proximal femur after total hip arthroplasty. *Clin Orthop Relat Res* **352,** 66-74.

Kwak, B. M., Lim, O. K., Kim, Y. Y., and Rim, K. (1979) Investigation of the effect of cement thickness on an implant by finite-element stress-analysis. *Int Orthop* **2,** 315-319.

Kwon, M. S., Kuskowski, M., Mulhall, K. J., Macaulay, W., Brown, T. E., and Saleh, K. J. (2006) Does surgical approach affect total hip arthroplasty dislocation rates? *Clin Orthop Relat Res* **447,** 34-38.

Langlais, F., Kerboull, M., Sedel, L., and Ling, R. S. (2003) The 'French paradox'. *J Bone Joint Surg Br* **85,** 17-20.

Lee, A. J., Ling, R. S., Gheduzzi, S., Simon, J. P., and Renfro, R. J. (2002) Factors affecting the mechanical and viscoelastic properties of acrylic bone cement. *J Mater Sci Mater Med* **13,** 723-733.

Lee, A. J., Ling, R. S., and Vangala, S. S. (1977) The mechanical properties of bone cements. *J Med Eng Technol* **1,** 137-140.

Lee, I. Y., Skinner, H. B., and Keyak, J. H. (1993) Effects of variation of cement thickness on bone and cement stress at the tip of a femoral implant. *Iowa Orthop J* **13,** 155-159.

Lee, I. Y., Skinner, H. B., and Keyak, J. H. (1994) Effects of variation of prosthesis size on cement stress at the tip of a femoral implant. *J Biomed Mater Res* **28,** 1055-1060.

Lennon, A. B. and Prendergast, P. J. (2001) Evaluation of cement stresses in finite element analyses of cemented orthopaedic implants. *J Biomech Eng* **123,** 623-628.

Lennon, A. B. and Prendergast, P. J. (2002) Residual stress due to curing can initiate damage in porous bone cement: experimental and theoretical evidence. *J Biomech* **35,** 311-321.

Lewis, G. (1997) Properties of acrylic bone cement: state of the art review. *J Biomed Mater Res* **38,** 155-182.

Lewis, G. (1999) Effect of mixing method and storage temperature of cement constituents on the fatigue and porosity of acrylic bone cement. *J Biomed Mater Res* **48,** 143-149.

Lewis, G. (2003) Fatigue testing and performance of acrylic bone-cement materials: state-of-the-art review. *J Biomed Mater Res [B]* **66,** 457-486.

Lewis, G. and Mladsi, S. (1998) Effect of sterilization method on properties of Palacos R acrylic bone cement. *Biomaterials* **19,** 117-124.

Lewis, J. L., Askew, M. J., Wixson, R. L., Kramer, G. M., and Tarr, R. R. (1984) The influence of prosthetic stem stiffness and of a calcar collar on stresses in the proximal end of the femur with a cemented femoral component. *J Bone Joint Surg Am* **66,** 280-286.

Li, C., Schmid, S. R., and Mason, J. J. (2003) Effects of pre-cooling and pre-heating procedures on cement polymerization and thermal osteonecrosis in cemented hip replacements. *Med Eng Phys* **25,** 559-564.

Li, C., Wang, Y., and Mason, J. (2004) The effects of curing history on residual stresses in bone cement during hip arthroplasty. *J Biomed Mater Res B Appl Biomater* **70,** 30-36.

Lichtinger, T. K., Schurmann, N., and Muller, R. T. (2000) [Early loosening of a cemented hip endoprosthesis stem of titanium]. *Unfallchirurg* **103,** 956-960.

Light, T. R. and Keggi, K. J. (1980) Anterior approach to hip arthroplasty. *Clin Orthop Relat Res* **152,** 255-260.

Lindgren, U. and Svenson, O. (1988) A new transtrochanteric approach to the hip. *Int Orthop* **12,** 37-41.

Lombardi, A. V., Mallory, T. H., and Fada, R. A. (2000) Surgical Technique in Total Hip Arthroplasty Utilizing the Anterolateral Approach. *Surg Technol Int* **IX,** 291-294.

Madsen, M. S., Ritter, M. A., Morris, H. H., Meding, J. B., Berend, M. E., Faris, P. M., and Vardaxis, V. G. (2004) The effect of total hip arthroplasty surgical approach on gait. *J Orthop Res* **22,** 44-50.

Malchau, H. and Herberts, P. (1998) Prognosis of total hip replacement. Revision and re-revision rate in THR: a revision-risk study of 148,359 primary operations. *Scientific Exhibition presented at the 65th Annual Meeting of the American Academy of Orthopaedic Surgeons, New Orleans, USA.*

Malchau, H., Herberts, P., Söderman, P., and Odén, A. (2000) Prognosis of total hip replacement. Update and validation of results from the Swedish National Hip Arthroplasty Register 1979-1998. *Scientific Exhibition presented at the 67th Annual Meeting of the American Academy of Orthopaedic Surgeons, Orlando, USA.*

Malik, M. H., Fisher, N., Gray, J., Wroblewski, B. M., and Kay, P. R. (2005) Prediction of Charnley femoral stem aseptic loosening by early post-operative radiological features. *Int Orthop* **29,** 268-271.

Maloney, W. J., Jasty, M., Rosenberg, A., and Harris, W. H. (1990) Bone lysis in well-fixed cemented femoral components. *J Bone Joint Surg Br* **72,** 966-970.

Mann, K. A., Bartel, D. L., Wright, T. M., and Ingraffea, A. R. (1991) Mechanical characteristics of the stem-cement interface. *J Orthop Res* **9,** 798-808.

Mann, K. A., Gupta, S., Race, A., Miller, M. A., Cleary, R. J., and Ayers, D. C. (2004) Cement microcracks in thin-mantle regions after in vitro fatigue loading. *J Arthroplasty* **19,** 605-612.

Masonis, J. L. and Bourne, R. B. (2002) Surgical approach, abductor function, and total hip arthroplasty dislocation. *Clin Orthop Relat Res* **405,** 46-53.

Massin, P., Astoin, E., and Lavaste, F. (2003) [Influence of proximal stem geometry and stem-cement interface characteristics on bone and cement stresses in femoral hip arthroplasty: finite element analysis]. *Rev Chir Orthop Reparatrice Appar Mot* **89,** 134-143.

Massoud, S. N., Hunter, J. B., Holdsworth, B. J., Wallace, W. A., and Juliusson, R. (1997) Early femoral loosening in one design of cemented hip replacement. *J Bone Joint Surg Br* **79,** 603-608.

Mau, H., Schelling, K., Heisel, C., Wang, J. S., and Breusch, S. J. (2004) Comparison of various vacuum mixing systems and bone cements as regards reliability, porosity and bending strength. *Acta Orthop Scand* **75,** 160-172.

McCaskie, A. W., Brown, A. R., Thompson, J. R., and Gregg, P. J. (1996) Radiological evaluation of the interfaces after cemented total hip replacement. Interobserver and intraobserver agreement. *J Bone Joint Surg Br* **78,** 191-194.

McCormack, B. A. and Prendergast, P. J. (1999) Microdamage accumulation in the cement layer of hip replacements under flexural loading. *J Biomech* **32,** 467-475.

McFarland, B. and Osborne, G. (1954) Approach to the hip: a suggested improvement on Kocher's method. *J Bone Joint Surg Br* **36,** 364-367.

Mellor, S. J., Ripley, L. G., and Ricketts, D. M. (2004) The femoral cement mantle in three total hip replacements. *Int Orthop* **28,** 40-43.

Miles, A. W. and Dall, D. M. (1985) An experimental study of femoral cement stress in total hip replacement--influence of structural stiffness of the femoral stem. *Eng Med* **14,** 133-135.

Mohler, C. G., Callaghan, J. J., Collis, D. K., and Johnston, R. C. (1995) Early loosening of the femoral component at the cement-prosthesis interface after total hip replacement. *J Bone Joint Surg Am* **77,** 1315-1322.

Morgan, E. F., Bayraktar, H. H., and Keaveny, T. M. (2003) Trabecular bone modulus-density relationships depend on anatomic site. *J Biomech* **36,** 897-904.

Mulroy, W. F., Estok, D. M., and Harris, W. H. (1995) Total hip arthroplasty with use of so-called second-generation cementing techniques. A fifteen-year-average follow-up study. *J Bone Joint Surg Am* **77,** 1845-1852.

Murphy, B. P. and Prendergast, P. J. (1999) Measurement of non-linear microcrack accumulation rates in polymethylmethacrylate bone cement under cyclic loading. *J Mater Sci Mater Med* **10,** 779-781.

Murphy, B. P. and Prendergast, P. J. (2002) The relationship between stress, porosity, and nonlinear damage accumulation in acrylic bone cement. *J Biomed Mater Res* **59,** 646-654.

Murphy, B. P. and Prendergast, P. J. (2003) Multi-axial fatigue failure of orthopedic bone cement - experiments with tubular specimens. *J Mater Sci Mater Med* **14,** 857-861.

Nazarian, S., Tisserand, P., Brunet, C., and Muller, M. E. (1987) Anatomic basis of the transgluteal approach to the hip. *Surg Radiol Anat* **9,** 27-35.

Nivbrant, B., Karrholm, J., and Soderlund, P. (1999) Increased migration of the SHP prosthesis: radiostereometric comparison with the Lubinus SP2 design in 40 cases. *Acta Orthop Scand* **70,** 569-577.

Noble, P. C., Collier, M. B., Maltry, J. A., Kamaric, E., and Tullos, H. S. (1998) Pressurization and centralization enhance the quality and reproducibility of cement mantles. *Clin Orthop Relat Res* **355,** 77-89.

Noble, P. C., Johnson, J. D., and Alexander, J. W. (2005) Cracking of the debonded cement mantle is the critical event in the aseptic loosening of cemented femoral stems. *Trans Orthop Res Soc* **51,** 9.

Norman, T. L., Kish, V., Blaha, J. D., Gruen, T. A., and Hustosky, K. (1995) Creep characteristics of hand- and vacuum-mixed acrylic bone cement at elevated stress levels. *J Biomed Mater Res* **29,** 495-501.

Nuno, N. and Avanzolini, G. (2002) Residual stresses at the stem-cement interface of an idealized cemented hip stem. *J Biomech* **35,** 849-852.

O'Connor, D. O., Burke, D. W., Jasty, M., Sedlacek, R. C., and Harris, W. H. (1996) In vitro measurement of strain in the bone cement surrounding the femoral component of total hip replacements during simulated gait and stair-climbing. *J Orthop Res* **14,** 769-777.

Ong, A., Wong, K. L., Lai, M., Garino, J. P., and Steinberg, M. E. (2002) Early failure of precoated femoral components in primary total hip arthroplasty. *J Bone Joint Surg Am* **84-A,** 786-792.

Orr, J. F., Dunne, N. J., and Quinn, J. C. (2003) Shrinkage stresses in bone cement. *Biomaterials* **24,** 2933-2940.

Pai, V. S. (2002) A modified direct lateral approach in total hip arthroplasty. *J Orthop Surg (Hong Kong)* **10,** 35-39.

Papini, M. and Zalzal, P. (2003) IGES solid model of the 'third generation composite femur #3306' made by Pacific Research Labs, Vashon, WA. http://www.biomed-town.org/biomed_town/LHDL/Reception/datarepository/repositories/BelRepWikiPages/3rdGenerationCompositeFemur. *Biomechanics European Laboratory Repository*.

Parks, M. L., Walsh, H. A., Salvati, E. A., and Li, S. (1998) Effect of increasing temperature on the properties of four bone cements. *Clin Orthop Relat Res* **355,** 238-248.

Pascarel, X., Dumont, D., Nehme, B., Dudreuilh, J. P., and Honton, J. L. (1989) [Total hip arthroplasty using the Hardinge approach. Clinical results in 63 cases]. *Rev Chir Orthop Reparatrice Appar Mot* **75,** 98-103.

Patiala, H., Lehto, K., Rokkanen, P., and Paavolainen, P. (1984) Posterior approach for total hip arthroplasty. A study of postoperative course, early results and early complications in 131 cases. *Arch Orthop Trauma Surg* **102,** 225-229.

Pellicci, P. M., Bostrom, M., and Poss, R. (1998) Posterior approach to total hip replacement using enhanced posterior soft tissue repair. *Clin Orthop Relat Res* **355,** 224-228.

Picado, C. H., Garcia, F. L., and Marques, W., Jr. (2006) Damage to the Superior Gluteal Nerve after Direct Lateral Approach to the Hip. *Clin Orthop Relat Res* **455,** 209-211.

Powers, C. M., Lee, I. Y., Skinner, H. B., and Keyak, J. H. (1998) Effects of distal cement voids on cement stress in total hip arthroplasty. *J Arthroplasty* **13,** 793-798.

Prendergast, P. J. (2002) Mechanics Applied to Skeletal Ontogeny and Phylogeny. *Meccanica* **37,** 317-334.

Prendergast, P. J., Monaghan, J., and Taylor, D. (1989) Materials selection in the artificial hip joint using finite element stress analysis. *Clin Mater* **4,** 361-376.

Prendergast, P. J. and Taylor, D. (1990) Stress analysis of the proximo-medial femur after total hip replacement. *J Biomed Eng* **12,** 379-382.

Race, A., Miller, M. A., Ayers, D. C., and Mann, K. A. (2003) Early cement damage around a femoral stem is concentrated at the cement/bone interface. *J Biomech* **36,** 489-496.

Reilly, D. T. and Burstein, A. H. (1975) The elastic and ultimate properties of compact bone tissue. *J Biomech* **8,** 393-405.

Ritter, M. A., Harty, L. D., Keating, M. E., Faris, P. M., and Meding, J. B. (2001) A clinical comparison of the anterolateral and posterolateral approaches to the hip. *Clin Orthop Relat Res* **385,** 95-99.

Ritter, M. A., Zhou, H., Keating, C. M., Keating, E. M., Faris, P. M., Meding, J. B., and Berend, M. E. (1999) Radiological factors influencing femoral and acetabular failure in cemented Charnley total hip arthroplasties. *J Bone Joint Surg Br* **81,** 982-986.

Roberts, J. M., Fu, F. H., McClain, E. J., and Ferguson, A. B., Jr. (1984) A comparison of the posterolateral and anterolateral approaches to total hip arthroplasty. *Clin Orthop Relat Res* **187,** 205-210.

Robertsson, O., Wingstrand, H., Kesteris, U., Jonsson, K., and Onnerfalt, R. (1997) Intracapsular pressure and loosening of hip prostheses. Preoperative measurements in 18 hips. *Acta Orthop Scand* **68,** 231-234.

Rohlmann, A., Mossner, U., Bergmann, G., Hees, G., and Kolbel, R. (1987) Effects of stem design and material properties on stresses in hip endoprostheses. *J Biomed Eng* **9,** 77-83.

Rohlmann, A., Mossner, U., Bergmann, G., and Kolbel, R. (1983) Finite-element-analysis and experimental investigation in a femur with hip endoprosthesis. *J Biomech* **16,** 727-742.

Roques, A., Browne, M., Taylor, A., New, A., and Baker, D. (2004) Quantitative measurement of the stresses induced during polymerisation of bone cement. *Biomaterials* **25,** 4415-4424.

Scheerlinck, T., de Mey, J., Deklerck, R., and Noble, P. C. (2006) CT analysis of defects of the cement mantle and alignment of the stem: in vitro comparison of Charnley-Kerboul femoral hip implants inserted line-to-line and undersized in paired femora. *J Bone Joint Surg Br* **88,** 19-25.

Schmalzried, T. P., Jasty, M., and Harris, W. H. (1992a) Periprosthetic bone loss in total hip arthroplasty. Polyethylene wear debris and the concept of the effective joint space. *J Bone Joint Surg Am* **74,** 849-863.

Schmalzried, T. P., Kwong, L. M., Jasty, M., Sedlacek, R. C., Haire, T. C., O'Connor, D. O., Bragdon, C. R., Kabo, J. M., Malcolm, A. J., and Harris, W. H. (1992b) The mechanism of loosening of cemented acetabular components in total hip arthroplasty. Analysis of specimens retrieved at autopsy. *Clin Orthop Relat Res* **274,** 60-78.

Schmalzried, T. P., Peters, P. C., Maurer, B. T., Bragdon, C. R., and Harris, W. H. (1996a) Long-duration metal-on-metal total hip arthroplasties with low wear of the articulating surfaces. *J Arthroplasty* **11,** 322-331.

Schmalzried, T. P., Szuszczewicz, E. S., Akizuki, K. H., Petersen, T. D., and Amstutz, H. C. (1996b) Factors correlating with long term survival of McKee-Farrar total hip prostheses. *Clin Orthop Relat Res* **329 Suppl,** S48-S59.

Schmolz, W., Gordon, D. R., Shields, A. J., Kirkwood, D., and Grigoris, P. (2000) The effect of stem geometry on stresses within the distal cement mantle in total hip replacement. *Technol Health Care* **8,** 67-73.

Shaw, J. A. (1991) Experience with a modified posterior approach to the hip joint. A technical note. *J Arthroplasty* **6,** 11-18.

Silva, M., Heisel, C., and Schmalzried, T. P. (2005) Metal-on-metal total hip replacement. *Clin Orthop Relat Res* **430,** 53-61.

Skinner, J. A., Todo, S., Taylor, M., Wang, J. S., Pinskerova, V., and Scott, G. (2003) Should the cement mantle around the femoral component be thick or thin? *J Bone Joint Surg Br* **85,** 45-51.

Smith, S. W., Estok, D. M., and Harris, W. H. (1998) Total hip arthroplasty with use of second-generation cementing techniques. An eighteen-year-average follow-up study. *J Bone Joint Surg Am* **80,** 1632-1640.

Smith-Petersen, M. N. (1949) Approach to and exposure of the hip joint for mold arthroplasty. *J Bone Joint Surg Am* **31,** 40-46.

Soni, R. K. (1997) An anterolateral approach to the hip joint. *Acta Orthop Scand* **68,** 490-494.

Star, M. J., Colwell, C. W., Jr., Kelman, G. J., Ballock, R. T., and Walker, R. H. (1994) Suboptimal (thin) distal cement mantle thickness as a contributory factor in total hip arthroplasty femoral component failure. A retrospective radiographic analysis favoring distal stem centralization. *J Arthroplasty* **9,** 143-149.

Stolk, J., Janssen, D., Huiskes, R., and Verdonschot, N. (2007) Finite Element-based Preclinical Testing of Cemented Total Hip Implants. *Clin Orthop Relat Res* **456,** 138-147.

Stolk, J., Maher, S. A., Verdonschot, N., Prendergast, P. J., and Huiskes, R. (2003a) Can finite element models detect clinically inferior cemented hip implants? *Clin Orthop Relat Res* **409,** 138-150.

Stolk, J., Verdonschot, N., and Huiskes, R. (2002) Stair climbing is more detrimental to the cement in hip replacement than walking. *Clin Orthop Relat Res* **405,** 294-305.

Stolk, J., Verdonschot, N., Mann, K. A., and Huiskes, R. (2003b) Prevention of mesh-dependent damage growth in finite element simulations of crack formation in acrylic bone cement. *J Biomech* **36,** 861-871.

Stolk, J., Verdonschot, N., Murphy, B. P., Prendergast, P. J., and Huiskes, R. (2004) Finite element simulation of anisotropic damage accumulation and creep in acrylic bone cement. *Eng Fract Mech* **71,** 513-528.

Suh, K. T., Park, B. G., and Choi, Y. J. (2004) A posterior approach to primary total hip arthroplasty with soft tissue repair. *Clin Orthop Relat Res* **418,** 162-167.

Swenson, L. W., Schurman, D. J., and Piziali, R. (1981) Finite element temperature analysis of a total hip replacement and measurement of PMMA curing temperatures. *J Biomed Mater Res* **15,** 83-96.

Sylvain, G. M., Kassab, S., Coutts, R., and Santore, R. (2001) Early failure of a roughened surface, precoated femoral component in total hip arthroplasty. *J Arthroplasty* **16,** 141-148.

Taylor, M., Tanner, K. E., Freeman, M. A., and Yettram, A. L. (1995) Cancellous bone stresses surrounding the femoral component of a hip prosthesis: an elastic-plastic finite element analysis. *Med Eng Phys* **17,** 544-550.

Thomas, S. R., Shukla, D., and Latham, P. D. (2004) Corrosion of cemented titanium femoral stems. *J Bone Joint Surg Br* **86,** 974-978.

Topoleski, L. D., Ducheyne, P., and Cuckler, J. M. (1990) A fractographic analysis of in vivo poly(methyl methacrylate) bone cement failure mechanisms. *J Biomed Mater Res* **24,** 135-154.

Topoleski, L. D., Ducheyne, P., and Cuckler, J. M. (1993) Microstructural pathway of fracture in poly(methyl methacrylate) bone cement. *Biomaterials* **14,** 1165-1172.

Topoleski, L. D., Ducheyne, P., and Cuckler, J. M. (1995) The effects of centrifugation and titanium fiber reinforcement on fatigue failure mechanisms in poly(methyl methacrylate) bone cement. *J Biomed Mater Res* **29,** 299-307.

Valdivia, G. G., Dunbar, M. J., Parker, D. A., Woolfrey, M. R., MacDonald, S. J., McCalden, R. W., Rorabeck, C. H., and Bourne, R. B. (2001) The John Charnley Award: Three-dimensional analysis of the cement mantle in total hip arthroplasty. *Clin Orthop Relat Res* **393,** 38-51.

Vallo, C. I. (2002) Flexural strength distribution of a PMMA-based bone cement. *J Biomed Mater Res* **63,** 226-236.

van der Linde, M. J. and Tonino, A. J. (1997) Nerve injury after hip arthroplasty. 5/600 cases after uncemented hip replacement, anterolateral approach versus direct lateral approach. *Acta Orthop Scand* **68,** 521-523.

van Stralen, G. M., Struben, P. J., and van Loon, C. J. (2003) The incidence of dislocation after primary total hip arthroplasty using posterior approach with posterior soft-tissue repair. *Arch Orthop Trauma Surg* **123,** 219-222.

Venesmaa, P. K., Kroger, H. P., Jurvelin, J. S., Miettinen, H. J., Suomalainen, O. T., and Alhava, E. M. (2003) Periprosthetic bone loss after cemented total hip arthroplasty: a prospective 5-year dual energy radiographic absorptiometry study of 15 patients. *Acta Orthop Scand* **74,** 31-36.

Verdonschot, N. (1995) Biomechanical failure scenarios for cemented total hip replacement. *PhD Thesis, University of Nijmegen.*

Verdonschot, N. (2005) Philosophies of stem designs in cemented total hip replacement. *Orthopedics* **28,** s833-s840.

Verdonschot, N. and Huiskes, R. (1994) Creep behavior of hand-mixed Simplex P bone cement under cyclic tensile loading. *J Appl Biomater* **5,** 235-243.

Verdonschot, N. and Huiskes, R. (1995) Dynamic creep behavior of acrylic bone cement. *J Biomed Mater Res* **29,** 575-581.

Verdonschot, N. and Huiskes, R. (1996a) Mechanical effects of stem cement interface characteristics in total hip replacement. *Clin Orthop Relat Res* **329,** 326-336.

Verdonschot, N. and Huiskes, R. (1996b) Subsidence of THA stems due to acrylic cement creep is extremely sensitive to interface friction. *J Biomech* **29,** 1569-1575.

Verdonschot, N. and Huiskes, R. (1997a) Cement debonding process of total hip arthroplasty stems. *Clin Orthop Relat Res* **336,** 297-307.

Verdonschot, N. and Huiskes, R. (1997b) The effects of cement-stem debonding in THA on the long-term failure probability of cement. *J Biomech* **30,** 795-802.

Verdonschot, N., Tanck, E., and Huiskes, R. (1998) Effects of prosthesis surface roughness on the failure process of cemented hip implants after stem-cement debonding. *J Biomed Mater Res* **42,** 554-559.

Vicar, A. J. and Coleman, C. R. (1984) A comparison of the anterolateral, transtrochanteric, and posterior surgical approaches in primary total hip arthroplasty. *Clin Orthop Relat Res* **188,** 152-159.

Viceconti, M., Casali, M., Massari, B., Cristofolini, L., Bassini, S., and Toni, A. (1996) The 'standardized femur program' proposal for a reference geometry to be used for the creation of finite element models of the femur. *J Biomech* **29,** 1241.

Wang, J. S., Franzen, H., Toksvig-Larsen, S., and Lidgren, L. (1995) Does vacuum mixing of bone cement affect heat generation? Analysis of four cement brands. *J Appl Biomater* **6,** 105-108.

Watson, M. B., Miles, A. W., and Clift, S. E. (1990) The influence of curing time and environment on the fracture properties of bone cement. *Clin Mater* **6,** 299-305.

Watson-Jones, R. (1936) Fractures of the neck of the femur. *Br J Surg* **23,** 787-808.

Weeden, S. H., Paprosky, W. G., and Bowling, J. W. (2003) The early dislocation rate in primary total hip arthroplasty following the posterior approach with posterior soft-tissue repair. *J Arthroplasty* **18,** 709-713.

Wheeler, J. P., Miles, A. W., and Clift, S. E. (1997) The influence of the stem-cement interface in total hip replacement--a comparison of experimental and finite element approaches. *Proc Inst Mech Eng [H]* **211,** 181-186.

Wiles, P. (1958) The surgery of the osteoarthritic hip. *Br J Surg* **45,** 488-497.

Wilkinson, J. M., Eveleigh, R. J., Hamer, A. J., Milne, A., Miles, A. W., and Stockley, I. (2000) Effect of mixing technique on the properties of acrylic bone-cement: a comparison of syringe and bowl mixing systems. *J Arthroplasty* **15,** 663-667.

Willert, H. G., Broback, L. G., Buchhorn, G. H., Jensen, P. H., Koster, G., Lang, I., Ochsner, P., and Schenk, R. (1996) Crevice corrosion of cemented titanium alloy stems in total hip replacements. *Clin Orthop Relat Res* **333,** 51-75.

Williams, J. L. and Johnson, W. J. (1989) Elastic constants of composites formed from PMMA bone cement and anisotropic bovine tibial cancellous bone. *J Biomech* **22,** 673-682.

Wong, A. S., New, A. M., Isaacs, G., and Taylor, M. (2005) Effect of bone material properties on the initial stability of a cementless hip stem: a finite element study. *Proc Inst Mech Eng [H]* **219,** 265-275.

Yetkinler, D. N. and Litsky, A. S. (1998) Viscoelastic behaviour of acrylic bone cements. *Biomaterials* **19,** 1551-1559.

Yettram, A. L. and Wright, K. W. (1979) Biomechanics of the femoral component of total hip prostheses with particular reference to the stress in the bone-cement. *J Biomed Eng* **1,** 281-285.

Yoon, Y. S., Jang, G. H., and Kim, Y. Y. (1989) Shape optimal design of the stem of a cemented hip prosthesis to minimize stress concentration in the cement layer. *J Biomech* **22,** 1279-1284.

Zimmerma, S., Hawkes, W. G., Hudson, J. I., Magaziner, J., Hebel, J. R., Towheed, T., Gardner, J., Provenzano, G., and Kenzora, J. E. (2002) Outcomes of surgical management of total HIP replacement in patients aged 65 years and older: cemented versus cementless femoral components and lateral or anterolateral versus posterior anatomical approach. *J Orthop Res* **20,** 182-191.

Appendix – Selected publications

DOES CHOICE OF FEMORAL CEMENT MANTLE THICKNESS DEPEND ON BONE DENSITY?

*Caruana, J; [+]Mannan, K; [+]Sanghrajka, A; [+]Higgs, D; Briggs, TW; *Blunn, GW
*Centre for Biomedical Engineering, Institute for Orthopaedics and Musculoskeletal Science, University College, London, UK
[+]Royal National Orthopaedic Hospital, Stanmore, UK
j.caruana@ucl.ac.uk

DO FEMORAL CEMENT MANTLE THICKNESS AND CENTRALISATION AFFECT CEMENT CRACKING IN TOTAL HIP REPLACEMENT?

+*Caruana, J; *Hon, CMY; **Whittingham-Jones, PM; **Briggs, TWR; *Hua, J; *Blunn, GW
+*Centre for Biomedical Engineering, Institute for Orthopaedics & Musculoskeletal Science, University College London, Stanmore, UK
j.caruana@ucl.ac.uk

DEBONDING IS CRITICAL TO FEMORAL CEMENT MANTLE DAMAGE IN TOTAL HIP REPLACEMENTS

+*Caruana, J; **Janssen, D; **Verdonschot, N; *Hua, J; *Blunn, GW
+*Centre for Biomedical Engineering, Institute of Orthopaedics & Musculoskeletal Science, University College London, Stanmore, UK
j.caruana@ucl.ac.uk

Hip International / Vol. 16 no. 2, 2006 / pp. 67-74

Anterior or posterior: does the surgical approach to the hip influence the quality of the femoral cement mantle?

A.P. SANGHRAJKA, P.M. WHITTINGHAM-JONES, D. HIGGS, J. CARUANA, G. BLUNN, T.W.R. BRIGGS

Royal National Orthopaedic Hospital, Stanmore, Middlesex - UK

UNIVERSITY OF LONDON

SENATE HOUSE. MALET STREET, LONDON, WCIE 7HU

REPRODUCTION OF THESES

A thesis which is accepted by the University for the award of a Research Degree is placed in the Library of the College and in the University of London Library. The copyright of the thesis is retained by the author.

As you are about to submit a thesis for a Research Degree, you are required to sign the declaration below. This declaration is separate from any which may be made under arrangements with the College at which you have *pursued* your course (for internal candidates only). The declaration will be destroyed if your thesis is not approved by the examiners, being either rejected or referred for revision.

Academic Registrar

To be completed by the candidate

NAME IN FULL (please type surname in BLOCK CAPITALS)

Jonathan CARUANA

THESIS TITLE Does Cement Mantle Thickness Really Matter?

DEGREE FOR WHICH THESIS IS PRESENTED Doctor of Philosophy (Ph.D.)

DATE OF AWARD OF DEGREE *(To be completed by the University):* _____

DECLARATION

1. I authorise that the thesis presented by me in *[2007] for examination for the MPhil/PhD Degree of the University of London shall, if a degree is awarded, be deposited in the library of the appropriate College and in the University of London Library and that, subject to the conditions set out below, my thesis be made available for public reference, inter-library loan and copying.

2. I authorise the College or University authorities as appropriate to supply a copy of the abstract of my thesis for inclusion in any published list of theses offered for higher degrees in British universities or in any supplement thereto, or for consultation in any central file of abstracts of such theses.

3. I authorise the College and the University of London Libraries, or their designated agents, to make a microform or digital copy of my thesis for the purposes of inter-library loan and the supply of copies.

4. I understand that before my thesis is made available for public reference, inter-library loan and copying, the following statement will have been included at the beginning of my thesis: The copyright of this thesis rests with the author and no quotation from it or information derived from it may be published without the prior written consent of the author.

5. I authorise the College and/or the University of London to make a microform or digital copy of my thesis in due course as the archival copy for permanent retention in substitution for the original copy.

6. I warrant that this authorisation does not, to the best of my belief, infringe the rights of any third party.

7. I understand that in the event of my thesis being not approved by the examiners, this declaration would become void.

***Please state year by hand, using a pen.**

DATE 22/08/07 SIGNATURE _____

Note: The University's Ordinances make provision for restriction of access to an MPhil/PhD thesis and/or the abstract but only in certain specified circumstances and for a maxiumum period of two years. If you wish to apply for such restriction, please enquire at your College about the conditions and procedures. External Students should enquire at the Research Degree Examinations Office, Room 261, Senate House.

THIS DECLARATION MUST BE COMPLETED AND RETURNED WITH THE EXAMINATION ENTRY FORM